The FAA's Center of Excellence for UAS Research
ASSURE
Alliance for System Safety of UAS through Research Excellence

THE OHIO STATE UNIVERSITY
COLLEGE OF ENGINEERING

NIAR
WICHITA STATE UNIVERSITY
NATIONAL INSTITUTE FOR AVIATION RESEARCH

Task A43: Airborne Collision Severity Evaluation – Engine Ingestion
Final Report

September 10, 2025

NOTICE

LEGAL DISCLAIMER

The information provided herein may include content supplied by third parties. Although the data and information contained herein has been produced or processed from sources believed to be reliable, the Federal Aviation Administration makes no warranty, expressed or implied, regarding the accuracy, adequacy, completeness, legality, reliability, or usefulness of any information, conclusions or recommendations provided herein. Distribution of the information contained herein does not constitute an endorsement or warranty of the data or information provided herein by the Federal Aviation Administration or the U.S. Department of Transportation. Neither the Federal Aviation Administration nor the U.S. Department of Transportation shall be held liable for any improper or incorrect use of the information contained herein and assumes no responsibility for anyone's use of the information. The Federal Aviation Administration and U.S. Department of Transportation shall not be liable for any claim for any loss, harm, or other damages arising from access to or use of data or information, including without limitation any direct, indirect, incidental, exemplary, special, or consequential damages, even if advised of the possibility of such damages. The Federal Aviation Administration shall not be liable to anyone for any decision made or action taken, or not taken, in reliance on the information contained herein.

THIRD PARTY RESEARCH. PENDING FAA REVIEW.

The FAA's Center of Excellence for UAS Research
ASSURE
Alliance for System Safety of UAS through Research Excellence

TECHNICAL REPORT DOCUMENTATION PAGE

1. Report No.	2. Government Accession No.	3. Recipient's Catalog No.
FAA A11L.UAS.58		

4. Title and Subtitle	5. Report Date
Task A43: High-Bypass Turbofan UAS Engine Ingestion Test 2021-2025	(month and year printed)
	6. Performing Organization Code ASSURE: OSU

7. Author(s)	8. Performing Organization Report No.
Professor Kiran D'Souza, The Ohio State University (OSU) Dr. Dushyanth Sirivolu (OSU) Mr. Mitchell Wong (OSU) Dr. Gerardo Olivares, National Institute for Aviation Research (NIAR) Mr. Luis Gomez, National Institute for Aviation Research (NIAR)	

9. Performing Organization Name and Address	10. Work Unit No. (TRAIS)
The Ohio State University Aerospace Research Center 2300 West Case Road Columbus, OH 43235	11. Contract or Grant No.

12. Sponsoring Agency Name and Address	13. Type of Report and Period Covered
U.S. Department of Transportation Federal Aviation Administration Office of Aviation Research Washington, DC 20591	Final Report
	14. Sponsoring Agency Code 5401

15. Supplementary Notes

The Federal Aviation Administration Aviation William J. Hughes Technical Center Research Division COR was

16. Abstract

The A43 study accomplished three main tasks: (1) overseeing and guiding the test partner's work in defining and executing a live ingestion of a UAS into an engine; and (2) analyzing the resulting test data to validate the computational modeling approach (3) showing the effectiveness in the open representative fan model for use in foreign object ingestion studies. The effort resulted in a successful ingestion of a UAS into a flightworthy CFM56-7B engine with a variety of data collected, including high-speed videos, strain gauges, digital image correlation, blade scans, and engine operational data. Based on the analysis of the data and comparison with numerical simulations, the research team concluded that the computational modeling approach is effective in predicting the damage level expected during a UAS ingestion. Moreover, the open representative fan model developed in the A17 work was also shown to behave in a similar manner as the actual engine model. These results bolster the conclusions in the previous study with the representative fan model, where a sensitivity study was conducted to identify the key parameters of the ingestion.

17. Key Words	18. Distribution Statement
Crashworthiness, Engine Ingestion, UAS, Ohio State University, OSU	This document is available to the U.S. public through the National Technical Information Service (NTIS), Springfield, Virginia 22161. This document is also available from the Federal Aviation Administration William J. Hughes Technical Center at actlibrary.tc.faa.gov.

19. Security Classif. (of this report)	20. Security Classif. (of this page)	21. No. of Pages	22. Price
Unclassified	Unclassified	97	

ACKNOWLEDGEMENTS

The researchers and the respective university Principal Investigators listed in the technical documentation page have made fundamental contributions to the content. Individuals from the National Institute for Aviation Research who also supported the work include Hoa Ly, Armando De Abreu, and Akhil Bhasin.

The A43 team would also like to recognize the contributions of the Naval Air Warfare Center Weapons Survivability Lab, which worked closely with the ASSURE team to define and carry out the test plan.

The authors would like to acknowledge the FAA's Center of Excellence for Unmanned Aircraft Systems, ASSURE, for supporting this work. The A43 team also recognizes the vital importance of the leadership at ASSURE in the completion of this project. Steve Luxion and Hannah Thach, along with the ASSURE leadership, have been strong supporters of the team throughout this project and have participated actively in a number of events.

The authors would also like to acknowledge the Ohio Super Computer Center[1] and the OSU SimCenter, which provided additional computing resources used to run the simulations presented in this work.

Finally, the A43 team would like to thank all the FAA personnel who have been involved in this research project. In particular, the authors would like to thank Sabrina Saunders-Hodge, Hector Rea, Nick Lento, Jorge Fernandez, Karen Davis, William Oehlschlager, John M Miller, and Bhanu Kota for their support throughout the project.

TABLE OF CONTENTS

Page

LIST OF FIGURES

LIST OF TABLES

LIST OF ACRONYMS

ASSURE	Alliance for System Safety of UAS through Research Excellence
AWG	LS-DYNA Aerospace Working Group
CAD	Computer-Aided Design
DIC	Digital Image Correlation
FAA	Federal Aviation Administration
FE	Finite Element
ITM	Integrated Test & Measurement
NAWC	Naval Air Warfare Center
NIAR	National Institute for Aviation Research
OEM	Original Equipment Manufacturer
OSU	The Ohio State University
RPM	Revolutions Per Minute
UAS	Uncrewed Aircraft System

EXECUTIVE SUMMARY

The A43 High-Bypass Turbofan Uncrewed Aircraft System (UAS) Engine Ingestion Test builds from two prior studies. The first is the A3 project, which had a small engine ingestion study that used a generic mid-sized business jet fan assembly model and developed a model of a UAS. The second is the A17 project that created a fan assembly model with representative structural features of a high bypass ratio fan commonly used in aircraft engines for commercial transport, validated the UAS model with experiments representative of a UAS being ingested into an engine, and used the representative fan assembly model and validated UAS model to conduct UAS ingestion studies. The primary goal of the A43 project was to conduct a live UAS ingestion into an engine to validate the overall computational modeling approach that had previously been used in the A3 and A17 research programs. The A43 team consisted of The Ohio State University (OSU) and the National Institute for Aviation Research (NIAR). The A43 team worked with the Naval Air Warfare Center (NAWC) to define and conduct the experiment.

A representative engine was chosen for the test, a flightworthy CFM56-7B engine. The DJI Phantom 3 standard UAS was chosen as the projectile to capitalize on the considerable effort that was expended in developing a high-fidelity Finite Element (FE) model that was validated at the conditions of an ingestion event. The ingestion conditions were selected to be at takeoff conditions for the engine, with the UAS impacting the outer radial span. The test conditions were chosen to result in one of the more severe ingestion scenarios for the given UAS, while also leveraging past research. Key data collected from the experiment to validate the modeling approach included high-definition and high-speed cameras capturing the ingestion, Digital Image Correlation (DIC), strain gauges, and post-test documentation.

The developed computational CFM56-7B fan assembly model was simulated in LS-DYNA at the same conditions as the live engine ingestion test in a similar manner as in the A17 work. The conditions of the ingestion (UAS speed, orientation, and location just before impact) were computed by analyzing the DIC data. Comparisons were made between the data gathered from the test and the numerical simulation. In particular, the overall damage to the fan blades was in very good agreement. There was a small amount of extra damage at the tips of all blades in the live ingestion due to the severe blade rub that occurred during the testing that was not present in the simulation. The main notable difference in damage between the two cases was that the upper portion of one blade in the experiment broke free, while in the simulation there was a significant crack along the leading edge in the corresponding blade. The overall fan damage severity level, as defined in the A17 research project, matched the experiment and numerical simulation. The strain gauge data and out-of-plane displacement on the impacted blades were compared with the simulation results and were in reasonably good agreement. Also, the kinematics of the ingestion were similar except for the explosion that was created in the experiment, which was not replicated in the numerical simulation.

The completion of this research program has validated the overall computational modeling approach for the ingestion of a UAS into a fan assembly model that was presented in the A17 program. Moreover, the open representative fan assembly model that was developed in the A17 program was compared with a fan assembly rig model of an actual engine in service (CFM56-7B) and found to be in good agreement. This gives high confidence in using this open representative fan assembly model in future foreign object ingestion studies in industry and academia to improve models and compare results with prior work.

1. BACKGROUND

The use of UAS has increased dramatically in recent years. As the number of UAS sold continues to increase, proper integration of UAS into the airspace is a major safety concern due to the potential for a UAS-airplane collision. Recreational users are the highest safety concern since they may be unaware or unconcerned with regulations and rules concerned with restricted operation of their devices in certain airspaces. These UAS tend to be relatively small and have the potential to be ingested into an engine. Currently, there are regulations on aircraft engines that require full-scale tests on new engines to demonstrate safe operation after certain bird and ice ingestions; the researchers do not intend to recommend additional certification tests for UAS ingestions. Moreover, the current tests and regulations cannot be transferred from birds to UAS since key components (motor, battery, camera) of these UAS contain materials that are much denser and stiffer than ice and birds (which are typically modeled as a fluid since they are over 70% water). Preliminary work on this topic has shown that UAS can cause significantly more damage than birds[2, 3]. Additional computational studies have recently been completed with a new representative fan model[4, 5] and a UAS model experimentally validated at the conditions of a UAS ingestion[6-9]. Due to the complexity of a UAS ingestion, the computational studies are focused on damage to the fan stage and the likely energy imparted to the casing. These representative models enable computational studies to understand the sensitivity to parameters of the ingestion that lead to worse damage scenarios (i.e., more severe blade damage, increased energy imparted to the casing, etc.) These recently completed[4, 10, 11] and future computational studies can be used by the nascent UAS industry to inform their design practices as well as by engine manufacturers as a starting point to focus their analysis with their proprietary models.

The key research question to be addressed in this study is: What is the actual damage to a large, single-aisle commercial air transport aircraft engine (both the fan and downstream components) during a UAS ingestion during a takeoff flight scenario? It is important to note that this test will provide a single point of data. While this test will be informative, its overall scope will be limited because it can only capture the effects of an impact at one UAS relative translational speed, circumferential and radial location, orientation, and rotor speed for a single UAS type and single engine architecture. The key benefits of the engine test include: (i) the ability to validate the computational modeling approach developed in previous phases of the research, which can be used to analyze many ingestion scenarios and engine architectures; (ii) gaining insight into the damage to the components downstream of the fan stage; (iii) understanding the effect of the ingestion on engine performance to inform flight training; and (iv) evaluating possible UAS battery fire or explosions during the impact.

2. SCOPE

The research was conducted over four years and included a peer review at the beginning of the research and a review of the final report at the end of the research program. The research was broken into two main research tasks, each subdivided into several sub-tasks to answer the key research questions.

2.1 TASK A: LIVE ENGINE TEST PROGRAM MANAGEMENT (OSU)

The research effort, centered on conducting a UAS ingestion test into an operating engine, was carried out in close collaboration with the test partner (NAWC) and the Federal Aviation

Administration (FAA). The test partner, in consultation with the FAA and the Alliance for System Safety of UAS through Research Excellence (ASSURE) team, selected an operational engine for the test. This task was focused on the coordination efforts to keep the FAA informed and up to date on the research throughout the research program through Program Management Reviews, Technical Interchange Meetings, interim reports, e-mails, and telephone meetings as appropriate to ensure the research validation objectives were met.

Assumptions and Limitations - The research assumed the following operating limitations:

1. Outside of the work done by the research team, updates and details of the research progress were limited by what was shared by the test partner with the research team.
2. DJI Phantom 3 Standard was used for testing to capitalize on previously validated computational models.

2.2 TASK B: TESTING OVERSIGHT (OSU, NIAR)

The objective of this research task was to serve as oversight for the testing conducted by the test partner and provide an independent review and analysis of the data gathered by the test partner. Moreover, the appropriate messaging for the testing and how it relates to recently completed computational research[12] was also analyzed.

Research Questions

1. What data should be generated and recorded from this test?
2. Since only one experiment could be conducted, what was the best impact condition for the UAS ingestion into the engine (speed, location, orientation, etc.)?
3. How well does the experiment correlate with the recently completed computational engine ingestion work?

Assumptions and Limitations - The research assumed the following operating limitations:

1. The independent analysis and connection to ongoing computational research required accurate scans of the fan blades pre- and post-test by the test partner.
2. The computational modeling in this project matches the computational modeling approach in the recently completed computational engine ingestion research program. Namely, the nose cone and containment ring have reasonable geometries compatible with the high bypass ratio engine fan to mainly provide a visual reference and were modeled with elastic material properties with no failure.
3. Material models for all the fan blades are provided by the test partner or the closest pre-existing publicly available material models were used in alignment with the current modeling approach used in the recently completed computational engine ingestion research.
4. All the reduced and processed data obtained by the test partner, including high-speed and regular-speed videos, strains and loads on the casing, onboard engine performance data during the test, ambient conditions, pre- and post-test scans of fan blades and interior components of the engine, and onboard and non-contact measurement system data from systems run by the ASSURE team or the test partner would be shared for an independent analysis.

3. OVERVIEW OF RESEARCH

The research was carried out in close collaboration with the test partner and the FAA. The ASSURE team helped inform and review the test plan created by the test partner. The ASSURE team was provided with scans of portions of the fan stage used in the experiment by the test partner. An FE model was created using the closest pre-existing material models in alignment with the modeling approach of the recently completed computational engine ingestion research[12]. The reduced and processed data obtained by the test partner, including high-speed and regular-speed videos, onboard engine performance data during the test, ambient conditions, and onboard and non-contact measurement system data from systems run by the test partners vendors, were shared with the ASSURE team after the test. The ASSURE team ran computational simulations at the conditions of the test using LS-DYNA (a finite element analysis software that specializes in highly nonlinear transient dynamic analysis) following the best practices set forth by the LS-DYNA Aerospace Working Group[13] (AWG). This work provides an analysis of the fan impact to inform the overall computational modeling approach conducted in the recently completed computational engine ingestion research. As a separate effort, NIAR will provide a final test report focusing on the analysis of the test event.

3.1 TASK A

The objective of this research task was to provide program management for the live engine ingestion test. This program management kept the FAA leadership team informed of the research progress as it occurred and integrated feedback from the FAA and stakeholders as the research occurred.

A kick-off meeting was held to gather key stakeholders in the research project, including the research team, test partner, ASSURE leadership, FAA technical monitors, and other participating agencies, to review task requirements, proposed approaches, execution roles and responsibilities, and performance expectations. A research task plan was created to provide a detailed work plan and schedule that tracks project activities after the test partner contract was signed.

Technical interchange meetings were held monthly to review the research progress made by the test partner and ASSURE team and keep relevant stakeholders up-to-date with the research project. These monthly updates took place after the test partner contract was signed and the kick-off meeting was held. Presentation material from these technical interchange meetings was posted within seven days of the meeting. One-page research summaries and additional briefings were also provided to update the project's progress and current status throughout the project when requested by the FAA.

3.2 TASK B

The objective of this research task was to provide testing oversight and analysis for the live engine ingestion test and to correlate the results with the computational modeling approach developed in previous phases of the research.

The objective of overseeing and providing feedback to the test plan was to ensure a valuable data set was obtained from the test for answering current and future research questions related to UAS engine ingestions. This task included coordinating with the recently completed computational

research program and the FAA to provide the test partner with input on the test plan. This included the planned conditions for the test (i.e., operating conditions of the engine, launch speed, location, and orientation of UAS). In consultation with the FAA/ASSURE team, the test partner selected an operational engine for the test. The ASSURE research team analyzed the ingestion of the experimentally validated UAS model into the representative fan model developed in the computational research program at the take-off and cruise conditions. The relative damage for these two phases of flight, as well as other considerations such as the likelihood of each scenario and the additional challenges of how to conduct an emergency landing for each case, were considered, and the take-off phase of flight was recommended for the test conditions. Considerations of the impact of the UAS at the inner versus outer radius of the fan blades were also discussed and incorporated into the recommendation for the test case. The test plan also included planned measurement instrumentation and setup location. The FAA ultimately decided on the conditions of the test case. The instrumentation and data to be collected included: strain gauges on the fan delivering the data through a wireless telemetry system; digital image correlation on the fan casing to capture deformation due to primary or secondary impacts with the casing, and digital image correlation of the rotating fan blades; high speed and high definition cameras capturing all views (front, top, bottom, side, back, oblique) of the ingestion event; engine control and monitoring to capture data on display to the flight crew to inform flight training and monitor engine performance during the ingestion; scans of the blades pre- and post-test for use in the computational studies; and images or scans of the interior of the engine pre- and post-test for comparison and additional understanding of downstream damage resulting from ingestion. The test partner was responsible for the overall test plan and incorporating all the needed instrumentation.

The research team also completed an independent post-test analysis of the engine ingestion test for comparison with the computational modeling approach. The test partner conducted their own analysis of the engine ingestion and provided the reduced and processed measurement data from the experiment. This task was focused on conducting a computational simulation of the ingestion event for comparison purposes. The test partner provided OSU/NIAR with scans of fan blades before the ingestion event. Similar to the ingestion work in the recently completed computational research program, the ingestion analysis focused on the damage from the primary impact of the UAS with the fan to evaluate damage in the blades of the fan section. The damage from the computational simulation was compared to the experiment. Elastic material properties were used for the casing and nose cone to provide appropriate boundary conditions and to determine secondary impacts and loading patterns.

The test data was also used to validate the overall computational modeling approach and demonstrate the effectiveness of the representative fan assembly model for use in foreign object ingestion studies. In particular, a comparison of the computational simulation of the ingestion with the full-scale test was conducted. Differences in the response and damage are expected due to the prior use of the actual fan and the unknown proprietary materials processing in the construction of the actual fan. Additionally, the CFM56-7B fan UAS ingestion case and the representative fan from the computational research were also compared to give a better frame of reference for how the damage in the representative fan compares to an actual in-service engine.

4. ORGANIZATION OF THIS REPORT

The remainder of this report is organized as follows. Section 5 discusses the computational modeling approach. Section 6 highlights the experimental live ingestion test. Section 7 presents the validation of the modeling approach with the test data. Section 8 compares the representative fan assembly model with the CFM56-7B fan assembly model. Section 9 provides conclusions for the UAS engine ingestion modeling and experimental work.

All tests and research were conducted by the Task A43 team in accordance with Section 2 and Section 3 and were approved by the FAA. Reviews of data and analysis were conducted monthly at technical interchange meetings with the FAA. The final report was reviewed by the FAA and approved for release on September 9, 2025.

5. COMPUTATIONAL MODELING APPROACH

One of the key objectives of this research program is to validate the overall computational modeling approach used in the previous UAS ingestion research funded by the FAA[2, 12]. So, a very similar modeling approach was employed in this work. In particular, LS-DYNA was the computational software tool that was used with the modeling following the best practices of the AWG[13]. The following subsections review the UAS model used, the representative fan model developed in the previous research program[4, 5, 10-12], the new fan assembly model for the engine used in the experiment, and modeling details for the ingestion simulations.

5.1 UAS MODEL

The UAS model used in the simulations for this work was developed from the DJI Phantom 3. This UAS was released almost a decade ago, with newer UAS being released onto the market, such as the DJI Phantom 4, in the intervening years. The DJI Phantom 3 quadcopter model that was used in the ingestion simulations was developed by NIAR using a physics-based Building Block Approach that was initially developed in the A3 Airborne Collision Studies[14], and validated experimentally for a wide range of conditions. It was originally chosen to be studied when it was the most common UAS on the market. The choice of using this older model is based on three primary factors. First, a significant amount of resources were invested in creating and experimentally validating this UAS model for a variety of impact cases, including ingestion into an engine[6, 8, 9, 15], making it one of the most high-fidelity UAS models available for engine ingestion studies. Second, the key components of the UAS (i.e., the battery, camera, and motors) are very similar in newer models, and these key components are the ones that are found to impart the most damage on the fan during the ingestion[2, 3]. Finally, one of the overall goals of this research project is to validate the overall computational modeling approach of the engine ingestion research[2-4, 10-12], and the UAS model has been a key part of this work.

The DJI Phantom 3's mass is about 1.22 kg (2.7 lbs) with the physical quadcopter shown in Figure 1a, the Computer Aided Design (CAD) model in Figure 1b, and the key components in Figure 1c. The Lithium-Polymer battery (342 g), camera (51.9 g), and four electric motors (51.0 g each) were identified as key components of the UAS based on their harder composition and likelihood of imparting damage in a high-speed impact scenario. These key components are comprised of harder, denser materials when compared to the rest of the UAS, such as the polycarbonate body

from which the primary structure of the UAS is made. Additional details about the composition of the UAS and the development of the UAS model can be found in previously published works[6, 14].

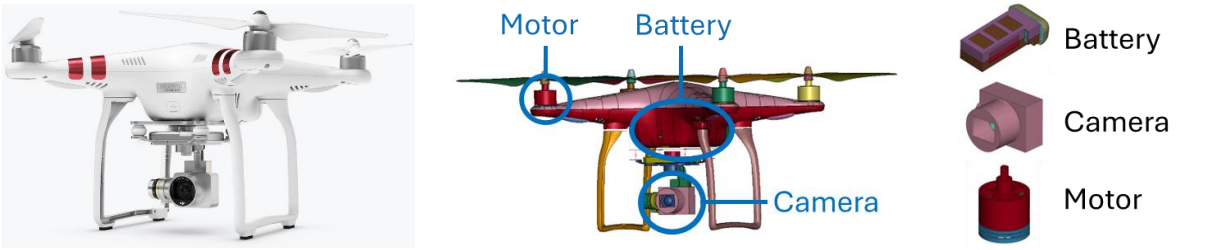

(a) Picture of UAS (b) CAD model of UAS (c) Key components

Figure 1. DJI Phantom 3 quadcopter.

5.2 REPRESENTATIVE FAN ASSEMBLY MODEL

There are a variety of fan designs that have been created for a number of engine architectures, and each engine's Original Equipment Manufacturer (OEM) tends to have its own preferences and designs. An open fan assembly model that is representative of key structural and vibratory features of fans commonly used in commercial transport was developed in the previous engine ingestion research[4, 12]. This work will compare the damage predicted by the representative fan assembly model with the fan assembly model developed to correspond to the assembly from the live ingestion test.

The representative fan was comprised of solid titanium blades with a 1.57 m (62 in) fan diameter. The fan geometry was created by scaling a smaller fan geometry up to the 1.57 m (62 in) fan diameter and removing proprietary features that were related to the aerodynamics and not the structural properties of the fan. Since building a truly representative containment ring and nose cone was not feasible due to the myriad of existing architectures, these models were included only to provide appropriate boundary conditions for the ingestion. The containment ring and nose cone models were designed with input from engine OEMs to have reasonable geometries for this representative fan. The containment ring was modeled with a linear elastic material with no failure defined to understand the expected loads it might encounter. The shaft was modeled as a rigid body.

A series of checks were done on the representative fan assembly model to ensure that it would meet the flightworthiness criteria. These tests included: (1) a pre-stress analysis to make sure that the fan could handle the maximum operating speed of the engine (5,175 Revolutions Per Minute - RPM) without any permanent deformation; (2) construction of the Campbell diagram for the fan blades to ensure there were no engine order one crossings over the operating speed range of the fan; and (3) large bird ingestion simulations to ensure that the damage to the fan was not excessive and consistent with prior bird ingestion experience.

The following subsections highlight some of the key features of the fan with the full description provided in the previous FAA report[4] and published papers[5, 10].

5.2.1 Fan Assembly Model Components and Geometry

The representative fan assembly model consists of the fan blade and disk assembly, nose cone, casing, and shaft, which can be seen in Figure 2.

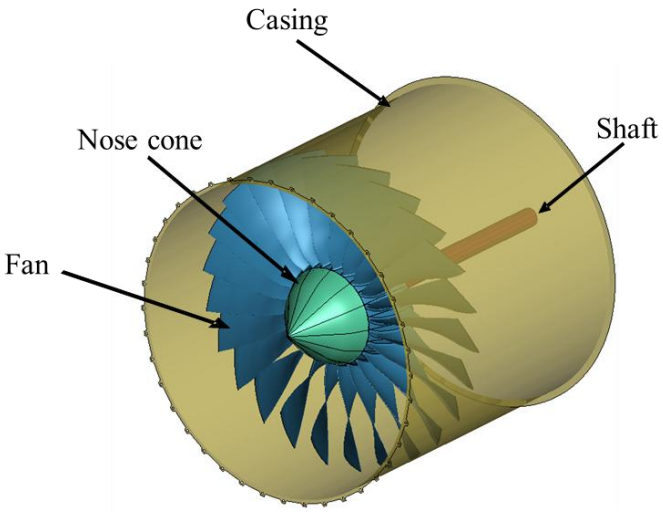

Figure 2. Components of the representative fan assembly model.

The casing used for the fan assembly model created in this project has a total length of 1.580 m (62.2 in) and an internal diameter of 1.586 m (62.44 in). A hot clearance (i.e., clearance when the fan is spinning at its nominal rotational speed) of 3.81 mm (0.15 in) is used between the airfoil and the internal diameter of the casing. The thickness of the casing at the inlet and outlet is 4.1 mm (0.16 in). In this model, the primary purpose of the casing is to provide an appropriate boundary condition for the fan to capture first-order effects of the UAS ingestion while also maximizing the parameter space for how the ingestions can occur (i.e., not having an inlet smaller than the fan diameter, which would restrict the UAS's entry into the engine).

The nose cone in the representative fan assembly model has a bi-conic like design and is modeled as aluminum. The overall thickness of the nose cone is 2.5 mm (0.1 in), and a clearance of 2.5 mm is maintained between the nose cone and the dovetail region. The nose cone is rigidly connected to the fan assembly through 24 bolt connections at the disk flange located on the front of the fan. The nose cone is only used as a boundary condition for the ingestion.

The low-pressure shaft connects the fan to the low-pressure turbine to form the low-pressure spool of the engine. The low-pressure turbine extracts energy from the flow to drive the fan through the low-pressure shaft. The CAD model for the shaft was based on drawings of the CFM56[16], a high bypass ratio turbofan. The shaft was modeled with steel, which is representative of the shaft material often used in turbofan engines. The cylindrical shaft had a total length of 0.915 m (36 in). The shaft has an internal diameter of 83.8 mm (3.3 in) and a thickness of 5 mm (0.2 in) for the majority of its length. There was a rapid expansion in diameter towards the forward face of the shaft, where it meets the disk.

The components of the fan blade and disk assembly include an airfoil, dovetail, retainer, retention ring, disk, and disk flange, which are all shown in Figure 3. In these types of fans, the airfoil and dovetail are a single unit, called a blade, that can be pulled out of their slot in the disk and replaced if damage or failure occurs (e.g., after a bird strike). There are a total of 24 blades in the representative fan model. Due to the nature of the disk flange, a two-blade model is needed to define a single cyclic sector model; therefore, there are 12 cyclic sectors that are repeated to form the 24-blade model.

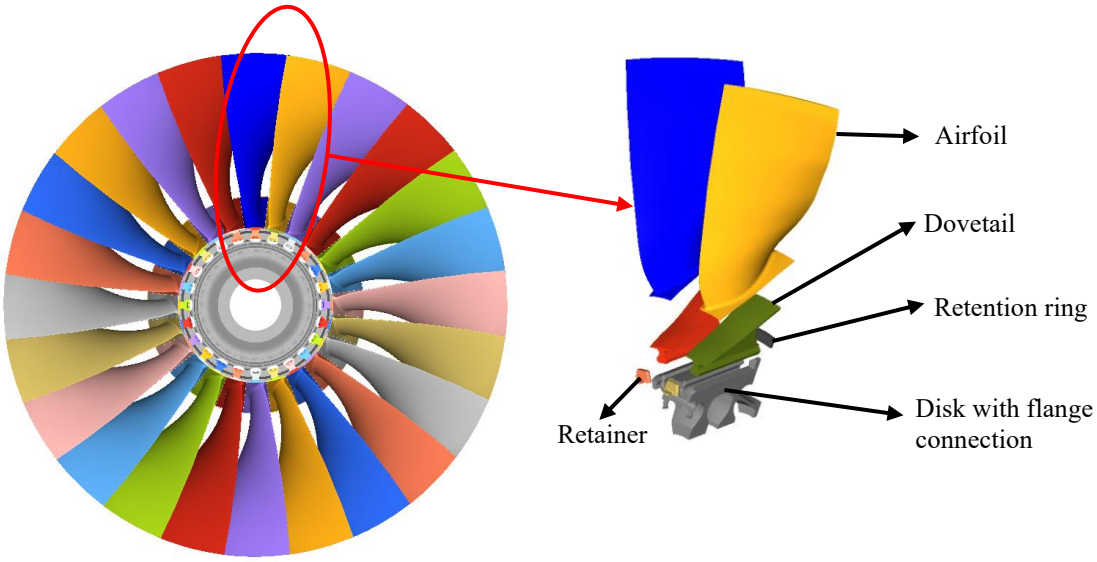

Figure 3. Components of the representative fan blade and disk assembly.

The airfoil retainer is used to secure the dovetail into the disk after it is installed. This retainer prevents the blade from moving forward in the axial direction. The retention ring, which is connected to the disk on the rear side of the fan, prevents the blades from sliding axially further than intended. The flange on the front of the disk provides a way to bolt the nose cone to the disk.

5.2.2 Fan Assembly Modeling Details

This section highlights some of the modeling details of the representative fan assembly model.

The disk, dovetail, airfoil, and retention ring are composed of a titanium alloy (Ti-6Al-4V) and were modeled using the *MAT_TABULATED_JOHNSON_COOK (*MAT_224) material model in LS-DYNA. The retainer is also composed of the same titanium alloy but was modeled as elastic using the *MAT_ELASTIC keyword. Material information for the Ti-6Al-4V alloy was obtained from a publicly available material model created in a previous FAA project[17, 18] and made available by the AWG [19, 20]. Images of the meshes of the fan blade and disk assembly components are shown in Figure 4.

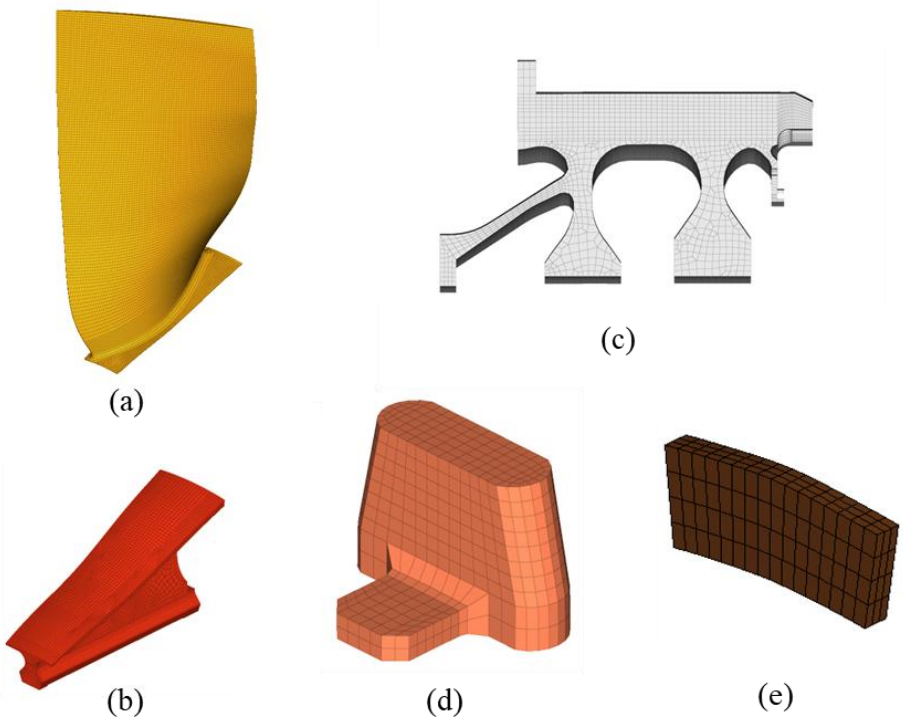

Figure 4. Mesh of fan blade and disk assembly components (a) airfoil, (b) platform and dovetail, (c) disk, (d) retainer, and (e) retention ring.

All components of the fan assembly were meshed using solid hexahedron elements and defined with a constant stress solid element (ELFORM=1) in their section cards. This under-integrated element formulation has the consequence of nonphysical, zero-energy modes of deformation called hourglass modes. Different algorithms in LS-DYNA can be invoked using the *HOURGLASS keyword to inhibit these hourglass modes. Each part with constant stress solid elements also had hourglass control defined with the type IHQ = 6 and the coefficient QM = 0.1. The contact card defined between the airfoil and the platform is *CONTACT_TIED_SURFACE_TO_SURFACE.

The casing was modeled with the Ti-6Al-4V alloy elastic material model using the *MAT_ELASTIC keyword, which had the exact same properties as the retainer. The casing was meshed with quadrilateral shell elements with a fully integrated shell element formulation (ELFORM=16). The bi-conic nose cone was composed of an aluminum 2024 alloy and was modeled as elastic using the *MAT_ELASTIC keyword. Material information for the aluminum 2024 alloy was obtained from prior FAA projects[21] with the material models being made available by AWG[22]. The nose cone was meshed using solid hexahedron elements, and the element formulation used was the constant stress solid element (ELFORM=1). The shaft was modeled as a rigid body using the *PART_INERTIA keyword with mass and inertia properties included. The shaft used the default Belytschko-Tsay shell element formulation (ELFORM=2). The keyword *MAT_RIGID was used to define the material for the shaft and the material properties were that of stainless steel[23]. The rotation of the shaft was prescribed using the

*BOUNDARY_PRESCRIBED_MOTION_RIGID keyword along with a vector in the direction of the rotational axis.

5.3 CFM56-7B FAN ASSEMBLY MODEL

The CFM56 engine is one of the most popular aircraft engines for commercial aviation use, with over 33,000 engines being sold and over 23,000 engines still in service in the 40+ years since its introduction to the market[24, 25]. This engine is primarily used to power single-aisle commercial aircraft such as the Airbus A320 family and the Boeing 737 family, and it has various versions, such as the CFM56-7B, which can be seen in Figure 5. The CFM56-7B variant has a 1.55 m (61 in.) fan diameter, and it is the exclusive engine used for Boeing's Next-Generation single-aisle airliner, with over 15,000 CFM56-7B engines being delivered and installed onto Boeing 737's around the world making it the most popular engine and aircraft combination in the world[16]. This made the CFM56-7B engine the ideal choice for an ingestion study due to the sheer number of engines currently in service, representing a large portion of the commercial aircraft engines in use today.

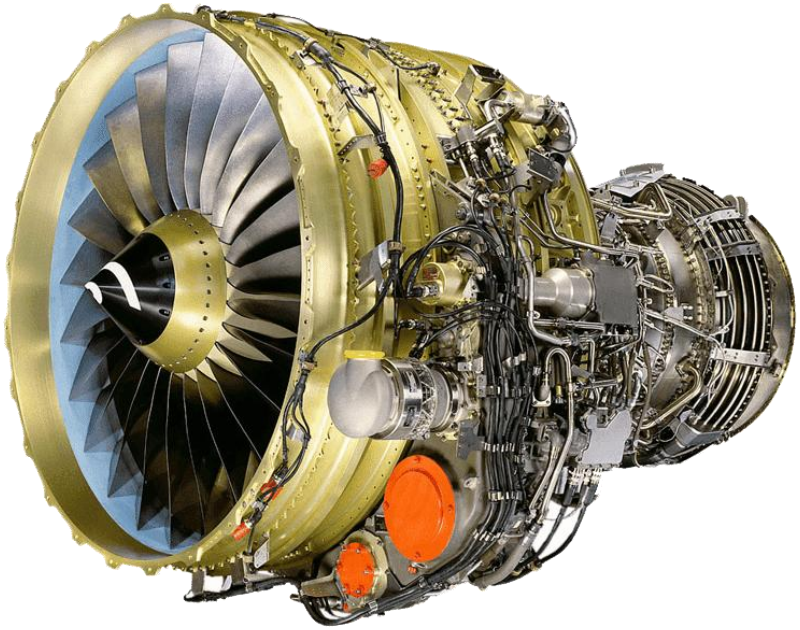

Figure 5. CFM56-7B engine[24].

The computational fan assembly model of the CFM56-7B was constructed to match the physical characteristics of the engine while following the AWG guidelines[13].

5.3.1 Sector-Level Model Development

To build the fan assembly model, NAWC took scans of the fan blades, nose cone, disk, platform, shims, and flange and shared them with OSU to be used to construct three-dimensional models of the fan assembly. NAWC also provided a description of how the parts were assembled to form the full fan assembly, but no detailed drawings or measurements were provided to show exactly how the parts were assembled.

The scans of the fan blade and nose cone were complete and did not require much additional postprocessing to obtain their CAD models. The CAD models were imported into HyperMesh to generate a mesh for these parts. Images of the scans and meshes of the blade and nose cone can be seen in Figure 6 and Figure 7, respectively.

(a) Fan blade scan (b) Fan blade mesh

Figure 6. Scan and mesh of CFM56-7B blade.

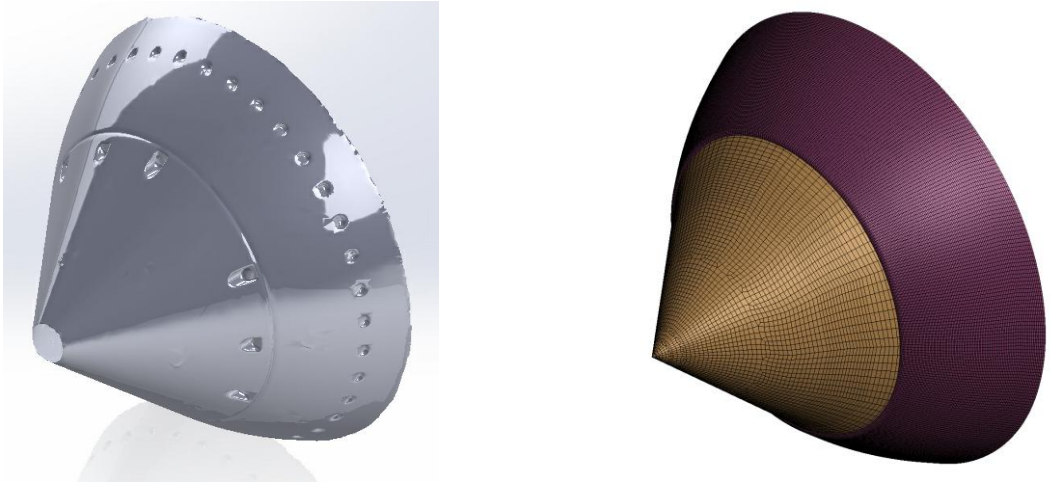

(a) Nose cone scan (b) Nose cone mesh

Figure 7. Scan and mesh of CFM56-7B nose cone.

The blades have three elements through the thickness, which matches the representative fan blade model. It is important to note that when meshing the fan blade part, several elements were of poor quality, such as having an aspect ratio greater than ten on the leading edge and the base of the fan blade mesh. Figure 8 shows the poor aspect ratio elements, and Table 1 summarizes the number of elements of poor quality in the fan blade. While these elements are of poor quality, they take up a small percentage of the total elements in the fan blades. Note that some nonrepresentative plastic

deformation can result in these poor-quality elements during a prestress analysis, which will be discussed in the next section.

(a) Fan blade side view (b) Elements with poor aspect ratio in the fan blade

Figure 8. Side view of the fan blade and poor aspect ratio elements.

Table 1. Element quality in fan blade.

Criteria	**Elements**
Total number of elements	62,244
Warpage	580 (1%) elements > 20° (Max = 84.6°)
Aspect ratio	1,072 (2%) elements > 10 (Max = 33.81)
Skew	300 elements > 60° (Max = 84.03°)
Jacobian	71 elements < 0.5 (Min = 0.34)

The scans of the other parts of the fan assembly provided by NAWC were all incomplete and needed significant processing to obtain a usable CAD model. The disk scan, in particular, was incomplete, and several approximations were required to construct a model. Figure 9 shows the process that was used to construct the CAD model of two sectors of the disk. First, the surfaces from the scan were cleaned up and stitched together in SolidWorks to get a complete surface that matched the surface of the disk scan. Next, to obtain a reasonable disk model with the incomplete information provided, the surface of the disk was combined with the disk model of the representative fan disk model. This was accomplished by creating a surface line approximation

from the disk scan to create the curved slot for the fan blade, then the rear side of the disk was merged with the representative fan disk model.

(a) Disk scan

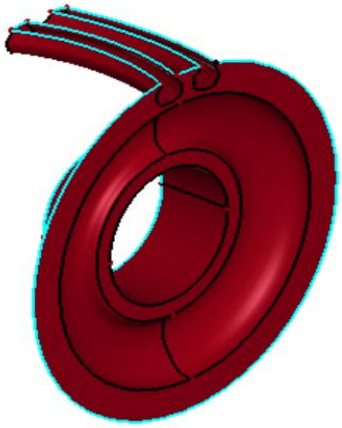

(b) Disk isolated and stitched surface

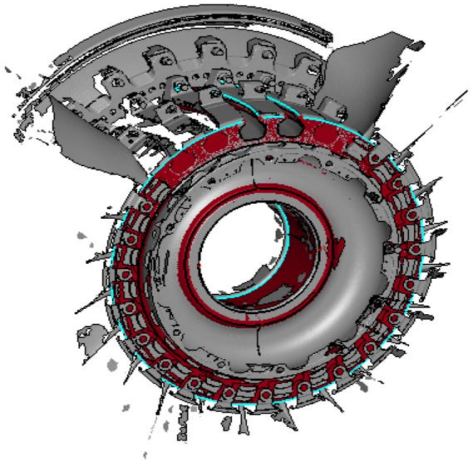

(c) Overlay of stitched surface on scan

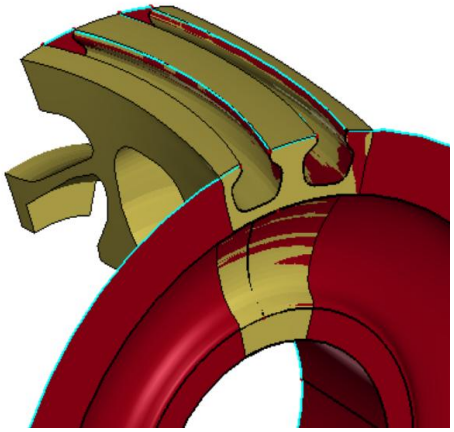

(d) Disk merged with representative fan disk design

Figure 9. Process for creating disk model.

The platform part also required significant post-processing to develop a usable CAD model. Figure 10 shows the process of creating the platform used in the fan assembly model. First, the surfaces had to be stitched together, and then the components had to be merged. Unfortunately, due to the incomplete scan and the required approximations in stitching together surfaces and combining parts, the inaccuracies of the platform model led to interference with the shim and fan blade when trying to assemble the fan assembly. Therefore, it was decided to simplify the platform part to retain just the upper surface of the platform. This simplification of the platform does not appreciably affect the overall fan model since the platforms are used for boundary conditions rather than the main focus of the impact in the simulation, such as the fan blades and disk.

(a) Platform scan

(b) Platform stitched surface

(c) Platform stitched part and scan overlay

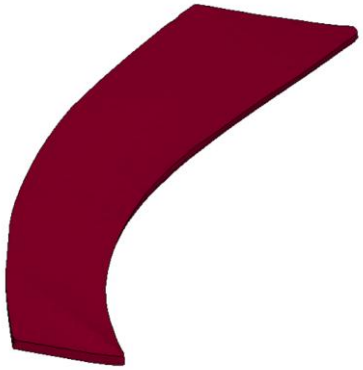

(d) Platform part simplified

Figure 10. Process for creating platform component.

The scan of the shim component also needed to be stitched together to create the CAD model. The scan, stitched together CAD model, and overlay are shown in Figure 11. The shim component also had to be modified by reducing the height of the shim by 6 mm so that the fan blade would fit in the slot.

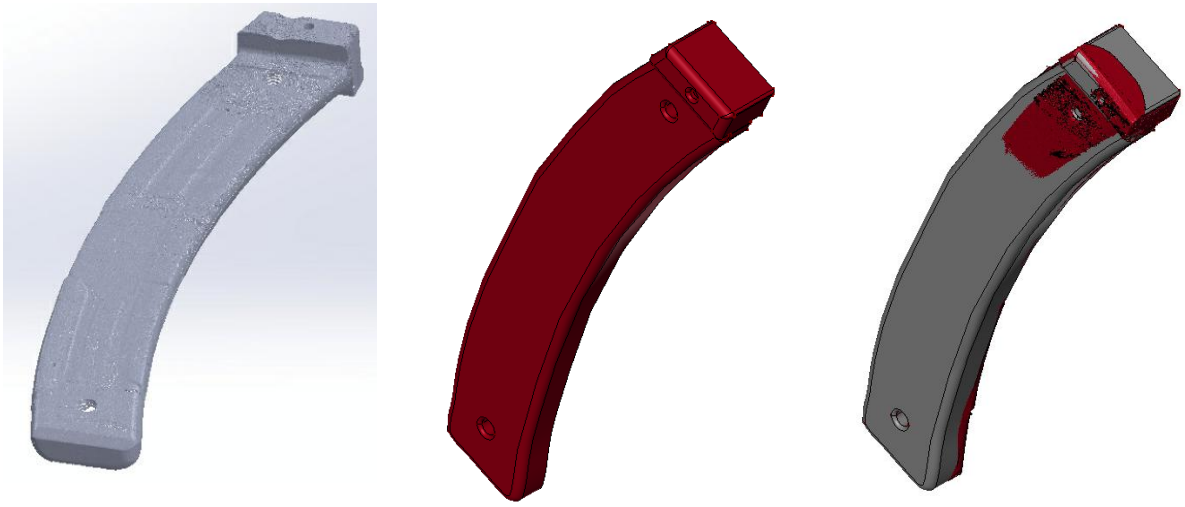

(a) Shim scan (b) Shim stitched surface (c) Overlay of stitched shim on scan

Figure 11. Scanned, stitched, and overlay of the shim component.

The scan of the retaining flange component also needed to be stitched together to create the CAD model. The scan, stitched together CAD model, and overlay are shown in Figure 12. Note that there are 12 bolt holes in the retaining flange and 24 blades in the fan, which means that the overall fan can be broken down into 12 identical sectors with two blades per sector (this is the same as the representative fan assembly model).

(a) Retaining flange scan (b) Retaining flange stitched surface (c) Overlay of stitched retaining flange on scan

Figure 12. Scanned, stitched, and overlay of the retaining flange component.

The scan of the retaining ring component also needed to be stitched together to create the CAD model. The scan, stitched together CAD model, and overlay are shown in Figure 13. Note that this retaining ring was eventually removed from the computational model to simplify the model.

(a) Retaining ring scan (b) Retaining ring stitched surface (c) Overlay of stitched retaining ring on scan

Figure 13. Scanned, stitched, and overlay of the retaining ring component.

A plate part was also added to the computational model, which was used to aid in the instrumentation of the strain gauges for the experiment. The plate was developed by Integrated Test & Measurement (ITM), and the drawings and models were provided to OSU from NAWC and can be seen in Figure 14.

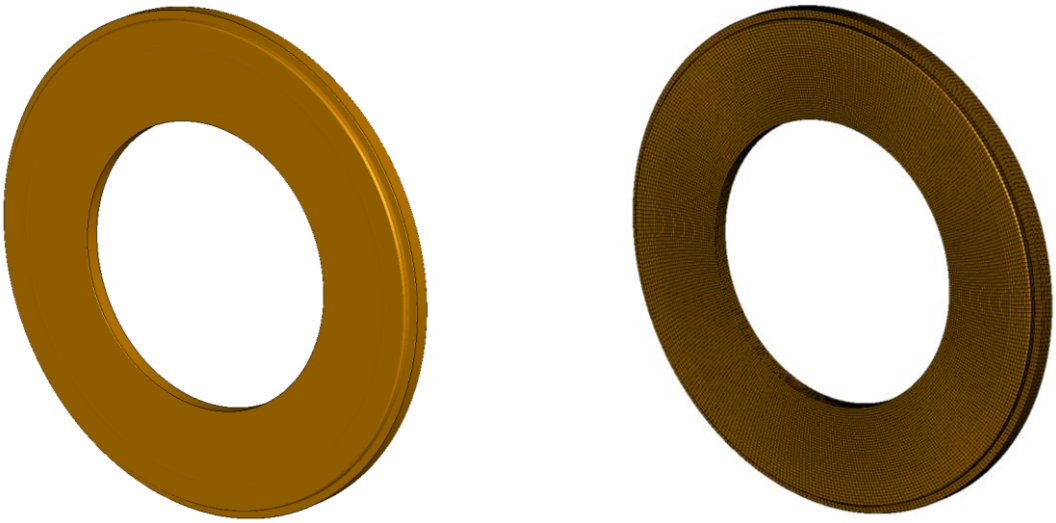

(a) Plate model (b) Plate mesh

Figure 14. Model and mesh of plate.

The material model chosen for the fan blades, disk, shim, flange, and platforms is an experimentally and computationally validated titanium alloy Ti-6Al-4V that was previously developed through a collaborative effort between George Mason University, OSU, the National Aeronautics and Space Administration, and the FAA[17]. Several tests, such as tension, compression, impact, shear, and biaxial stress state data, were collected, as well as temperature and strain rate effects, to create a Johnson-Cook material model for LS-DYNA using *MAT_224. This material model was made available through the AWG[22] and has also been used in previous UAS ingestion

research[2-4, 8-11]. However, it is important to note that while the CFM56-7B fan blade is made of a titanium alloy, the specific processing procedure and the corresponding material properties are not publicly available since this is proprietary information. The AWG titanium alloy material model is used because it is the closest available high-fidelity material model that is publicly available and also makes it consistent with the prior engine ingestion research. Linear elastic model *MAT_001 of aluminum, steel, and titanium were used for the nose cone, plate, and casing parts, respectively, since these parts were used for boundary conditions, and damage in these parts was not investigated. The lower fidelity material model for these parts greatly lowers the computational demand during the computationally intensive simulations. This was again consistent with the prior engine ingestion research where parts that were used for the boundary conditions were typically modeled as elastic or elastic-plastic materials with failure turned off to lower the computational demands of the simulations.

Underintegrated hexahedral elements were chosen for this study for modeling the fan assembly components due to having more accurate results than shell elements while being more computationally efficient and stable when compared to fully integrated hexahedral elements for crash front simulations. Underintegrated hexahedral elements were also used in the representative fan assembly model, used in the previous engine ingestion research.

The meshed parts were combined to create a two-blade (single sector) model of the fan assembly. The single-sector model and an exploded view of this model are shown in Figure 15. Using a smaller portion of the full fan assembly model reduces the computational demand by taking advantage of the rotational symmetry of the full fan assembly system by using cyclic boundary conditions for some preliminary analysis. A pre-stress analysis was conducted using the single-sector model to determine the initial displacements and stresses in the elements of the fan model from the rotation before the actual ingestion simulations. A two-step, first implicit then explicit prestress method, was chosen for this study as recommended by the AWG modeling guidelines[13] and is discussed in the next section. The number of elements and nodes for each component of the sector model is given in Table 2.

Table 2. Number of elements and nodes in single sector components.

Component	Number of Nodes	Number of Elements
Nose cone	18,444	13,148
Plate	10,695	8,670
Flange	5,512	3,513
Disk	31,092	24,453
Blade	84,099	62,244
Shim	5,114	2,439
Platform	7,448	5,253

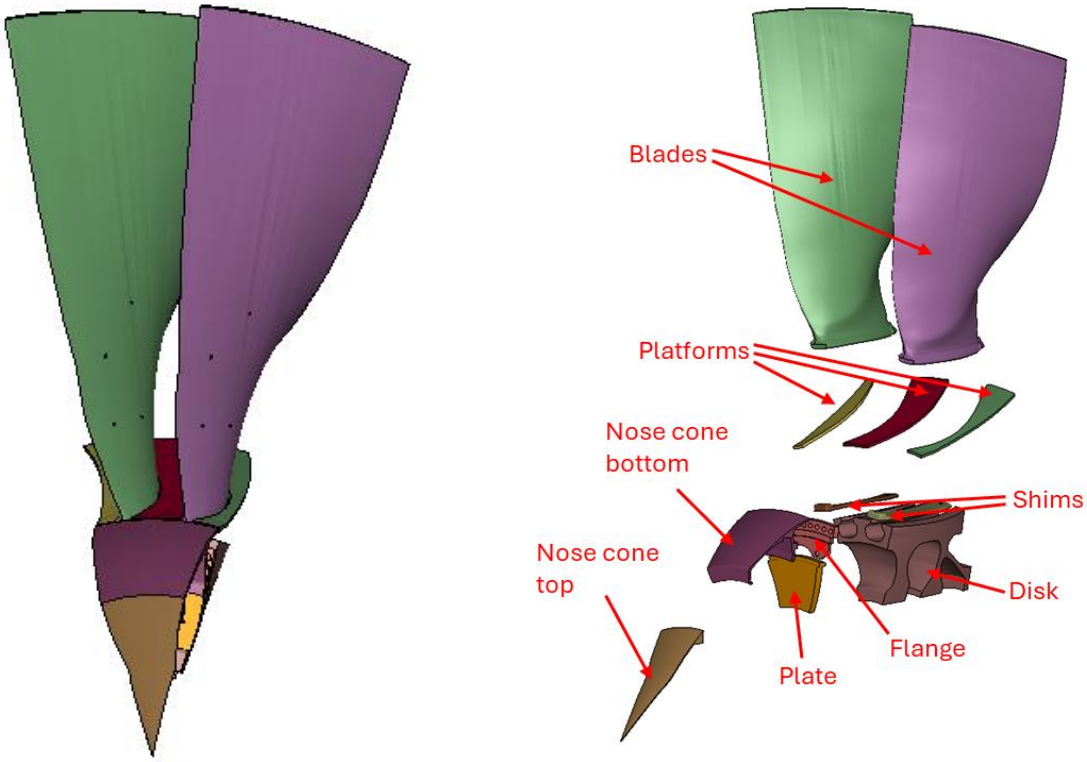

(a) Single sector model (b) Exploded view of single sector model

Figure 15. Single sector fan model with exploded view.

5.3.2 Prestress Analysis

A prestress analysis needed to be conducted on the fan model to obtain the positions of the nodes and stresses in the elements of the fan due to their rotation. A two-step, first implicit then explicit analysis, was used in the same way as done for the representative fan assembly model.

To apply the prestress on the sector model, a centrifugal force is applied in an implicit step. This simulates the blade rotating up to a specified angular velocity by applying a force onto the parts by calculating the centrifugal force (see Equation (1)) it would be experiencing at a specified angular velocity.

$$F = mr\omega^2 \tag{1}$$

In the implicit model, the mass (m), angular velocity (ω), and radial distance from the axis of rotation to the body's center of gravity (r) are given, and the centrifugal force (F) is calculated and then applied to the parts. Using *DEFINE_CURVE in LS-DYNA, a load curve for ω that gradually ramps up to the desired constant angular velocity can be used to apply the prestress onto the fan model, as seen in Figure 16.

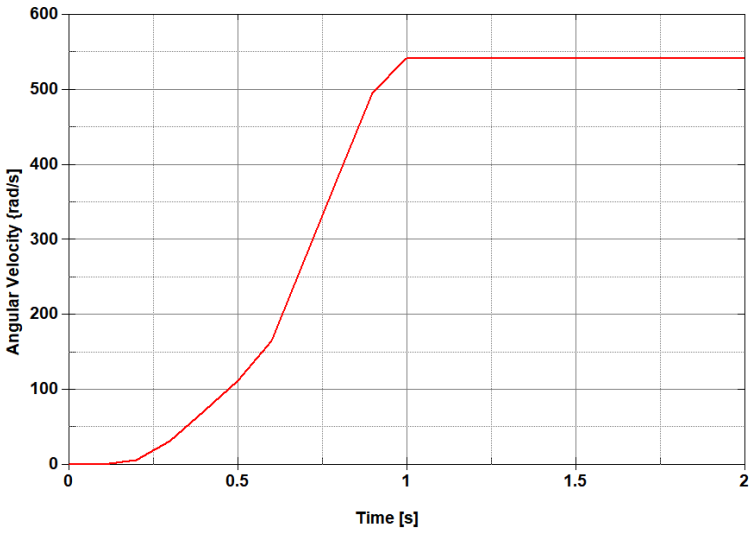

Figure 16. Load curve for ω.

Symmetric contacts were defined between the blade, shim, disk, nose cone, and platform parts of the model using *CONTACT_AUTOMATIC_SURFACE_TO_SURFACE. This uses the penalty contact method with symmetric contacts defined by the AUTOMATIC contact type, with the user defining the contact surfaces between the master and slave surfaces. Additional contacts using *CONTACT_AUTOMATIC_NODES_TO_SURFACE were added for the disk to shim contacts. The AUTOMATIC type contact was chosen as it is recommended in crashfront simulations as the orientation of parts can change, and large deformations cannot always be anticipated. Nonsymmetric contacts were then defined for the nose cone, plate, flange, and shim parts using *CONTACT_TIED_SURFACE_TO_SURFACE, which uses the constraint contact method with nonsymmetric contacts. Boundary conditions were defined to constrain the model and take advantage of the rotational symmetry in the model using *BOUNDARY_SPC_NODE, *BOUNDARY_SPC_SET, and *BOUNDARY_CYCLIC. The von Mises stress contour plot of the sector model after the implicit prestress step can be seen in Figure 17.

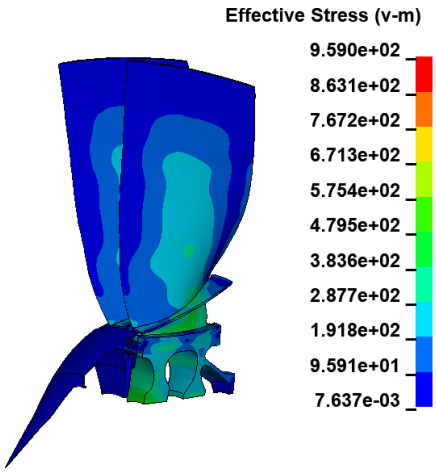

Figure 17. Sector implicit fan model von Mises stress contour plot.

Once the implicit simulation was complete, a dynain file was created, which contains the nodal deformation as well as the final stress and strain acting on the implicit model in the cards *INITIAL_STRAIN_SOLID and *INITIAL_STRESS_SOLID. This file can be used to create an explicit model by using the same contacts as the implicit model, but different boundary conditions are used. *BOUNDARY_PRESCRIBED_MOTION_SET is defined to apply a constant angular velocity on the parts that had the cyclic boundary condition applied to it. An additional boundary condition is also applied here, driving the root of the disk at a constant angular velocity while fixing any radial motion. *BOUNDARY_SPC_SET is defined to prevent translational movement in the disk and blades in any direction, allowing rotation only on one axis. *INITIAL_VELOCITY_GENERATION is also applied to the model to give an initial velocity instead of having an initial velocity of zero that immediately jumps up to the defined constant angular velocity.

The explicit model was then rotated for two full revolutions, and the forces in the disk and forces and stresses in the fan blades were monitored to ensure there were no large oscillations in the total force. In the explicit model, oscillations were seen during the first two rotations, so to dampen the total forces seen in the root of the disk, it was rotated for four revolutions with the force in the root of the disk shown in Figure 18.

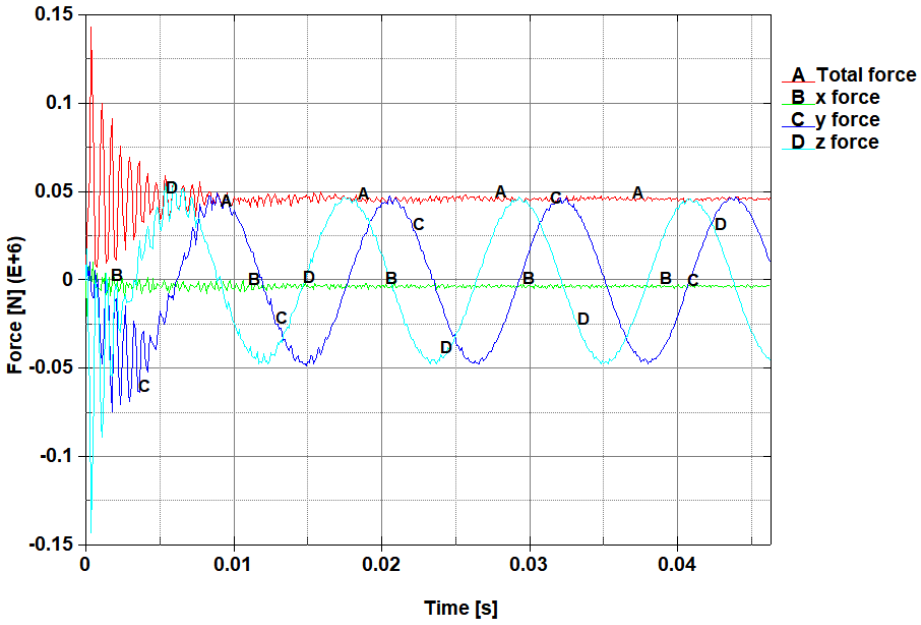

Figure 18. Forces at the root of the disk for four full explicit revolutions.

The von Mises stress was also checked to ensure that the explicit model did not reach material failure from the rotation. The stress contours at the end of the four revolutions are given in Figure 19. The maximum von Mises stress at the end of the four revolutions is 984 MPa, which is lower than the 1150 MPa yield strength used in the titanium alloy Ti-6Al-4V material model used for the fan.

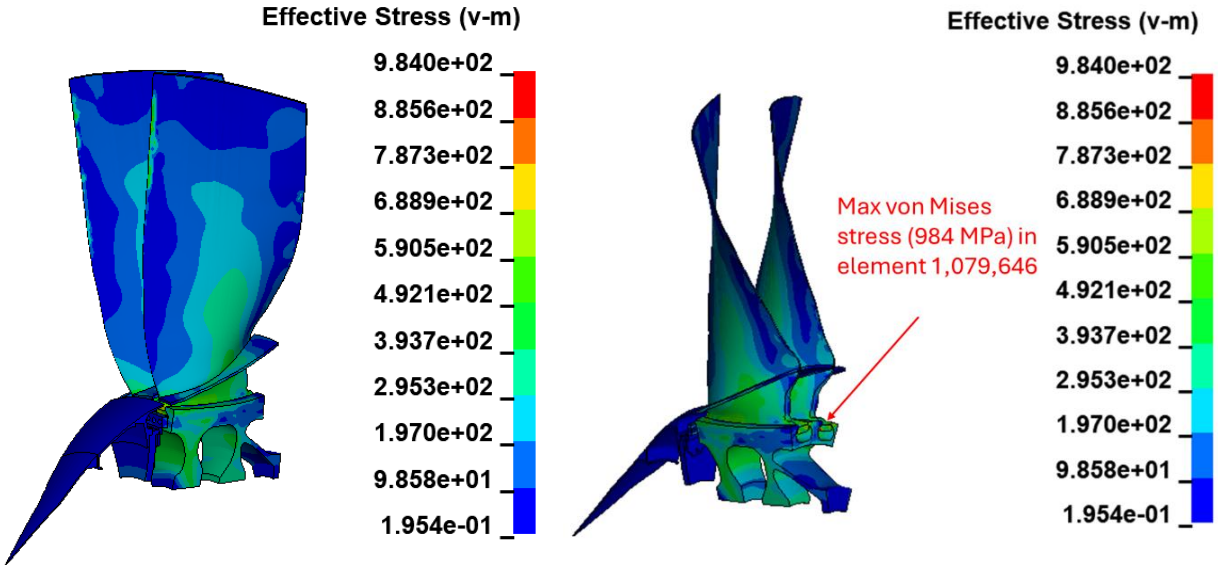

Figure 19. Explicit pre-stress von Mises stress contour plot.

However, when looking at the von Mises stress during the four revolutions, a few elements in the model passed the yield stress in the initial stages of the explicit model rotation when the large oscillations of force were seen in the root of the disk. Due to this, some portions of the model experienced plastic deformation, such as the disk and leading edge of the fan blades. Note that these elements generally correspond to the ones that did not meet the AWG guidelines and are highlighted in Figure 8. Figure 20a shows a graph of two elements in the disk part, with one element remaining in the elastic region and experiencing no plastic strain, while the other element was plastically deformed during the initial transient motion. This result can be attributed to the poor mesh quality of a few of the elements noted in Figure 8 and other approximations made in the fan blade model development from the resolution of the scans, incompleteness of the scans, and modifications to the models to remove interferences in components. However, this should not affect the main results from the simulation since the forces settle back down to a level below the material model yield strength and the main focus of this study is looking at the fan blade damage sustained during a UAS ingestion into a commercial aircraft engine. Note that this will result in some fictitious damage to the leading edge of all the blades in the ingestion simulations, but this damage is small compared to the overall damage from the ingestion. Further information on this process of applying a prestress onto a sector-level model can be found in the AWG modeling guidelines[13].

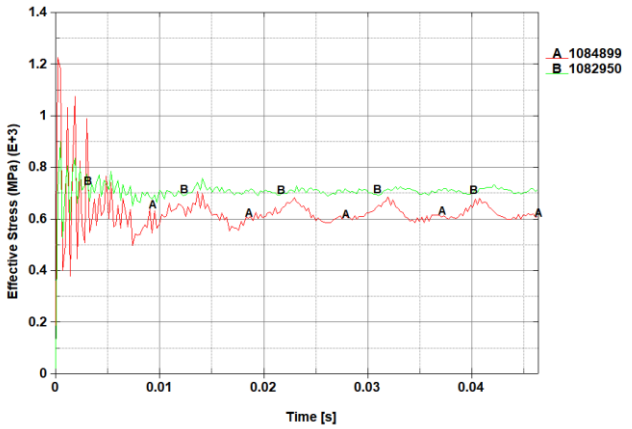

(a) Effective Stress in the elastic and plastically deformed elements of the disk during explicit simulation

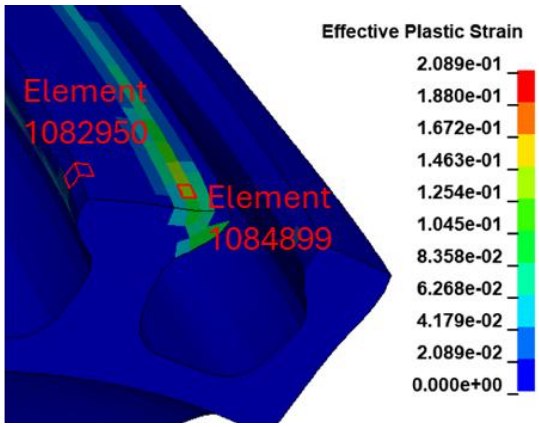

(b) Element identification

Figure 20. Effective Stress in the elastic and plastically deformed elements during explicit prestress simulation.

5.3.3 Full Fan Assembly Model

The full fan assembly model has 12 sectors and 24 blades, meaning that the single sector model needs to be rotated 12 times in 30° increments to complete the full fan assembly model. When doing this, care needed to be taken to renumber the nodes, elements, parts, contacts, boundary conditions, and sets so they have unique identification numbers, as well as renaming the contacts, boundary conditions, and sets so they have unique titles and correctly reference the parts they are referring to. Once this is complete, the parts can then be combined to make the full fan assembly model. Duplicate nodes in the flange, plate, nose cone, and disk can be merged at this point to form one full part for the plate, disk, and nose cone, while 24 separate parts for the platforms were created. The full fan assembly model can be seen in Figure 21.

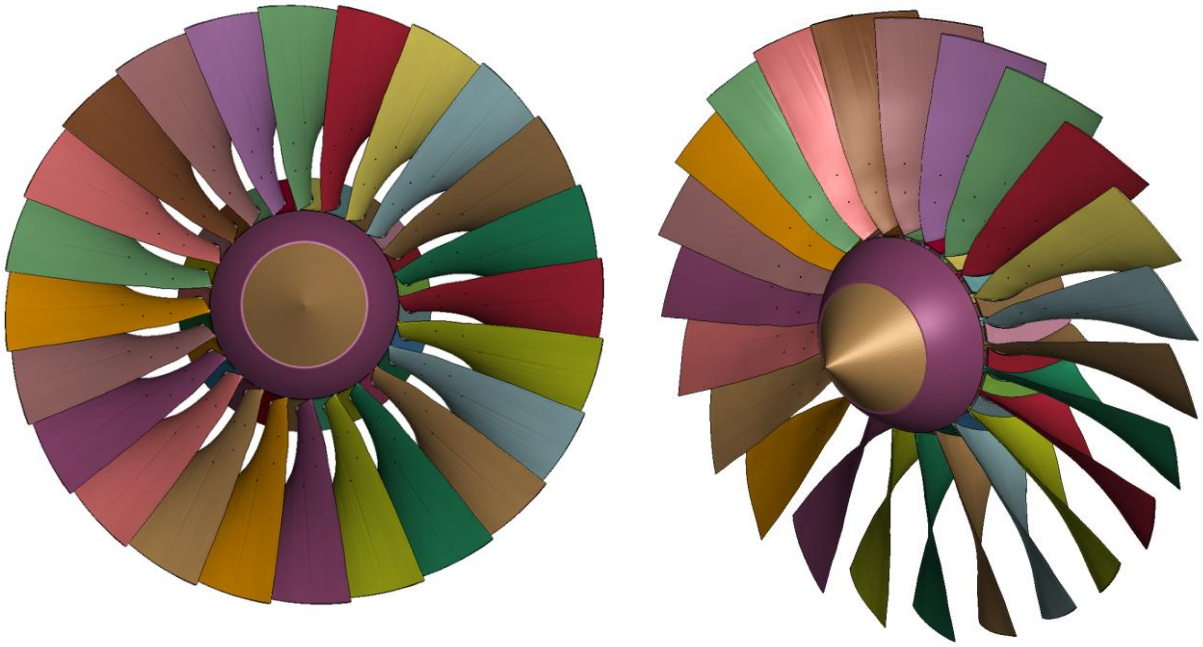

(a) Front view (b) Isometric view

Figure 21. Fan assembly model of the CFM56-7B engine.

Additional contacts need to be defined for the fan assembly model to behave correctly for UAS ingestion simulations. *CONTACT_ERODING_SINGLE_SURFACE is used for blade self-contact. Single-surface contacts behave similarly to surface-to-surface contacts, meaning they use the penalty-based contact method, but only a slave surface is defined. This single surface will then check for contact between all parts listed on the slave part list, including self-contact. The ERODING type contact was chosen as eroding contacts can automatically update the contact surface when elements are deleted. So, in a crashfront simulation where material failure is expected, which can be represented in FE analysis through element deletion, the ERODING type contact can automatically update the contact surfaces if an element from the user-defined contact surface is deleted due to material failure. *CONTACT_ERODING_SURFACE_TO_SURFACE is used for both UAS and fan assembly contact as well as fan blades and casing contact, while *CONTACT_AUTOMATIC_NODES_TO_SURFACE was added for UAS and casing contact. Additionally, the *INITIAL_VELOCITY_GENERATION card was used on the fan assembly model to give it an initial angular velocity equal to the angular velocity that was defined during the prestress step instead of jumping from a value of 0 to the desired angular velocity. This card was also used to apply the correct initial translational velocity to the UAS.

A generic casing was added to the fan assembly model to provide boundary conditions for the blade tips and the UAS parts during the ingestion. A scan of the interior of the casing was done after the ingestion test, which is shown in Figure 22a. The hole in the casing was caused by damage to the interior of the casing during the experiment. The same process that was used to develop the other fan blade assembly parts was applied to the casing to stitch the surface together. The scan given to OSU only included up to the fan region, so it was extended in the axial direction to represent the actual casing size better, as can be seen in Figure 22b.

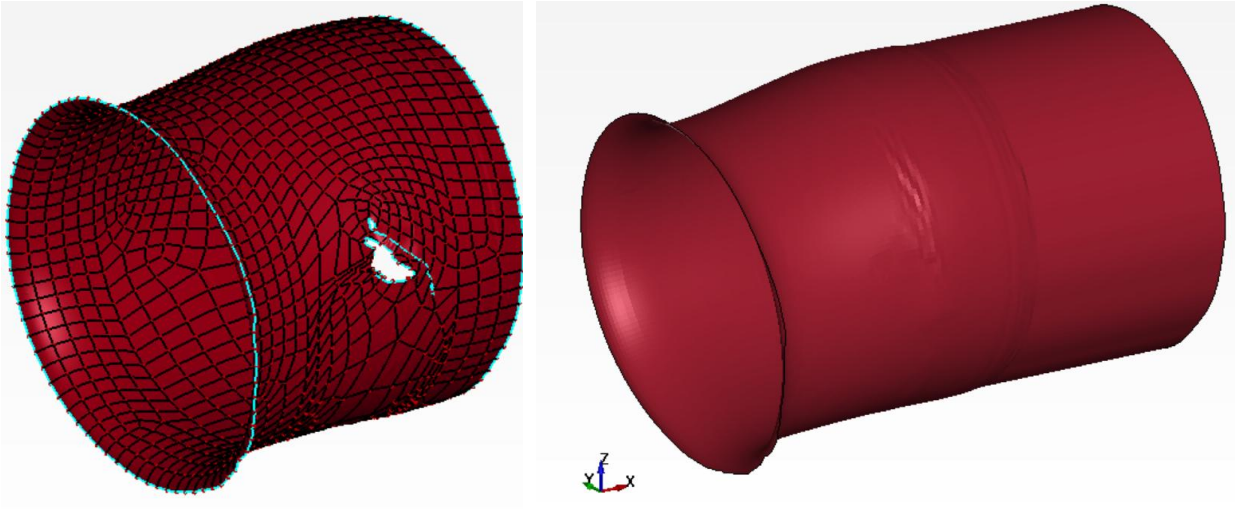

(a) Casing scan after ingestion test

(b) Casing model stitched and extended in axial direction

Figure 22. Casing model.

Shell elements were selected to be used for the casing component since only the energy absorbed by the casing was extracted from the simulation. The stress and damage to the casing are not the primary focus of this study, which is also why a linear elastic titanium material model was chosen for the casing part to reduce the computational time of the simulation. This matches the modeling approach of the previous engine ingestion research.

6. LIVE INGESTION EXPERIMENT

The live engine ingestion test was conducted at the NAWC China Lake facility in California. The team at the NAWC was responsible for all aspects of defining and conducting the test in agreement with the FAA. The ASSURE team was responsible for reviewing test plans and providing input on test conditions and instrumentation to try and obtain a useful set of data for computational validation of the engine ingestion modeling approach and additional data for future studies. This section highlights the test conditions, test facility, and instrumentation used in the test, particularly where ASSURE had input.

The engine chosen for the test was a CFM56-7B. It was chosen since it is one of the most common ones used today for commercial transport. Although the engine used was no longer in service, it was certified to be flightworthy and was deemed representative of engines currently in operation. An image of the used engine is given in Figure 23. The UAS chosen for the test is the DJI Phantom 3 standard. This UAS was chosen so that the computational modeling approach could be validated by the test since there has been a significant investment in creating this high-fidelity quadcopter model that has been validated for engine ingestion conditions.

Figure 23. CFM56-7B engine used for ingestion test.

6.1 TEST CONDITIONS

The conditions of the ingestion were chosen to obtain one of the more severe ingestion events. The prior engine ingestion research showed that the flight conditions for the worst-case damage were during takeoff conditions (which has the highest fan rotational speeds)[4]. Also, the impact location that does the most damage to the fan is near the outer radial span of the engine. While the UAS impact orientation can make a difference in the level of damage, it is a secondary factor, and the orientation that was easiest to launch while keeping the UAS intact was chosen. It should be noted that impacting the fan at the outer radius lowers the probability of core ingestion of UAS parts and, therefore, decreases the expected damage to downstream components in the engine for this test condition. The OSU team also did a number of simulations with the representative fan assembly model to ensure that changing the angle of the impact of the UAS would result in similar levels of damage to settle on the final planned test setup.

The fan rotational speed for takeoff conditions for the CFM56-7B engine is 5,175 RPM, which was chosen for the test conditions. The relative translational speed of the UAS to be launched into the engine was 92.6 m/s (180 knots). This corresponds to the sum of the maximum takeoff speed for the CFM56-7B and the maximum speed of UAS of similar size as the DJI Phantom 3. The UAS would impact 22.75 inches vertically above the nose cone, which is around 75% of the radial span of the fan blades. The orientation would be -12.8° pitch due to the angle of the gas gun and engine on the test stand, as seen in Figure 24. The CFM56-7B engine was mounted on a test stand with the nose cone tip 3.75 m (147.5 in.) above the test pad and the fan disk oriented 3.7° to the horizon, as seen in Figure 24.

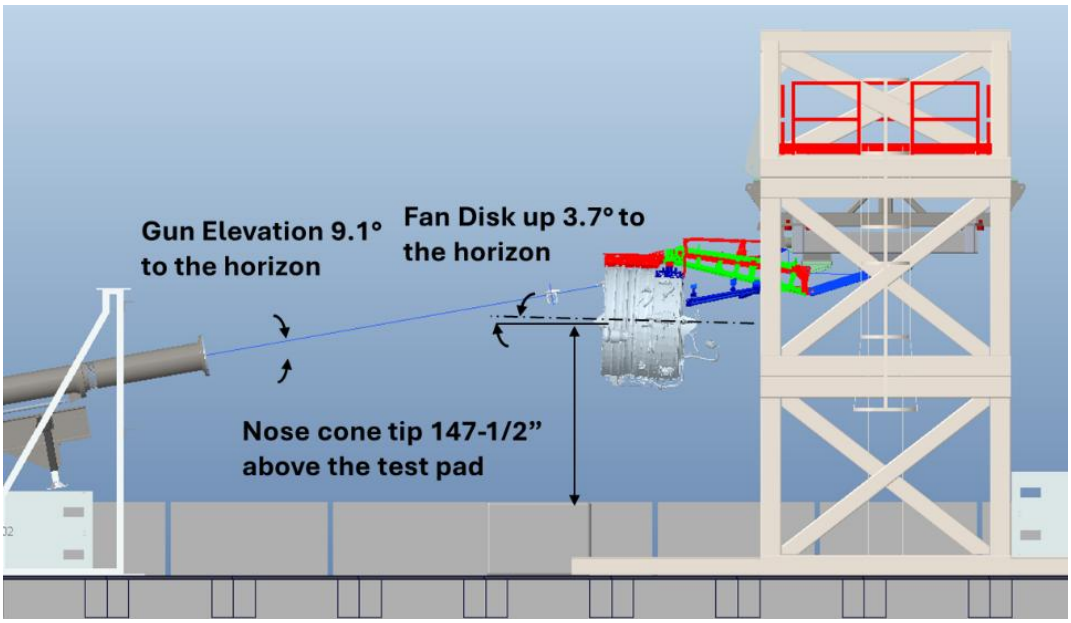

Figure 24. Planned test setup.

The UAS test item was a DJI Phantom 3 Standard version, which consists of an airframe body with four arms and rotors. The rigid plastic body houses the electronics, battery, and rotor motors. Suspended below the center of the airframe is a gimbal-mounted camera. The UAS weight (battery and propellers included) is 1.216 kg (2.68 pounds). The overall dimensions without the blades are 381 x 356 x 210 mm. The battery is a 4480mAh, 15.2V Lithium Polymer. The blades are made of light, thin plastic with little contribution to the event, so they were removed to facilitate better holding and launching of the UAS. The soft gimbal mount was stiffened with adhesive to help with a stable launch and flight. A DIC speckle pattern was painted onto the UAS, which will be discussed in the next section.

The test matrix given in Table 3 contains the test parameters for the test event. Test conditions during the execution of the event will be discussed in the following sections.

Table 3. Test impact conditions.

Test Event	Engine Speed (RPM)	Fan Speed (RPM)	UAS velocity (m/s)	Elevation	Aim Point	Target Distance (m)
1	14,460	5,175	92.6 (180 kts)	9.1°	75% Radius	6.1

6.2 TEST FACILITY

The test was conducted at the NAWC China Lake facility in California. The CFM56-7B engine pylon was mounted to a test frame, as shown in Figure 25. The test frame needed to be robust enough to withstand the thrust loads of the engine and the transient disturbances due to the UAS ingestion impact without sustaining any plastic/permanent deformation at the engine connection points while also limiting elastic deformation. The bridge mount was proposed by NAWC, as

shown in Figure 25. This mount would also allow the engine to roll as it would on the actual aircraft wing to aid the pylon connection. The test stand would hold the engine about 3.7 m (12 ft) in the air over the test pad and is able to react to 222,411 N (50,000 lbs) of thrust.

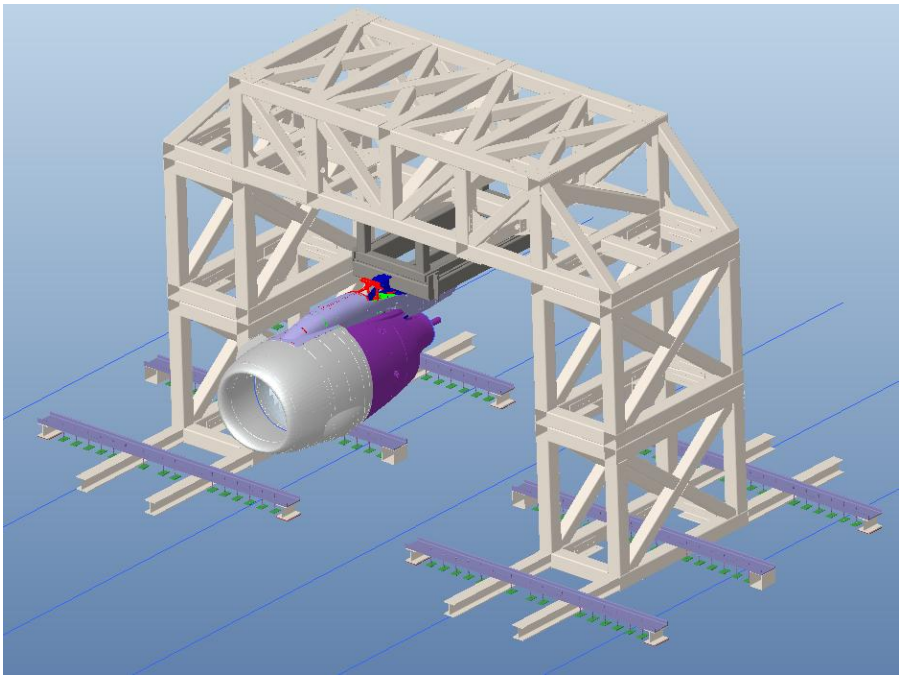

Figure 25. Schematic of CFM56-7B engine mounted to test frame.

A sabot was designed to support the UAS as it was accelerated to its desired velocity. The sabot was made using an aluminum inner shell with a foam support placed inside to support the UAS. The sabot had a mass of 3.69 kg (8.14 lbs) and can be seen in Figure 26.

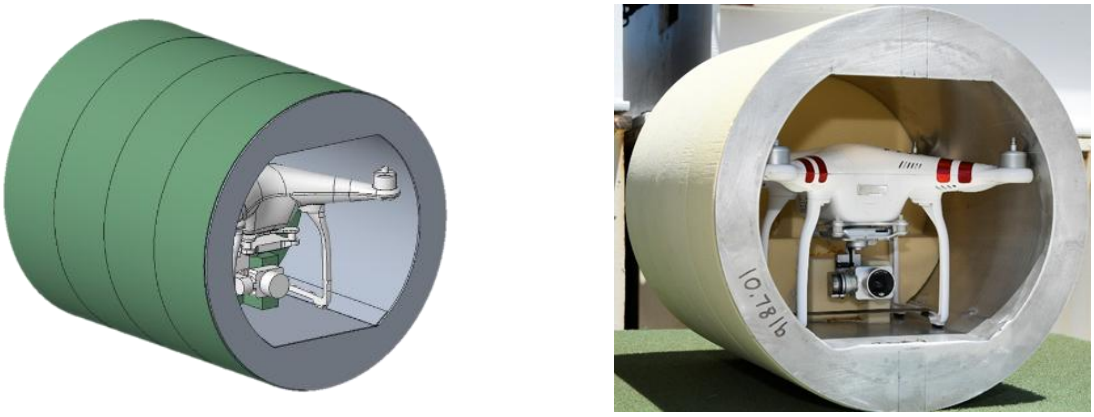

(a) Sabot model (b) Actual sabot

Figure 26. Sabot used to support UAS in launch gun.

In the gas gun barrel, attenuation segments were added in the interior to stop and prevent the sabot from being projected outside the barrel along with the UAS.

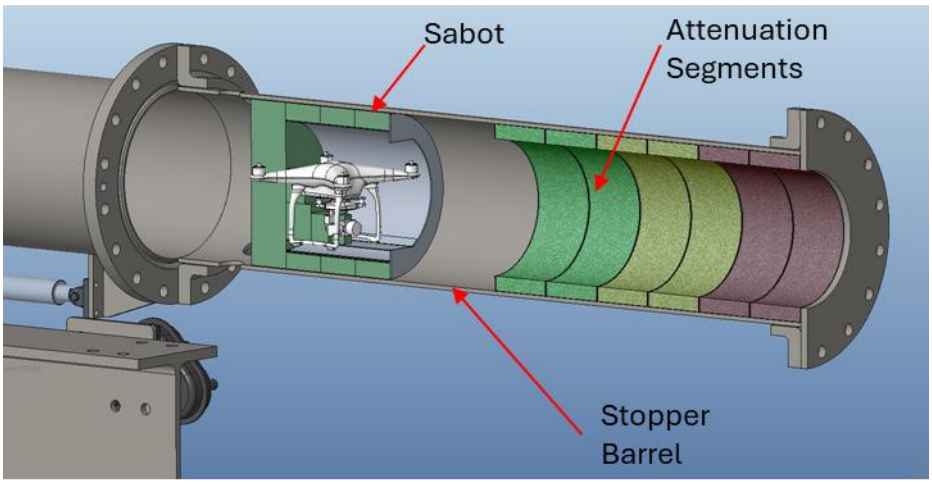

Figure 27. CAD model of sabot stopper design.

The overall setup of the launcher and engine mounted on the test stand can be seen in Figure 28.

Figure 28. Image of the test setup with launcher and engine mounted on the test stand.

6.3 INSTRUMENTATION

The purpose of the instrumentation for the testing was to thoroughly document the live ingestion test and provide a source of data for validating the computational modeling approach as well as for future studies (i.e., flight training). The data recorded from the test included:

- Recording engine parameters during the test using the Full Authority Digital Engine Control and other atmospheric conditions during the test.
- Recording different views of the test using a variety of high-definition and high-speed cameras to capture the ingestion from many different angles and to perform DIC.
- Recording strains on select locations on the blades during the ingestion.
- Scanning and documenting the blades post-impact to characterize the damage from the ingestion event.

Several engine parameters were monitored live and recorded during the test, including the fan speed (*N1*), core speed (*N2*), exhaust temperature (EGT), and fuel flow (*Wf*), along with several more parameters, limits, exceedances, cautions, and warnings. Additional facility data monitoring included zero time, oil pressure and temperature, fuel feed pressure, start air pressure, and start handle position, which were also recorded.

Several high-speed cameras were used for DIC to obtain the trajectory of the UAS as it was ingested into the engine and monitor the displacements of the fan and engine nacelle during the test. Unfortunately, the NAWC and outside vendor Trilion Quality Systems were unable to work out the proper lighting requirements before the test, and the speckling pattern on the blades was too small for the available lighting. As a result, the cameras had to record at a reduced resolution, causing the fan blade surface strain data to have a much higher noise level than desired, which could not be used for comparison with the numerical simulation. Along with the reduced recording resolution, part of the sabot, UAS debris, and a fireball created during the ingestion event created gaps in the DIC data due to obscuring the view of the camera during the ingestion event. As a result of this, only limited displacement data was obtained from the blades. The speckle pattern that was applied to the fan blades, nose cone, and cowling can be seen in

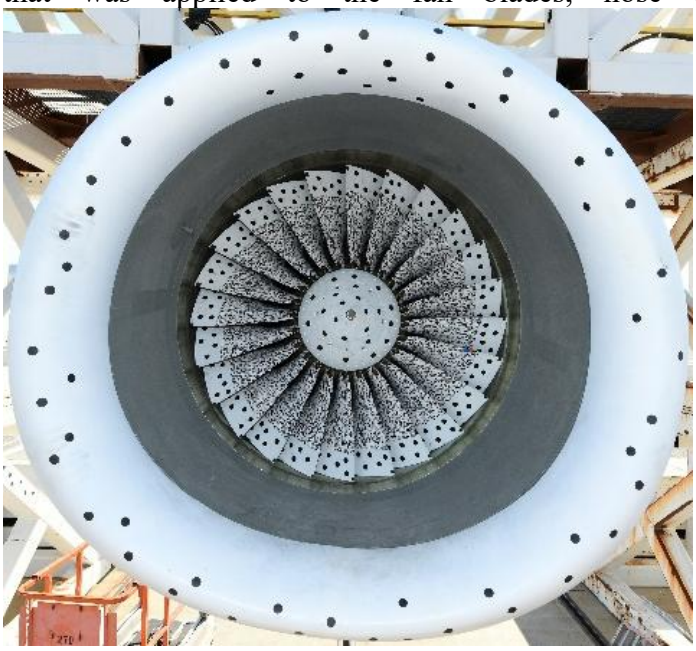

Figure 29. The DIC cameras used to record the ingestion are summarized in Table 4.

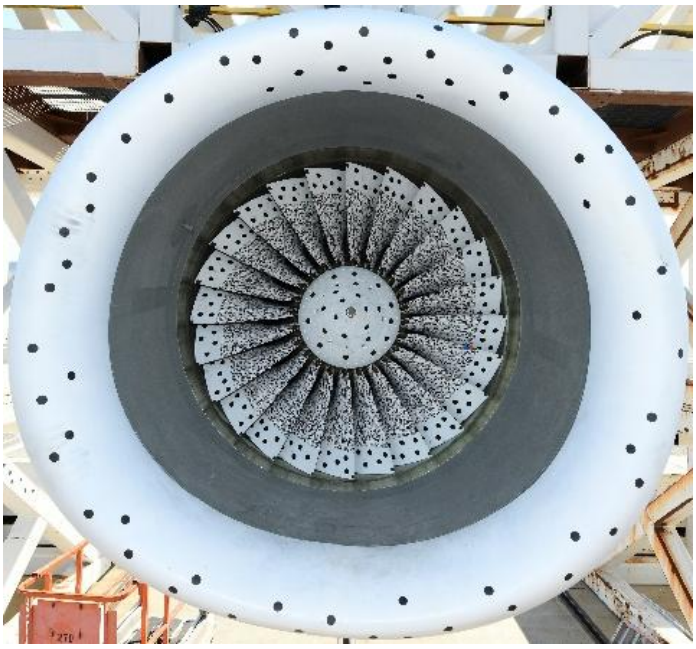

Figure 29. Speckle pattern applied in the experiment for DIC.

Table 4. DIC camera placement and specifications.

View	Quantity	Model	Resolution	Frame Rate	Measuring Volume	M/C
1 – 2D Front and Center	1	Phantom v2512	896 x 800 pixels	20,000 FPS	N/A	Color
2 – Stereo Drone Ingestion	2	Photron SAZ	1024 x 1024 pixels	20,000 FPS	1350 x 1350 x 1350 mm	Mono
3 – Stereo Close-Up Blades Near Impact Zone	2	Phantom T4040	1280 x 832 pixels (binning)	10,000 FPS	1220 x 795 x 795 mm	Mono
4 – Stereo Front and Center	2	Phantom T1340	1024 x 976 pixels (binning)	7,500 FPS	2080 x 2005 x 2005 mm	Mono
5 – Stereo Engine Nacelle Side View	2	Photron SA5	1024 x 1000 pixels	7,500 FPS	3845 x 4050 x 4050 mm	Color

The five viewing angles described in Table 4 all successfully captured data during the UAS ingestion into the CFM56-7B engine. View 1 was the only 2D analysis and was able to capture the fan blades' angular velocity, nose cone *y* and *z* displacements, and casing *y* and *z* displacements. However, since this was a 2D analysis and the camera was not completely planar with the engine, the data is more noisy and less accurate than the other viewing angles.

The rest of the views used two cameras for stereo analysis, allowing for more accurate measurements to be taken. View 2 successfully determined the 6-degrees of freedom orientation of the UAS before impact with the fan blades relative to the global coordinate system (*x*-axis in line with the centerline of the nose cone, *y*-axis horizontal, and *z*-axis vertical), UAS translational velocity, and the angular velocity of the nose cone, which can be seen in Figure 30.

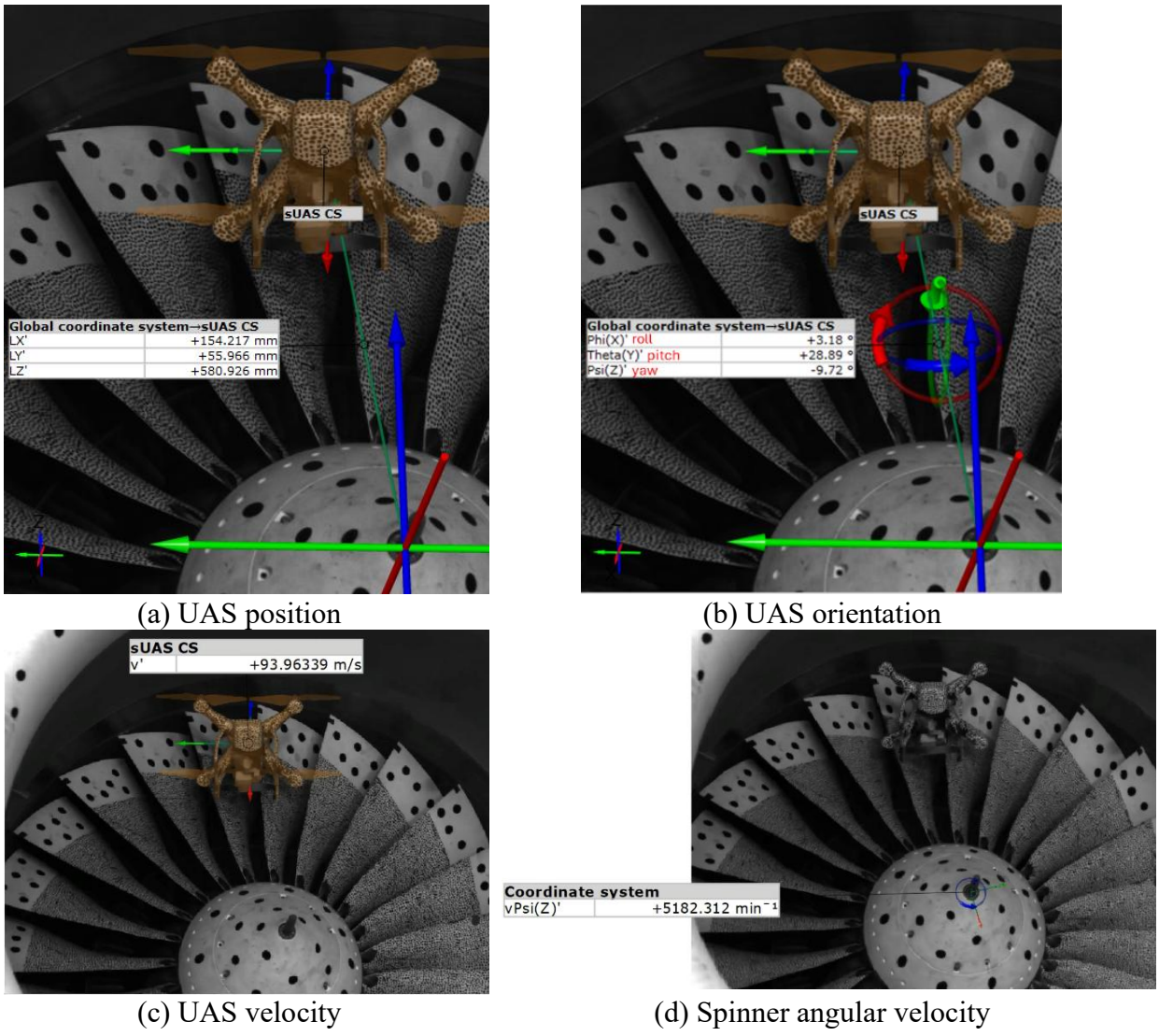

(a) UAS position (b) UAS orientation

(c) UAS velocity (d) Spinner angular velocity

Figure 30. Data extracted from view 2.

View 3 was able to confirm the analysis from view 2 for the 6-degrees of freedom orientation of the UAS before it impacted with the fan blades as well as capture the out-of-plane motion of points on the fan blades as shown in Figure 31.

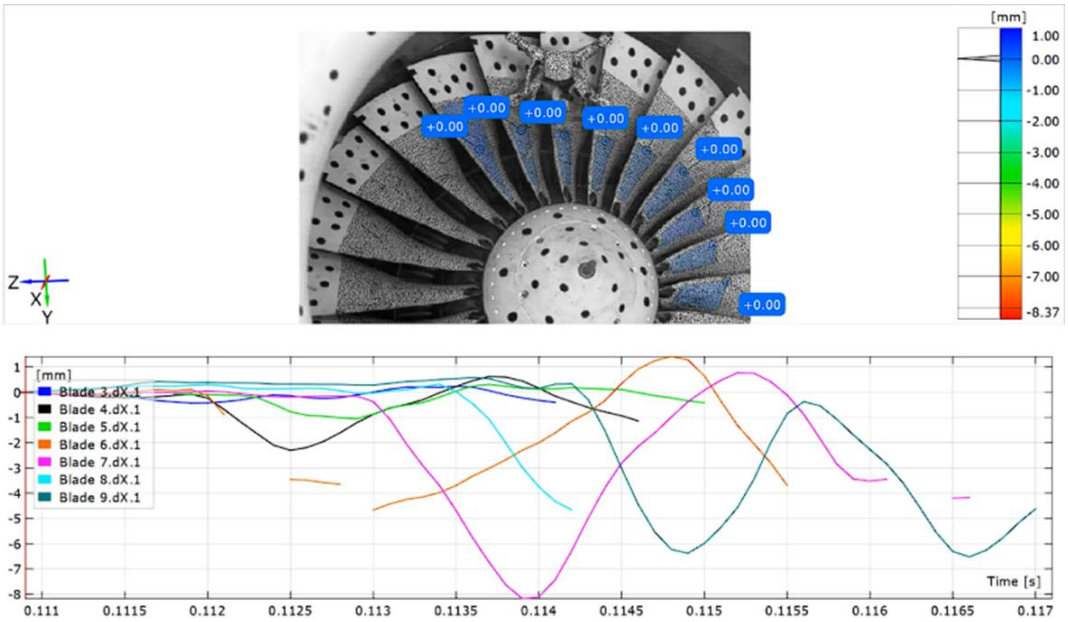

Figure 31. Out-of-plane motion extracted from view 3.

View 4 successfully determined the fan blades' angular velocity, nose cone *x*, *y*, and *z* displacements, and the *x*, *y*, and *z* displacements of the casing. View 5 successfully determined the *x*, *y*, and *z* displacements of the engine nacelle relative to both the lower portion of the engine test stand and the engine body itself.

Additional high-speed video, standard-speed video, still photos, and infrared video were captured before, during, and after the test event from facility cameras. A summary of these cameras is given in Table 5.

Table 5. Facility camera placement and specifications.

Name	FOV	Camera	Lens mm	x (px)	y (px)	FPS	f/stop	Shutter	M/C
SHIVAS	Port side overall	UX-100	28	1280	1024	2000	2.8	0.04ms	Color
West Tower	Starboard side overall	VEO-410	20	1280	800	2000	2.8	0.006ms	Color
Upper Muzzle	Full Fan	V2512	85	896	800	20000	1.4	0.0015ms	Color
Lower Muzzle	Full Fan	TMX6410	50	1280	800	60000	2.8	0.001ms	Mono
Velocity	Muzzle to Inlet	NOVA S12	50	1024	688	4000	4	0.005ms	Mono
Rear View	Port side rear view 45°	NOVA S12	35	1024	512	10000	4	0.02ms	Color
FLIR	Rear Exhaust	FLIR X8581	25	1280	640	280	2.5	0.01ms	Color

ITM was contracted to install 64 strain gauges on the fan blades and an onboard telemetry system with a sampling rate of 10 kHz. ITM suggested a variety of candidate positions for the placement of strain gauges. OSU evaluated each of the positions in preliminary ingestion simulations to provide recommendations for the strain gauge locations with two strain gauges placed on all fan blades to resolve the tangential and axial impact loads and two on every third fan blade for additional data closer to the impact location. The location and orientation of these strain gauges are indicated in Figure 32.

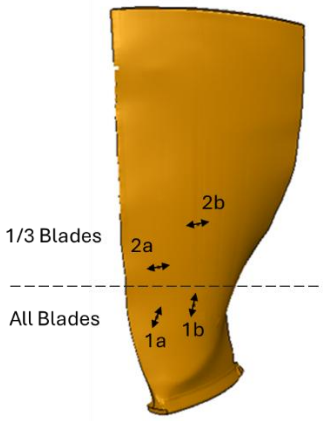

Figure 32. Strain gauge locations and orientations on the fan blade.

Scanning of the blades post-impact was conducted by NIAR, and comparisons of the blades post-impact with the numerical simulations will be highlighted in the next section.

7. VALIDATION OF MODELLING APPROACH

This section focuses on comparing key results from the live engine ingestion test with the CFM56-7B fan assembly model developed in this work. Note that results from the open representative fan assembly model are, in general, not compared with the experiment due to the differences in geometry, making comparisons of data at specific points on the model not useful. However, more general results like the final damage in the blades and the kinematics of the ingestion are useful points of comparison to show how representative the structural features of the fan assembly model are.

To set up the computational simulations, the orientation, location, and speed of the UAS and rotational speed of the fan were identified from the DIC camera views discussed in Section 6.3 Instrumentation. A summary of this information identified from the different camera views is given in Table 6. For the UAS ingestion simulations, the fan was prescribed with the desired rotational speed after a pre-stress analysis was conducted (as described in Section 5.3.2 Prestress Analysis). The UAS was given the prescribed initial orientation and placed with its center of mass at the desired location.

Table 6. Summary of initial conditions estimated from experiments using DIC cameras.

Camera View	Fan Angular Velocity [RPM]	UAS position (x, y, z) [mm]	UAS orientation (ϕ, θ, ψ)	UAS velocity [m/s]
1	5,179	-	-	-
2	5,182	(154.2, 56.0, 580.9)	(3.18°, 28.89°, -9.72°)	93.96
3	-	(154.1, 51.0, 582.9)	(3.44°, 28.94°, -9.71°)	-
4	5,183	-	-	-

Images of the UAS position and orientation just before impact for the experiment and the corresponding numerical simulation are shown in Figure 33.

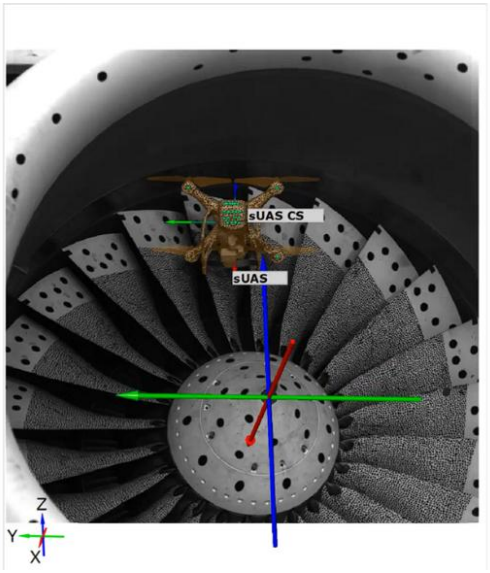

(a) Front view: experiment

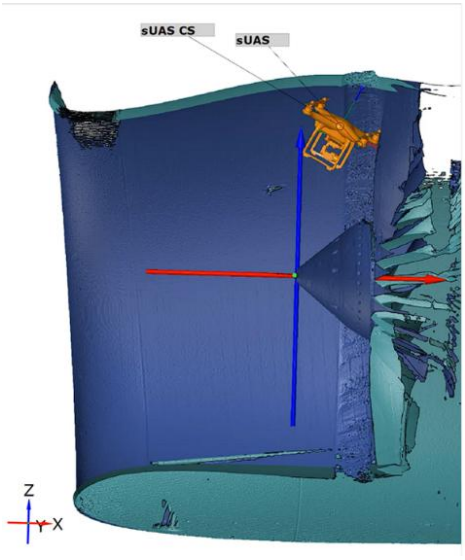

(b) Side view: experiment (predicted)

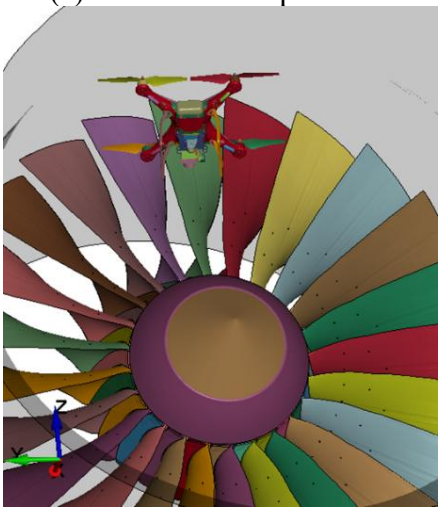

(c) Front view: simulation

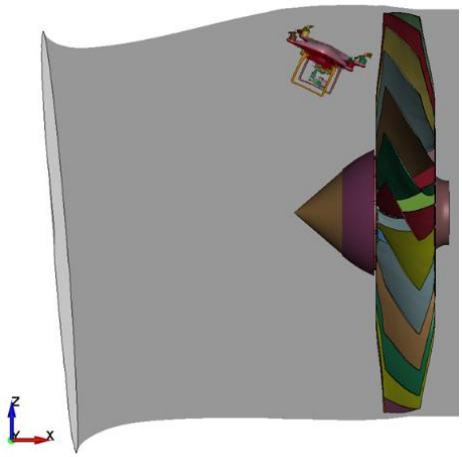

(d) Side view: simulation

Figure 33. Placement and orientation of UAS before impact.

The experiment resulted in significant damage to a number of blades. An image and scan of the blades after the experiment is shown in Figure 34. The numbering of the blades corresponds to the numbering done by ITM for the DIC computation. The first blade to make contact with the UAS is blade number 18, and the last one to make contact is blade number 12.

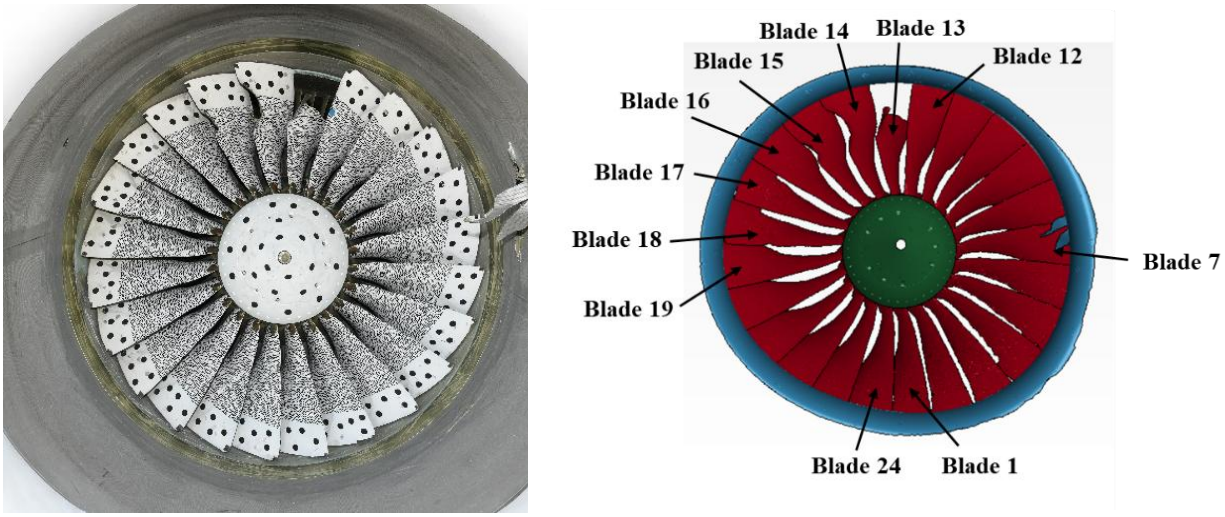

(a) Image of the fan after the experiment

(b) Scan of the fan after the experiment

Figure 34. Fan after ingestion with blades numbered.

In the following subsections, the kinematics of the ingestion are compared between the experiment, CFM56-7B fan assembly model, and open representative fan assembly model. Next, the final blade damage is compared for the physical fan blades, the fan blades from the CFM56-7B fan assembly model, and the fan blades from the open representative fan assembly model. After that, comparisons are made with the strain gauge data from the experiments and the strains in the model of the CFM56-7B fan blades at the locations of the strain gauges. Then, out-of-plane displacement measured using the DIC from the experiment is compared with the corresponding motion for the CFM56-7B fan assembly model. Finally, the overall fan damage severity evaluation defined in previous work is used to classify the damage in the fan for the experiment, the CFM56-7B fan assembly model, and the open representative fan assembly model.

7.1 KINEMATICS

The kinematics of the ingestion event from DIC view 1 can be seen in Figure 35. It should be noted that due to different sabot and UAS debris blocking portions of the camera view and the fireball created during the explosion as a result of the ingestion, data could not be recorded during this time. The data loss can be seen in the DIC measurements from view 3 in Figure 31.

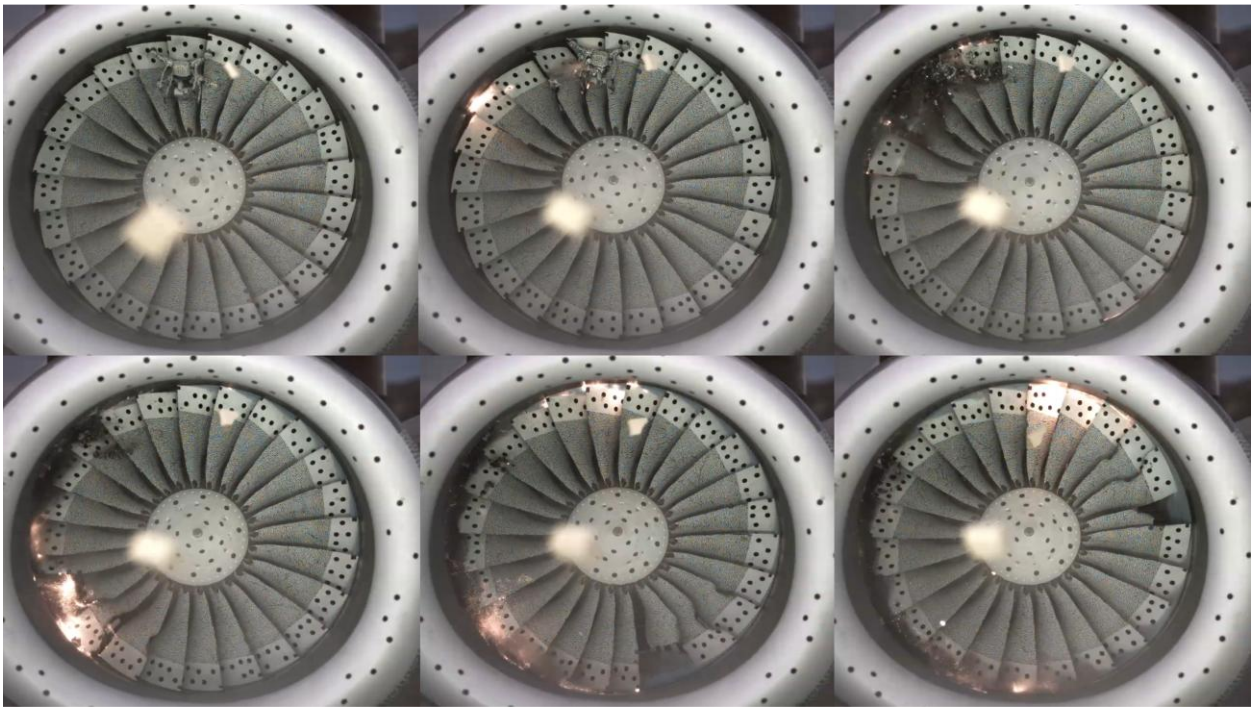

Figure 35. Ingestion kinematics from the experiment.

The kinematics of the ingestion event for the CFM56-7B fan assembly model can be seen in Figure 36. The fan was simulated to make one full revolution, which was around 11.6 ms. It should be noted that the UAS parts were deleted once they cleared the contact region with the fan blades, which was around 10 ms, to improve the computational efficiency.

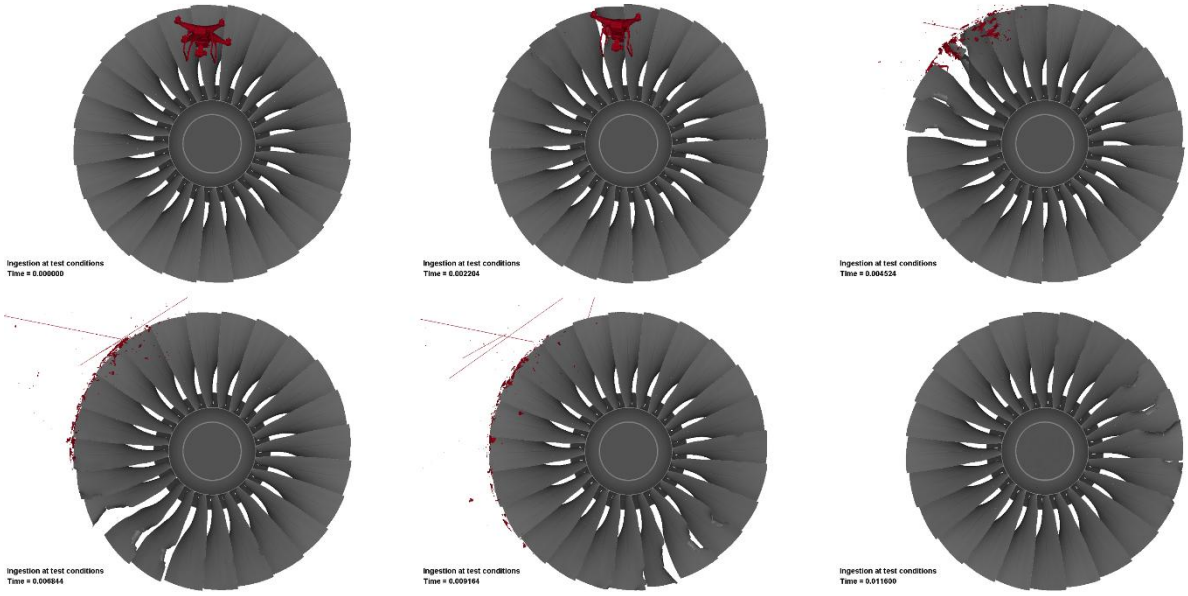

(a) Front view

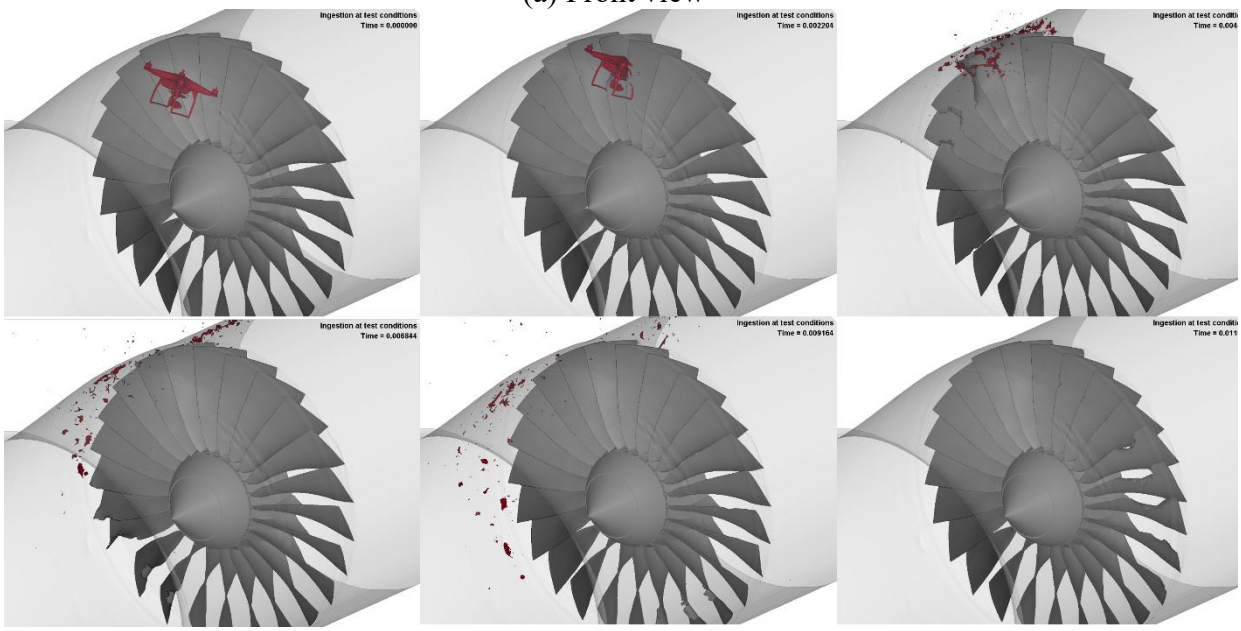

(b) Isometric view

Figure 36. CFM56-7B fan assembly model ingestion kinematics.

The kinematics of the ingestion event for the representative fan assembly model can be seen in Figure 37. The fan was simulated to make one full revolution, which was around 11.6 ms. It should be noted that the UAS parts were deleted once they cleared the contact region with the fan blades, which was around 10 ms to improve the computational efficiency.

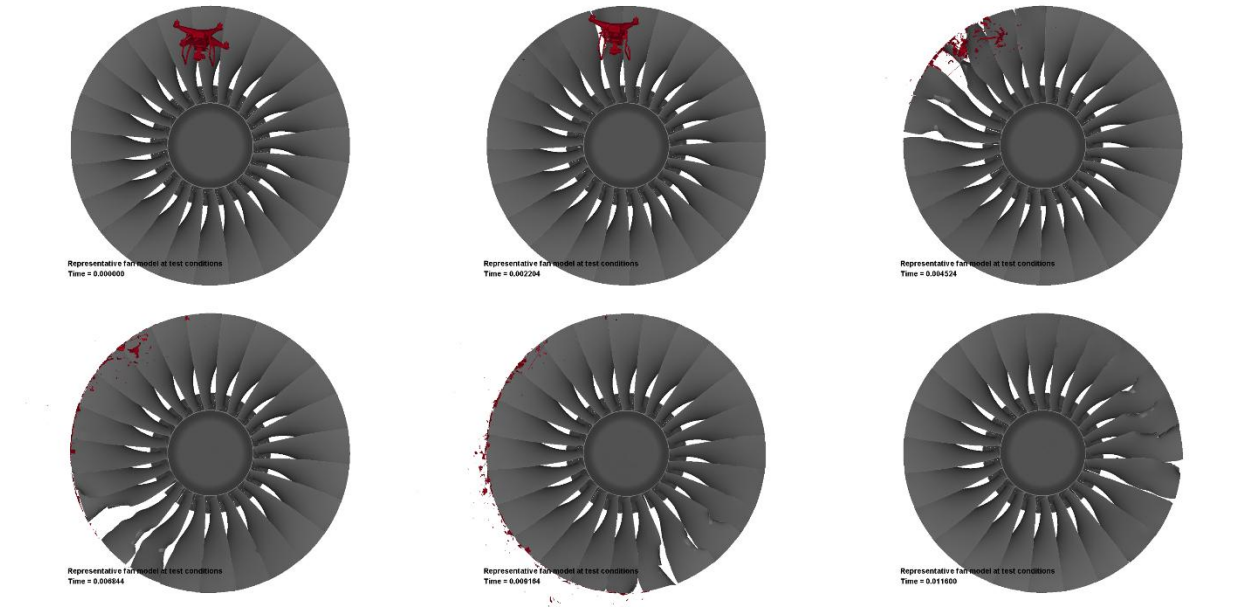

(a) Front view

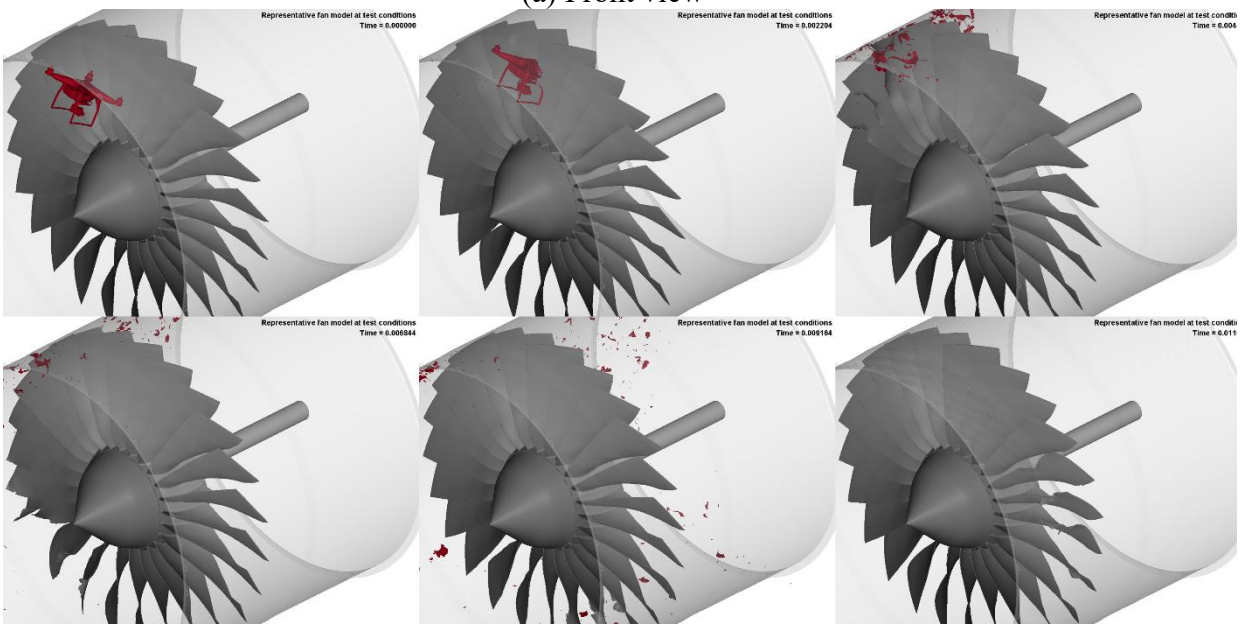

(b) Isometric view

Figure 37. Representative fan assembly model ingestion kinematics.

The similarity in the ingestion kinematics is evident for the three cases (actual test, CFM56-7B fan assembly, and the representative fan assembly). The UAS is completely obliterated during the ingestion, and very similar blades in the fan are impacted and damaged. Note that the largest difference is the explosion that occurs in the experiment, which the numerical simulation in LS-DYNA cannot capture.

7.2 FAN BLADE DAMAGE

In this section, images of the fan blade after the ingestion event are compared with plots of the effective plastic strain in the blades after the impact. The fan blades in the experiment did experience extra damage due to excessive blade tip rubbing, so some blade tip damage from the physical blades is not expected to be captured in the numerical results. The comparison is made for blades 12 through 18 (blade numbers shown in Figure 34), where blade 18 is the first blade that comes in contact with the UAS, and blade 12 is the last. The comparison shows the fan blade after one full revolution for both computational models, while the physical fan blade is after the conclusion of the test (the fan rotates many times after the UAS impact before it comes to a stop).

A comparison of blade 12 after the ingestion test with the CFM56-7B fan blade after the ingestion simulation and the representative fan blade after the ingestion simulation is shown in Figure 38. There is some small material loss along the leading edge of each of the blades. Note that the physical blade has some blade tip loss, most likely due to the tip rub that resulted during the experiment.

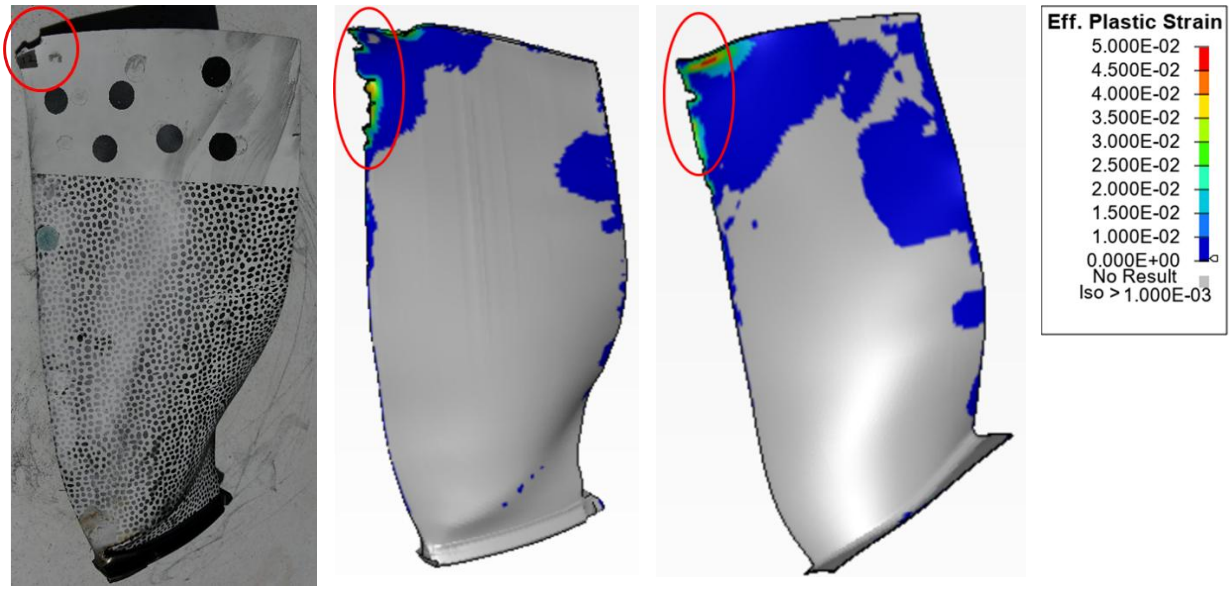

(a) Picture of blade (b) CFM56-7B model (c) Representative model

Figure 38. Blade 12 after the ingestion experiment/simulation.

A comparison of blade 13 after the ingestion test with the CFM56-7B fan blade after the ingestion simulation and the representative fan blade after the ingestion simulation is shown in Figure 39. A significant portion of the top of the physical blade broke off due to the impact of the UAS. Both the CFM56-7B and representative fan assembly model show a significant tear in the fan blade in a similar region to where the experimental blade tip liberated itself. This could potentially lead to the computational fan blade tips also liberating themselves from the fan blade if further rotated. This was noted in the previous UAS ingestion research, which discussed how portions of the blade could break free due to significant cracking along the leading edge[4].

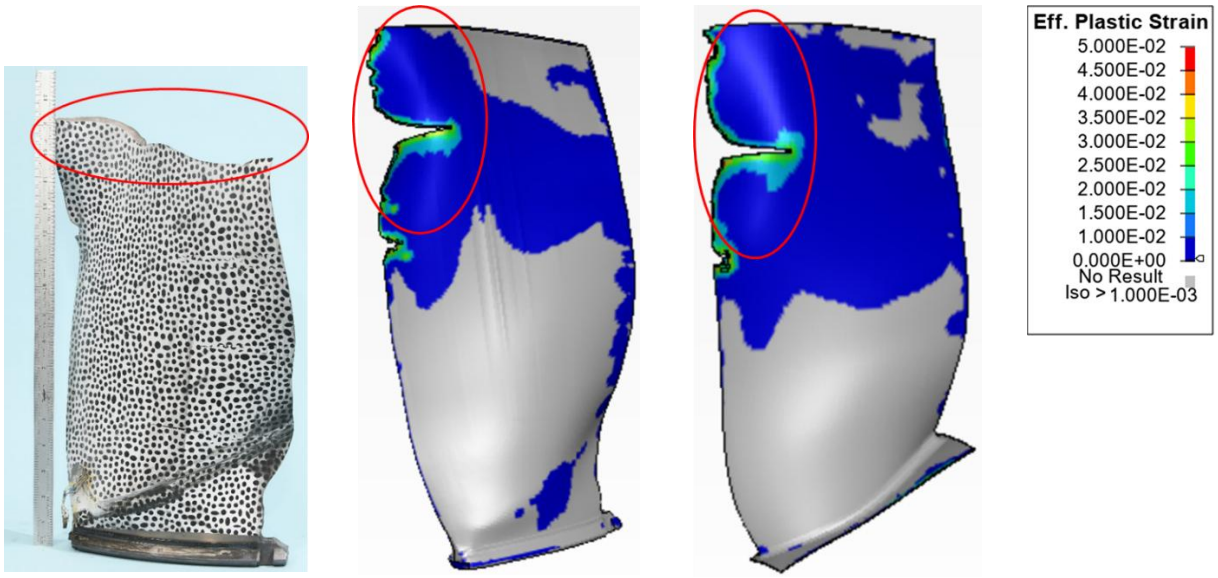

(a) Picture of blade (b) CFM56-7B model (c) Representative model

Figure 39. Blade 13 after the ingestion experiment/simulation.

A comparison of blade 14 after the ingestion test with the CFM56-7B fan blade after the ingestion simulation and the representative fan blade after the ingestion simulation is shown in Figure 40. There is a large notch made in the leading edge of the blades of similar size for all three cases.

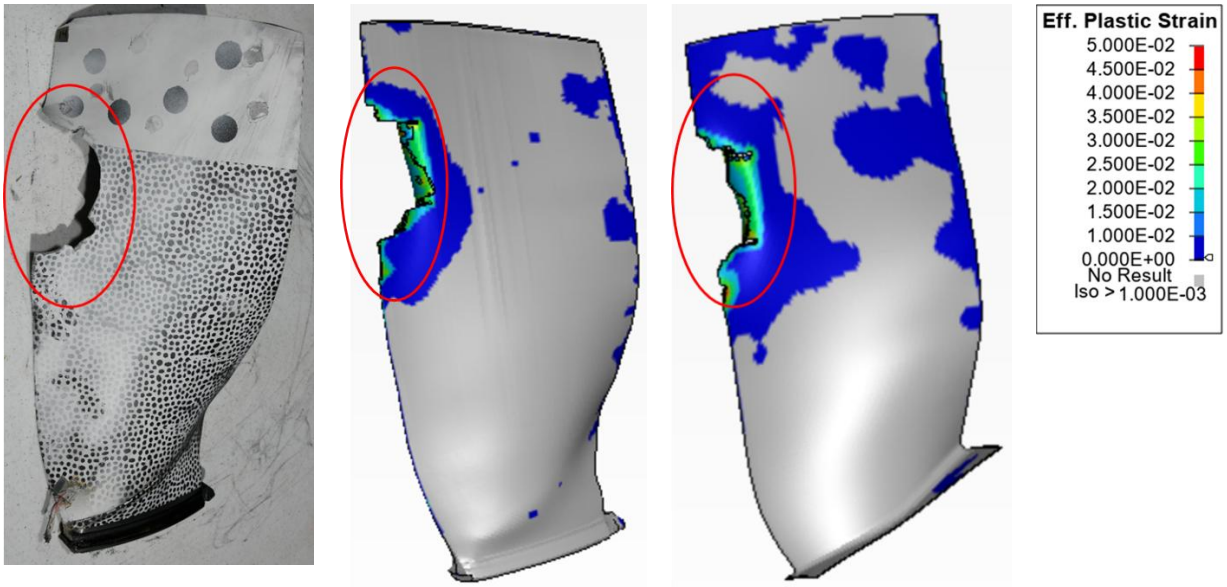

(a) Picture of blade (b) CFM56-7B model (c) Representative model

Figure 40. Blade 14 after the ingestion experiment/simulation.

A comparison of blade 15 after the ingestion test with the CFM56-7B fan blade after the ingestion simulation and the representative fan blade after the ingestion simulation is shown in Figure 41. There is a significant notch made on the leading edge of the blades, with the physical blade notch being slightly smaller than the notch made on the blades from the simulations.

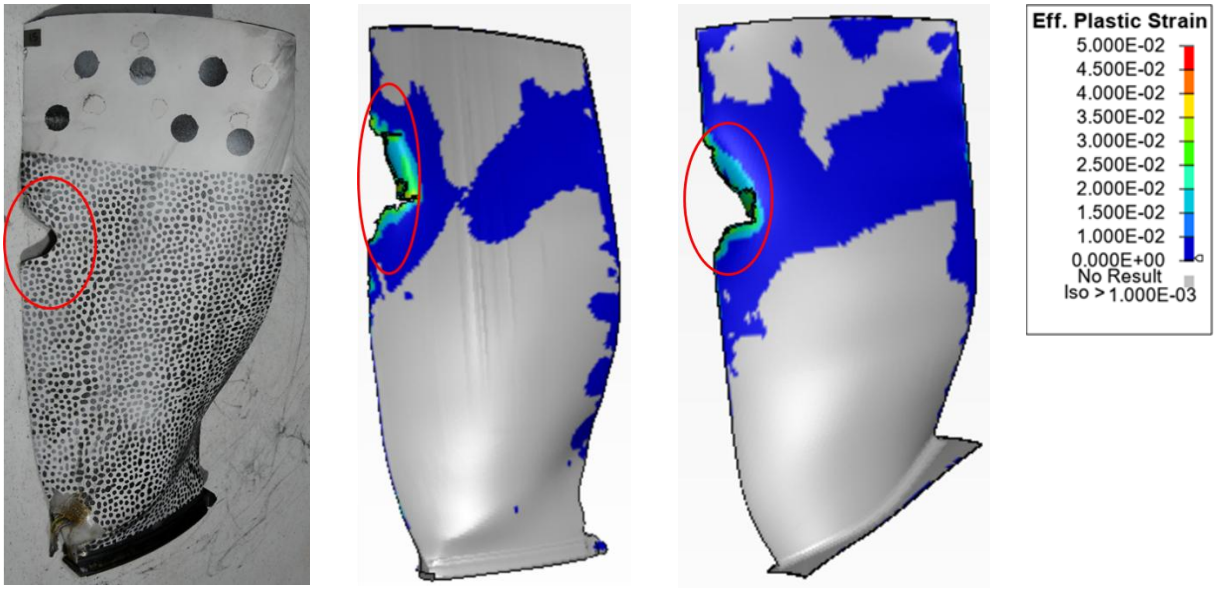

(a) Picture of blade (b) CFM56-7B model (c) Representative model

Figure 41. Blade 15 after the ingestion experiment/simulation.

A comparison of blade 16 after the ingestion test with the CFM56-7B fan blade after the ingestion simulation and the representative fan blade after the ingestion simulation is shown in Figure 42. There is minor damage to the leading edge of the blades for all three cases.

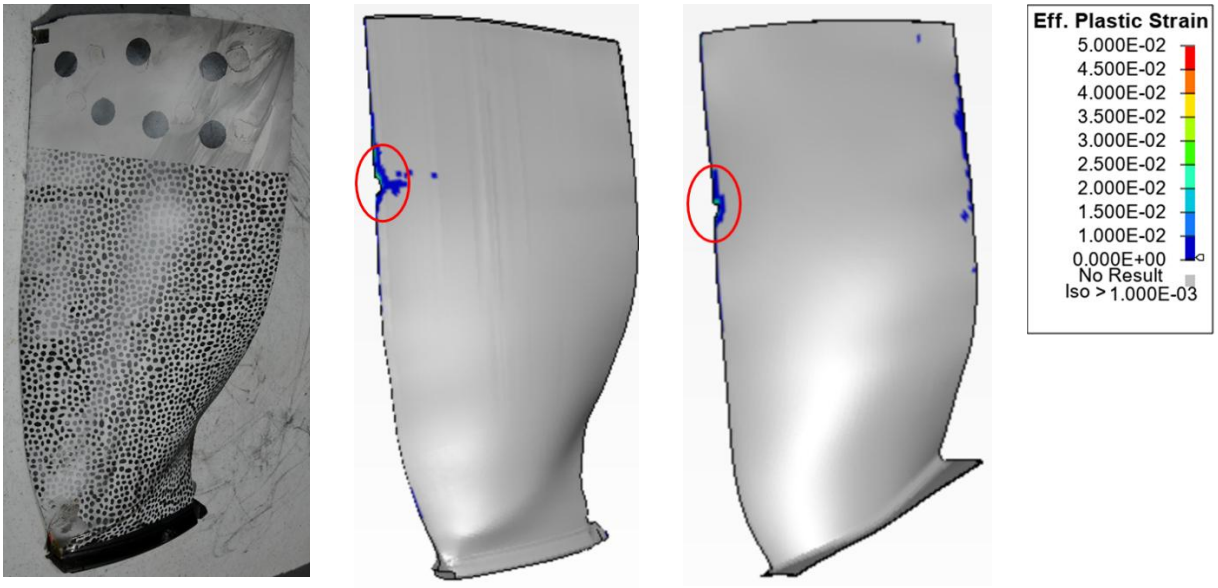

(a) Picture of blade (b) CFM56-7B model (c) Representative model

Figure 42. Blade 16 after the ingestion experiment/simulation.

A comparison of blade 17 after the ingestion test with the CFM56-7B fan blade after the ingestion simulation and the representative fan blade after the ingestion simulation is shown in Figure 43. There is a similar level of minor damage to the leading edge of all the blades. The physical blade also had a piece missing along the tip, most likely resulting from a severe tip rub.

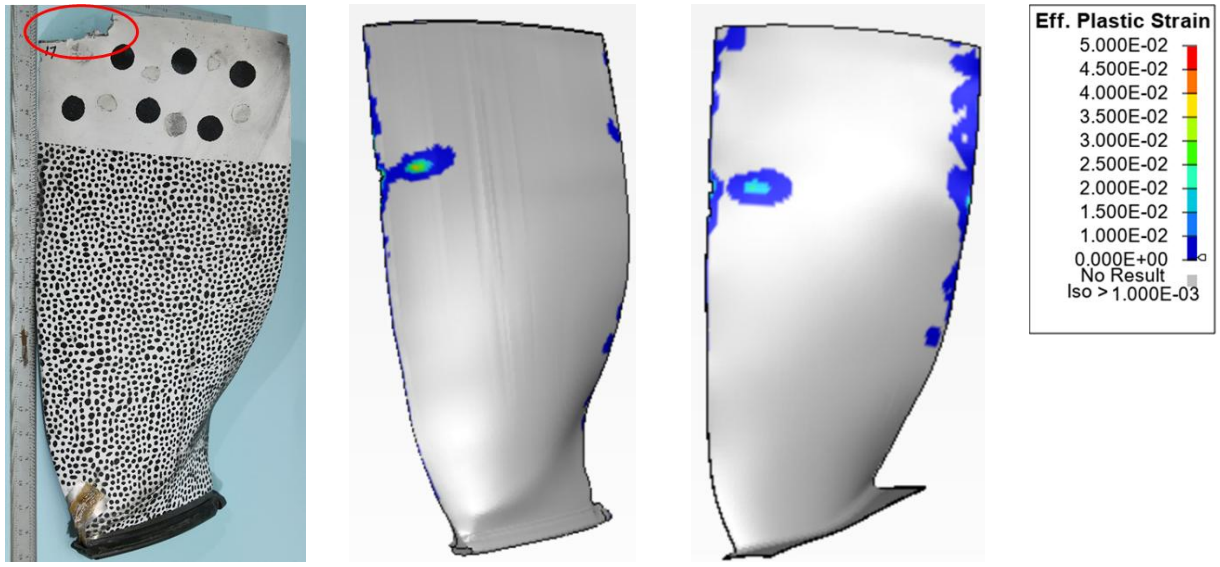

(a) Picture of blade (b) CFM56-7B model (c) Representative model

Figure 43. Blade 17 after the ingestion experiment/simulation.

A comparison of blade 18 after the ingestion test with the CFM56-7B fan blade after the ingestion simulation and the representative fan blade after the ingestion simulation is shown in Figure 44. There is a small notch made in the leading edge of the blades of similar size for all three cases. Additionally, the physical blade also had a small piece missing along the tip, most likely resulting from a tip rub.

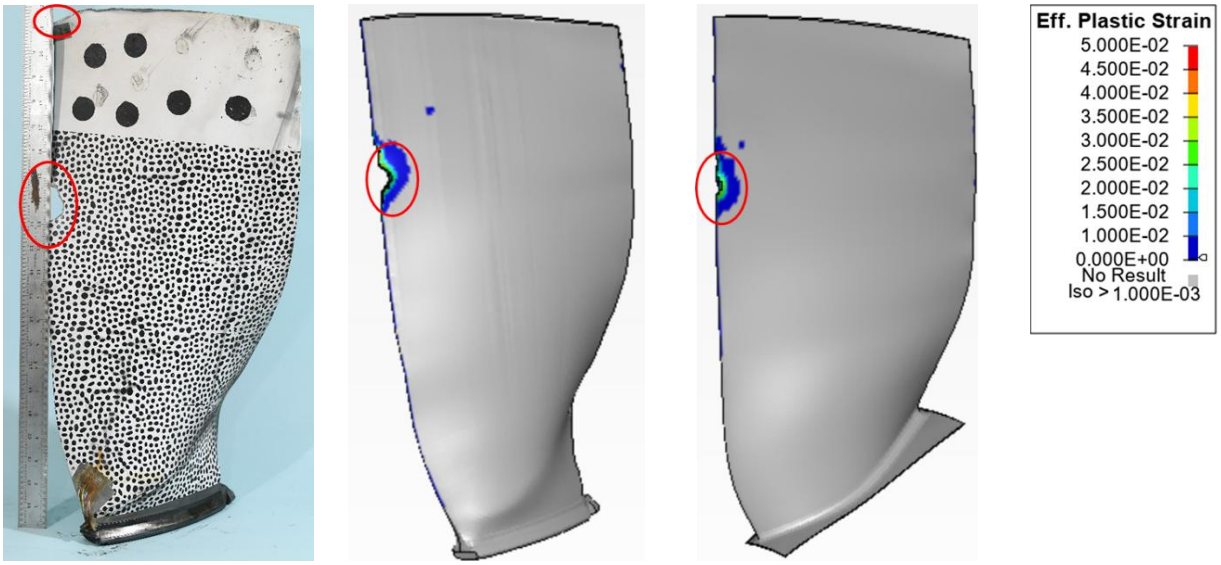

(a) Picture of blade (b) CFM56-7B model (c) Representative model

Figure 44. Blade 18 after the ingestion experiment/simulation.

The damage to all the impacted fan blades is very consistent between the experiment and simulations from the actual UAS impact. There is some additional tip damage in the physical blades from the experiments that result from blade tip rubs not captured in the simulation.

7.3 STRAIN GAUGE DATA

Strains from two locations on every blade and two additional locations on every third blade were obtained during the experiment. Strain gauge elements were placed in the same location on the CFM56-7B fan blades for the simulation. The location and orientation of the strain gauges are shown in Figure 32. A comparison of the strains for the impacted blades (blades 12-18) is given in Figure 45-Figure 51. The start of UAS contact, the time when instability occurs in the test, and the time when the UAS parts are deleted in the simulation are noted on the plots with datum lines. The data should only be compared before the instability occurs. The instability occurs when the explosion occurs during the ingestion, and the data from the strain gauges is questionable after this point. Taking into account all the assumptions in the numerical model, the agreement in the strain data between the simulation and the experiment before the instability is reasonable.

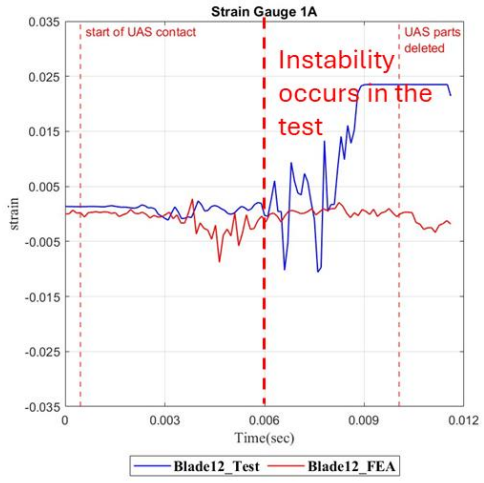

(a) Strain gauge 1A

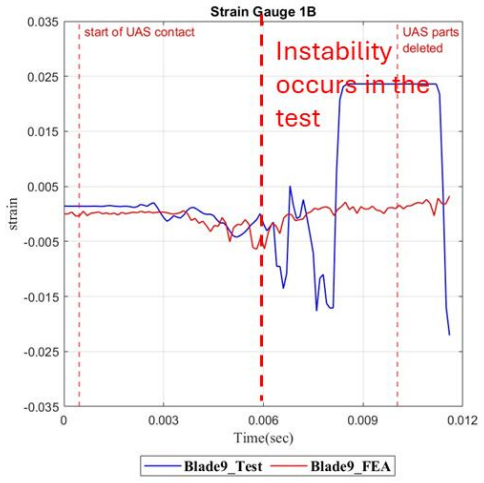

(b) Strain Gauge 1B

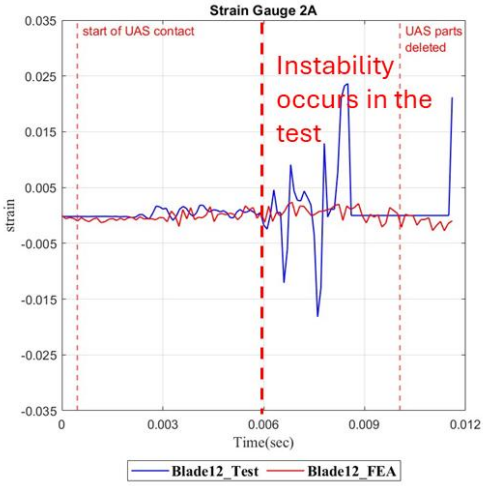

(c) Strain gauge 2A

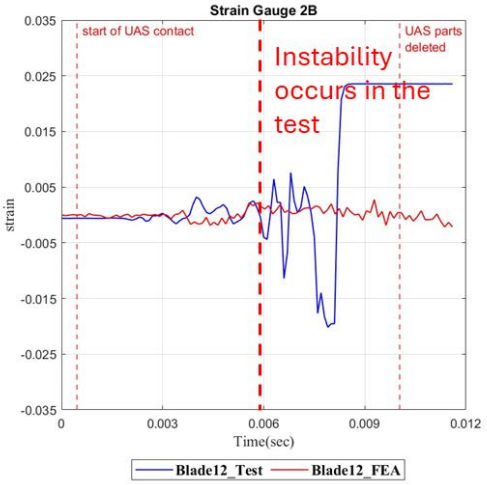

(d) Strain gauge 2B

Figure 45. Strain comparison for blade 12.

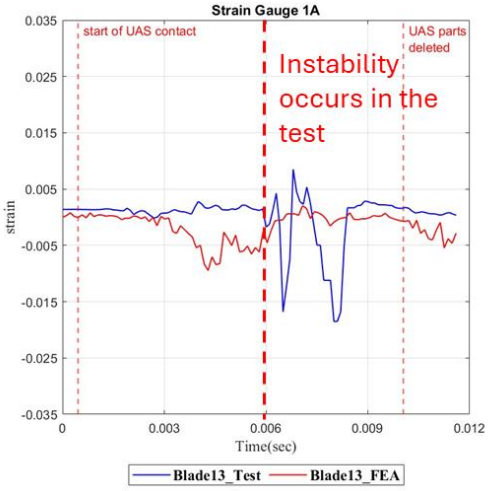

(a) Strain gauge 1A

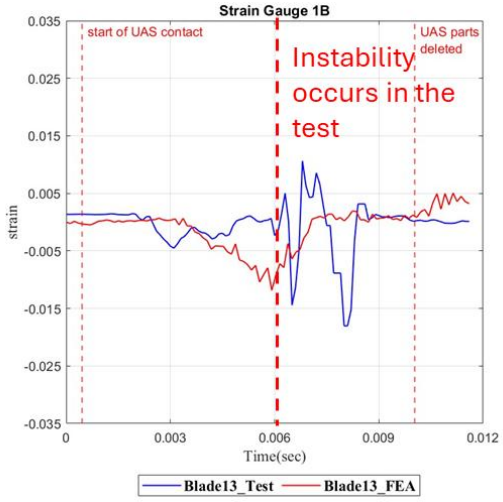

(b) Strain gauge 1B

Figure 46. Strain comparison for blade 13.

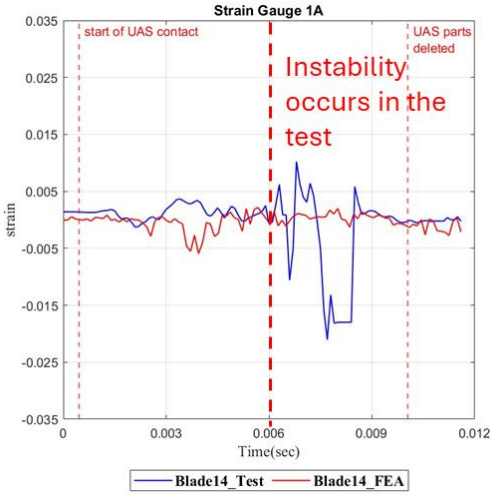

(a) Strain gauge 1A

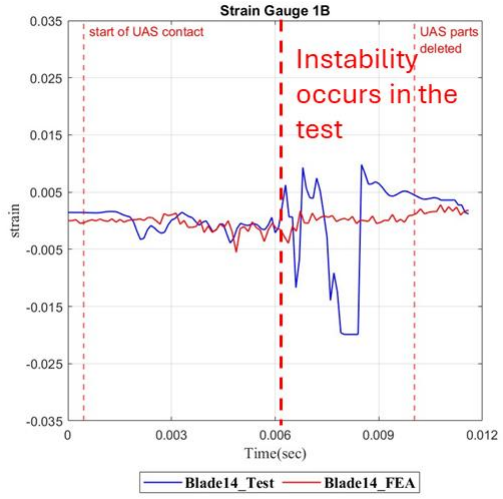

(b) Strain gauge 1B

Figure 47. Strain comparison for blade 14.

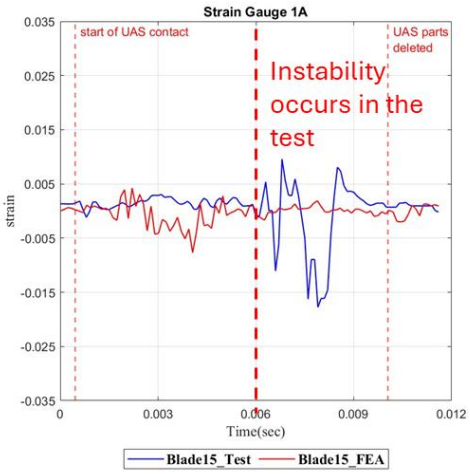

(a) Strain gauge 1A

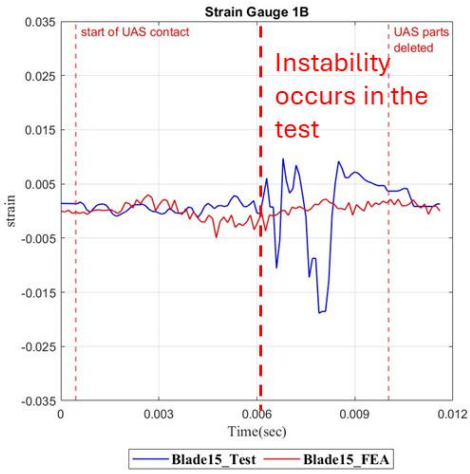

(b) Strain Gauge 1B

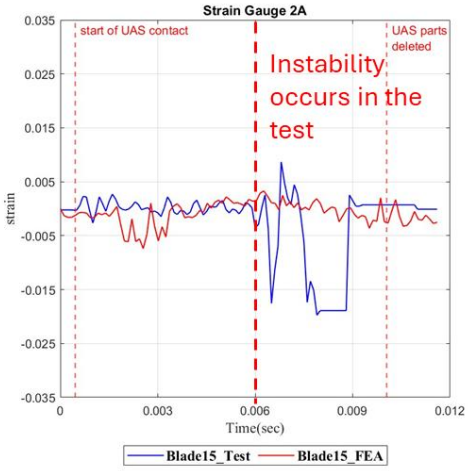

(c) Strain gauge 2A

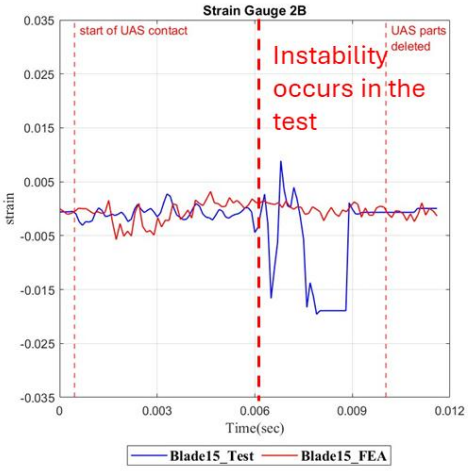

(d) Strain gauge 2B

Figure 48. Strain comparison for blade 15.

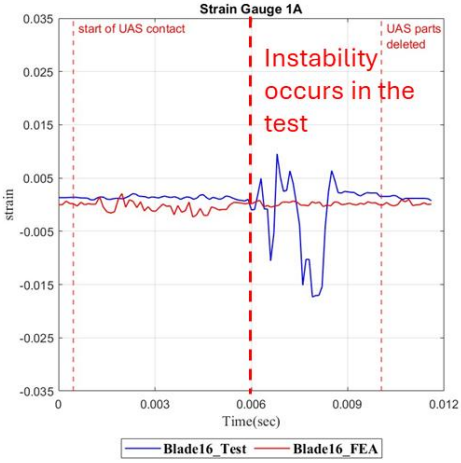

(a) Strain gauge 1A

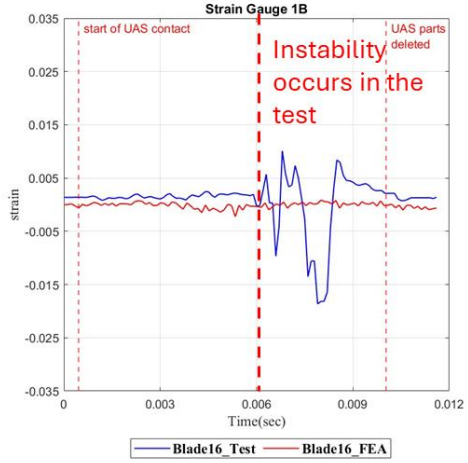

(b) Strain gauge 1B

Figure 49. Strain comparison for blade 16.

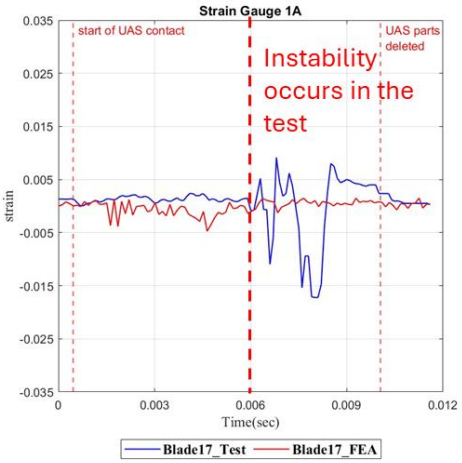

(a) Strain gauge 1A

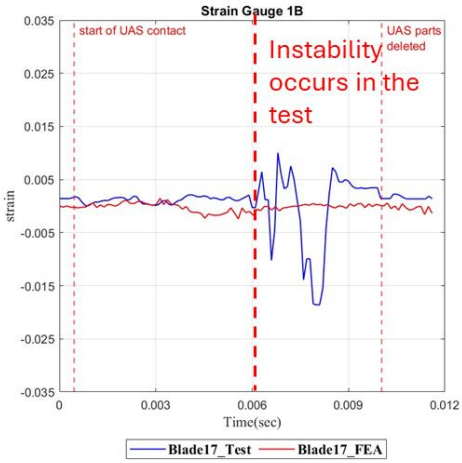

(b) Strain gauge 1B

Figure 50. Strain comparison for blade 17.

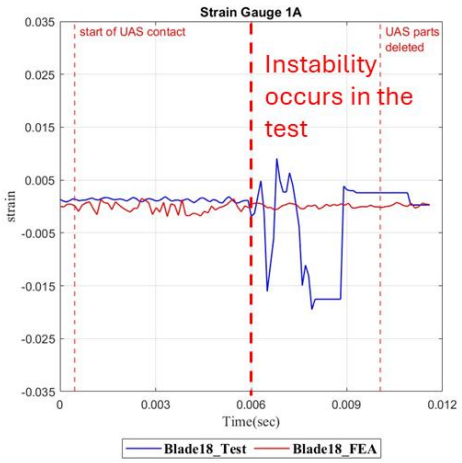

(a) Strain gauge 1A

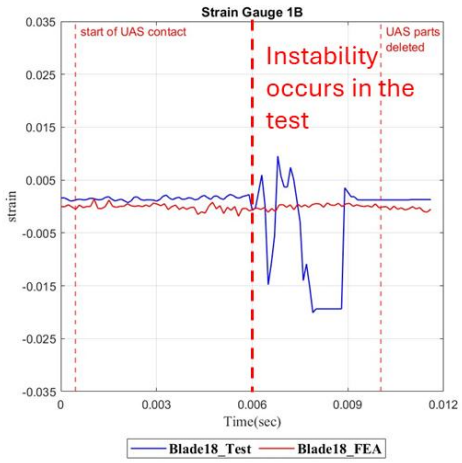

(b) Strain Gauge 1B

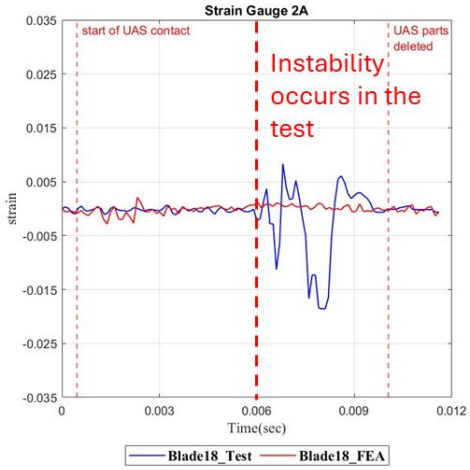

(c) Strain gauge 2A

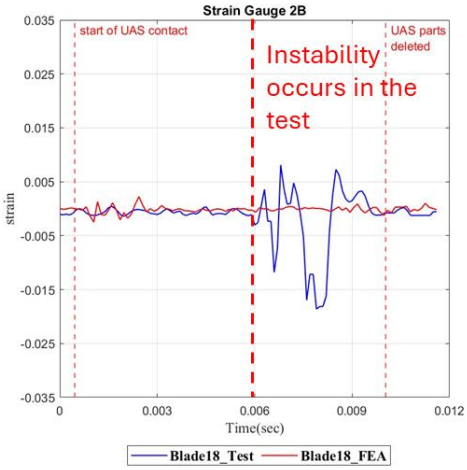

(d) Strain gauge 2B

Figure 51. Strain comparison for blade 18.

7.4 DIC DATA

The experimental DIC data of the fan blades was difficult to compare with the CFM56-7B fan assembly model simulation data. A point along the leading edge of the computational model was chosen to compare against the out-of-plane displacement information provided by Trilion for blades 12-18. It should be noted that there are gaps in the experimental data due to parts of the sabot, UAS debris, and a fireball created during the UAS ingestion event obscuring the view of the high-speed cameras, preventing them from recording the fan blade surfaces. However, the data that was recorded matches the computational model reasonably well, with similar initial and peak displacement values, as shown in Figure 52.

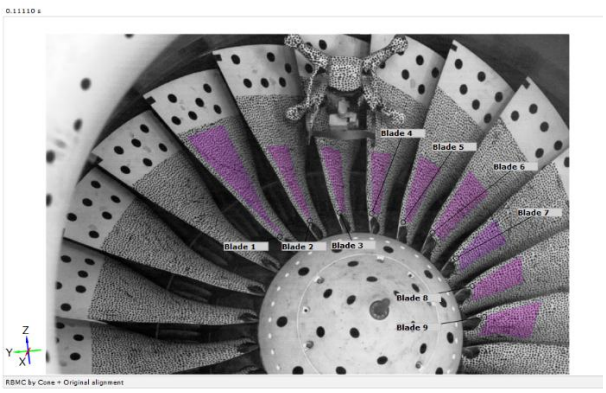

(a) Blade surface construction from DIC

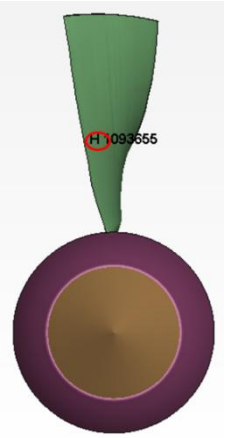

(b) Element location on the model used for displacement measurement

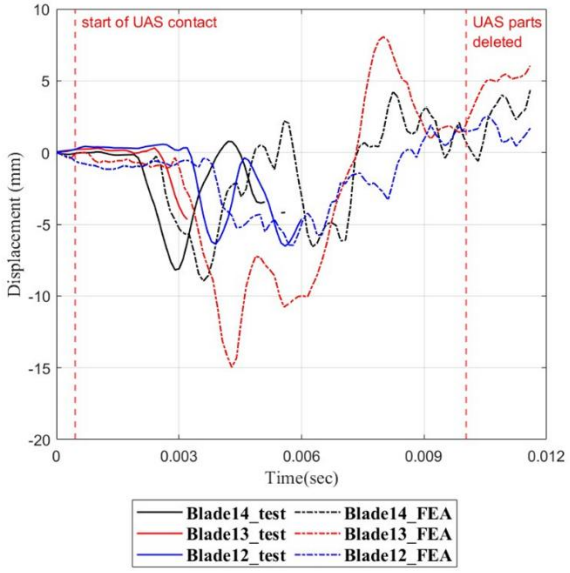

(c) Blades 12-14

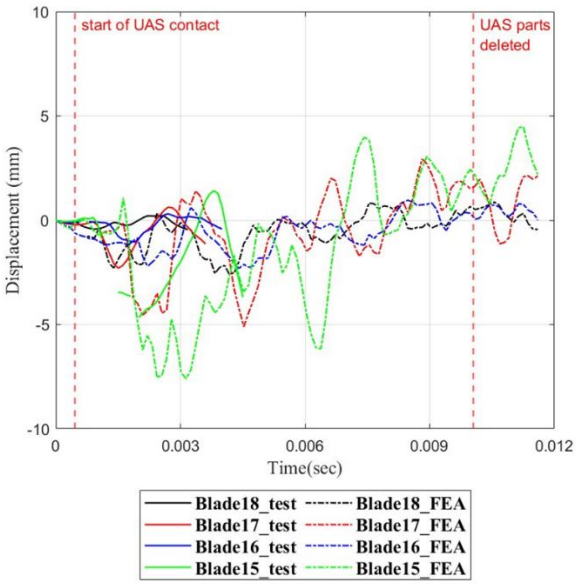

(d) Blades 15-18

Figure 52. Out-of-plane displacement measured by DIC.

7.5 DAMAGE SEVERITY LEVEL

The simulations conducted in the prior engine ingestion research were focused on understanding the effect of the UAS collision with an aircraft engine as it relates to damage in the fan in particular[4]. This fan damage has implications on rotor imbalance, blockage (which impacts thrust), containment, and retainment mechanisms. Note that the fan rig assembly model does not contain most of the downstream components of the fan (i.e., compressor, combustor, and turbine), and therefore, any damage to these components is out of scope when using the fan assembly rig models. The live ingestion test can be used to fill in some of these blanks. In the previous research effort, the damage was separated into four severity levels based on discussion with the research team and the industrial partners, which are detailed in Table 7. Table 7 has four columns: (i) the damage severity level; (ii) the fan damage and its corresponding likely effect on the engine; (iii) the corresponding aircraft operational impact for that same level of engine damage; and (iv) the typical associated damage in the fan for the damage severity level. Note that severity levels 1-3 are within the engine certification envelope and correspond to damage that would be typically seen up to a single blade-out event, which engines must be certified to be able to contain and shut down safely from. Severity level 4 is outside the certification envelope, which means the engine is not certified for these damage levels but makes no claims about the danger or safety at this level since it is unknown.

Table 7. Damage severity level classification.

Severity	Fan (Engine) Damage	Aircraft Operational Impact	Typical Associated Damage
Level 1	Slight damage – Continued operation with negligible to small reduced thrust Within engine certification envelope	Minimal effect – Continued flight to destination. Inspection after landing.	• Small deformation of fan blades • No crack initiation (blade or disk)
Level 2	Moderate damage – More significant reduced thrust Within engine certification envelope	Moderate effect – Continued flight or rerouting as needed. Inspection after landing.	• Significant deformation of fan blades • Material loss of leading edges of blades • Visible cracking in **single** blade above mid-span • No disk crack initiation
Level 3	Significant damage – Potential engine shutdown Within engine certification envelope	Significant effect – Fewer options for rerouting. Emergency landing may be needed if damage occurs at critical flight phase. Inspection after landing.	• Significant material loss leading to an imbalance that is less than or equal to a single-blade loss • Visible cracking in **single** blade below mid-span • Visible cracking in **multiple** blades above mid-span • No disk crack initiation
Level 4	Damage outside of design criteria and certification – Potential hazardous engine effect Beyond engine certification envelope	Significant effect – Ranging from need to reroute to emergency landing to catastrophic failure. Inspection after landing.	• Significant material loss in blades leading to an imbalance that is more than a single blade loss • High-energy forward arc debris • Visible cracking of **multiple** blades below mid-span • Crack initiation in **disk**

It is important to note that Table 7 only provides an initial assessment of the fan damage and does not classify overall engine damage (since the model does not include most of the downstream components of the engine).

The damage severity level classification for the live ingestion test and the simulation of the CFM56-7B fan assembly and open representative fan assembly models all resulted in very similar damage to the fan. Each of these cases is in agreement and would lead to a level 3 severity level classification with significant material loss to the leading edge of multiple blades with cracks or notches occurring in multiple blades above the mid-span. The overall imbalance and damage to the fan is less than that of a fan blade out event and, therefore, would be within the engine certification envelope. The consistency in the level of damage and the damage severity level for the fan assembly gives confidence in the overall computational modeling approach.

8. COMPARISON OF REPRESENTATIVE FAN MODEL AND CFM56-7B MODEL

In this section, a more detailed comparison of the ingestion results for the representative fan assembly model and CFM56-7B fan assembly model is discussed. For each ingestion simulation, several types of analyses were conducted. First, several steps were taken to ensure the stability and accuracy of the solution. Then, the simulation data was processed in several ways to provide useful metrics to understand and compare the ingestion for each fan assembly model.

To ensure the stability and accuracy of the solution, several steps were taken for each simulation. First, the animations of the simulations were carefully inspected to ensure that all the contacts were behaving properly and that parts of the UAS and fan did not fictitiously pass through each other. Also, the total energy in the system, as well as energy in individual components, were analyzed to ensure reasonable transmission of energy between components and the overall stability of the simulation.

To analyze and compare the results of the different ingestion simulations, several analyses were performed to assess the relative difference between cases in terms of (i) overall damage to the fan, (ii) imbalance in the rotor, and (iii) containment.

(i) Two analyses are used to understand the overall damage in the system. Both analyses are important in understanding the ability of the fan to continue to provide thrust. The first analysis involves understanding the overall effective plastic strain in the fan at the end of the simulation. This is achieved by plotting the overall effective plastic strain in the fan at the end of the simulation to show the distribution of the damage over the entire fan surface and to understand the localized damage in each blade and how close it is to failure. The second analysis is a quantitative measure of the overall damage in the fan using the damage indicator D that is defined on each element as

$$D = \int \frac{\dot{\epsilon}_p}{\epsilon_{pf}} dt, \tag{1}$$

where $\dot{\epsilon}_p$ is the plastic strain evolution and ϵ_{pf} is the plastic failure strain. Note that D varies from 0 (no damage) to 1 (element failure) and is a measure of the cumulative plastic strain in the element. In order to get a quantitative assessment of the whole fan, a mass-weighted average of D is used for all elements to get a composite D_{fan}

$$D_{fan} = \frac{\sum_i^N m_i D_i}{\sum_i^N m_i}, \tag{2}$$

where N is the number of elements in the fan, m_i is the mass of the i^{th} element and D_i is the cumulative plastic strain in the i^{th} element. The D_{fan} metric quantifies the damage to the fan as a whole structure.

(ii) To understand the imbalance in the rotor due to the ingestion two analyses were carried out. Understanding the imbalance loads is important since it defines the structural and mount loads of the fan on the shaft. The first analysis identifies the center of gravity of each of the blades. A comparison of the pre- and post-impact center of gravities shows where damage occurs in the fan and how it relates to the steady state imbalance in the rotor. The second analysis computes the forces in the disk that are acting on the rigid shaft during the simulation. These forces give the overall transient loads acting on the shaft during and just after the UAS ingestion.

(iii) To understand the relative difference between the UAS ingestions in relation to containment, the energy imparted to the casing is tracked using the MATSUM card in LS-DYNA. It is important to understand if the ingestion is likely to produce high-energy debris beyond the capability of the containment system. Note that the predicted loads are expected to be very different for the two models based on the construction of the casing model. However, the trend in the energy imparted to the casing should be similar for the two different fan assembly models.

The following subsection will present a detailed comparison of the results from the live ingestion conditions, showing the plastic strain in the fans after the ingestion, the center of mass of the blades, loads on damaged and undamaged blades, and energies in components. After that, four additional cases will be compared to highlight the representative fan assembly model's similarity to the CFM56-7B fan assembly model and its ability to capture similar trends for different ingestion scenarios. Finally, a summary comparing the ingestions into the representative and CFM56-7B fan assembly models will be presented.

8.1 LIVE INGESTION CONDITIONS

This subsection provides a detailed comparison of the simulations of the UAS ingestion into the representative and CFM56-7B fan assembly models at the conditions of the live ingestion experiment. Note that the kinematics are shown in Section 7.1, and the individual blade damage is compared in Section 7.2, and both were found to be in very good agreement.

Contour plots of the front and rear views of the CFM56-7B and representative fan assembly models' effective plastic strain can be seen in Figure 53. These contour plots highlight the areas that sustained the most damage in the ingestion event. It should be noted that while similar plastic strain distribution is seen in the damaged blades, there is some small plastic strain in the leading edge area for all blades of the CFM56-7B model that is not seen in the representative model.

Additionally, there is more plastic strain in the disk of the CFM56-7B model when compared to the representative model, which can be attributed to the manner in which the model was created, as discussed in Section 5.3.2. Figure 53 shows that the damage is focused on the leading edge of several fan blades, causing plastic deformation. Several blades exhibit material loss along the leading edge, and one blade potentially leads to the liberation of a fan blade tip above the mid-span line. This would create an imbalance in the fan blades that would be less than the loss of a full fan blade, corresponding to a damage severity level 3 for both computational models. The damage level D_{fan} is 0.00156 for the CFM56-7B model and 0.00177 for the representative model, so there is slightly more overall damage in the representative fan assembly model.

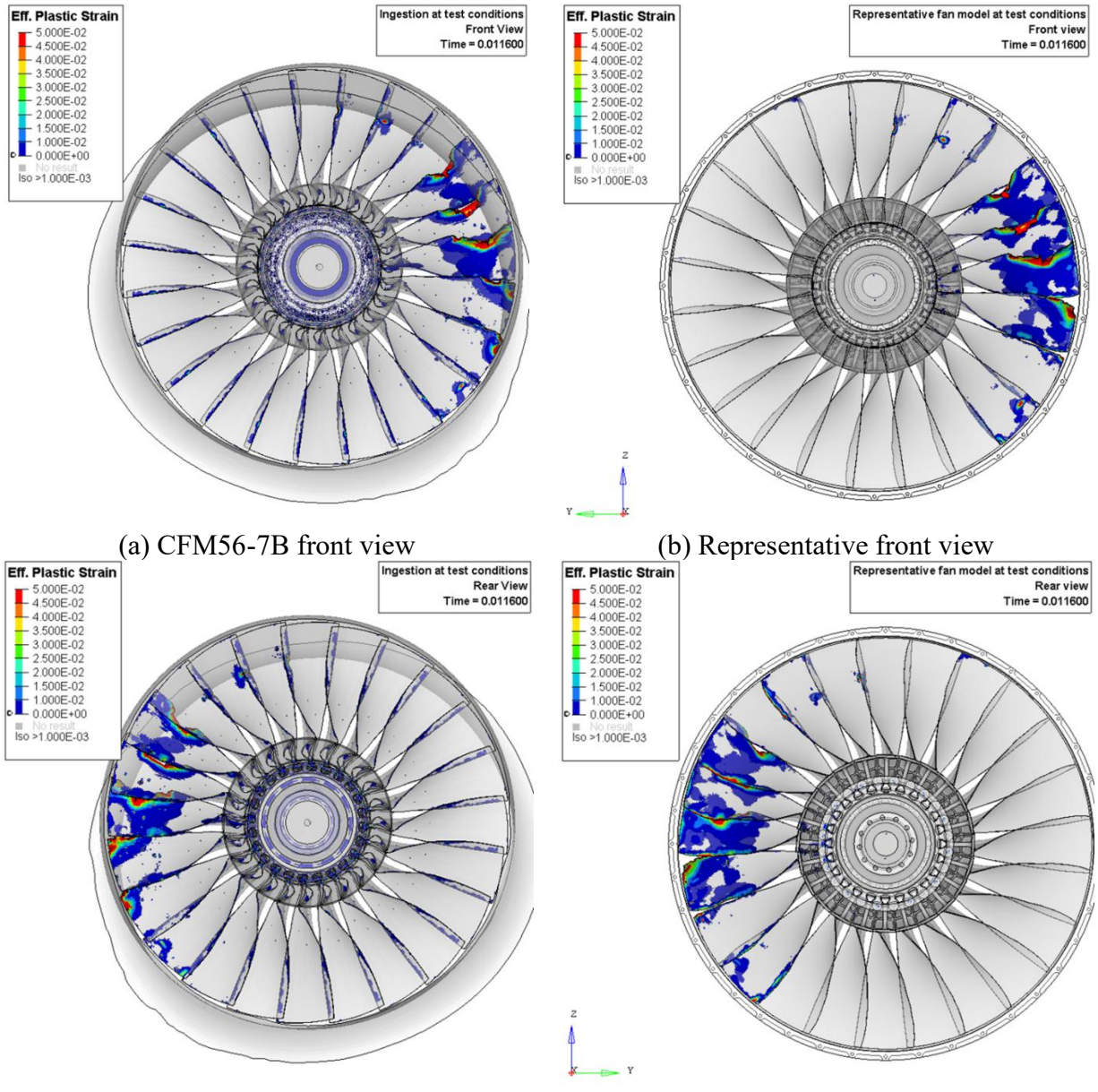

(a) CFM56-7B front view (b) Representative front view

(c) CFM56-7B rear view (d) Representative rear view

Figure 53. Effective plastic strain in the fan assembly models.

The steady-state imbalances in the fan assembly models can be related to the change in position of the center of mass of each fan blade from the ingestion event. The plots of this change for the CFM56-7B and representative fan assembly models are shown in Figure 54. It is clear that the change is very similar for both models, with a decrease in the center of mass of the blades that sustained the most damage, as can be seen in Figure 53a and Figure 53b. It should be noted that even though both computational models have similar fan diameters, the representative fan assembly model does not account for the dovetail in the center of mass calculation, while the CFM56-7B fan assembly model does. This accounts for the large difference in the average center of mass of the fan blades, given the fan diameters are similar in size. The resultant force in the disk is also looked at to gain an understanding of transient loads in the fan assembly during and just after the impact, and those results are included in Section 8.3.

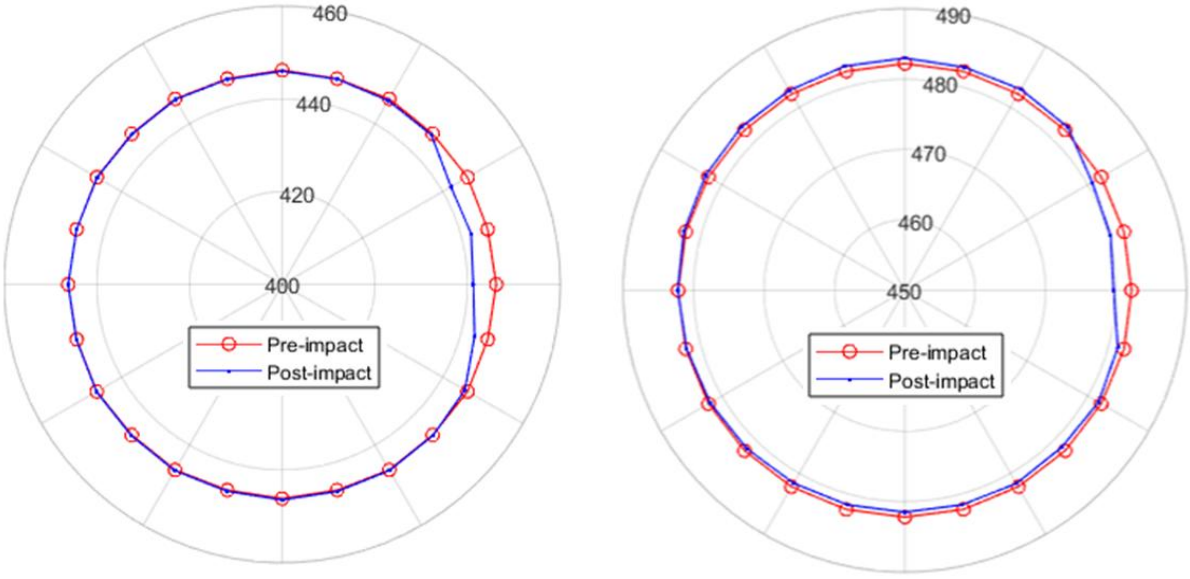

(a) CFM56-7B (b) Representative

Figure 54. Center of mass of blades pre- and post-impact.

The resultant force and moments from a sectional plane in both a damaged (impacted) and undamaged (not impacted) fan blade for both fan assemblies can be seen in Figure 55. The CFM56-7B and representative fan blades have very similar forcing and moment values for the impacted blades. For the moments on the undamaged blades, the magnitudes are similar but are out of phase. Overall, the agreement between the models is good.

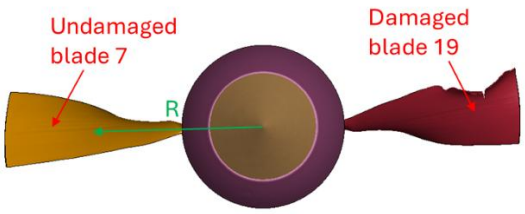

(a) Location of forces and moments of sectional plane on blades

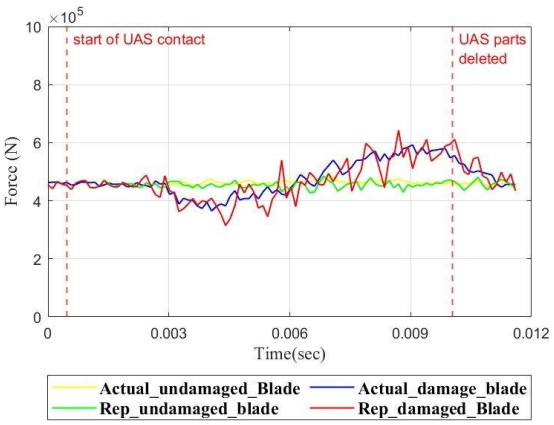

(b) Sectional force

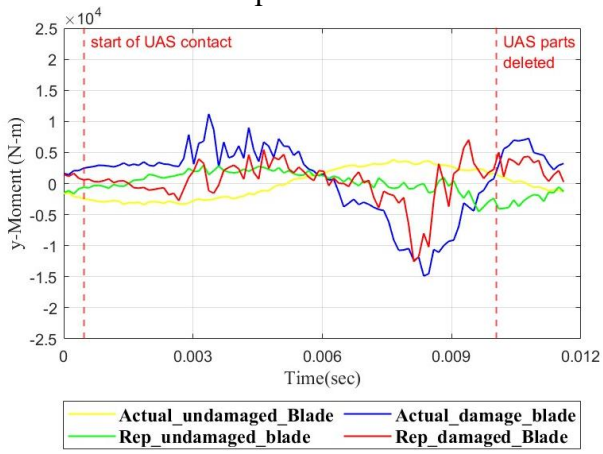

(c) Sectional moment in y-direction

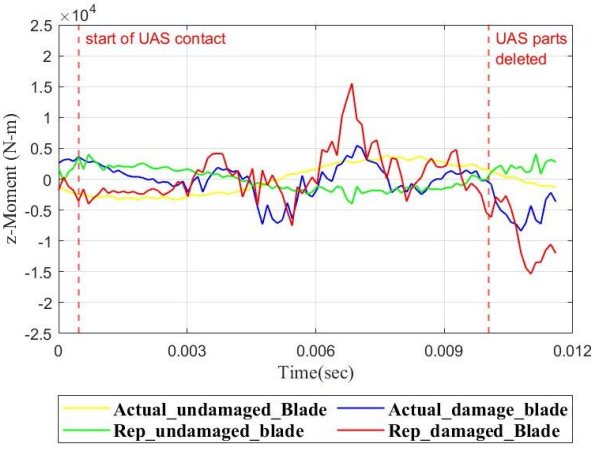

(d) Sectional moment in z-direction

Figure 55. Comparison of sectional force and moments in fan models.

Finally, overall energy and energy in particular components were explored and compared. The overall energy for the ingestion simulation can be seen in Figure 56. The energy is very similar for both simulations, where the bulk of the energy is in the kinetic energy of the rotating fan, and some additional kinetic energy is in the UAS. Internal and sliding interface energy increases from zero due to the impact. External work is due to the fan being driven, so external work is added to the fan to keep it at a maintained speed during the ingestion event. Hourglass energy is very small throughout the ingestion for both cases. The internal energy of both systems is of a different order of magnitude than the kinetic energy, making it difficult to see in the overall energy plots. This will be discussed more in the breakdown of the UAS and fan blade energies.

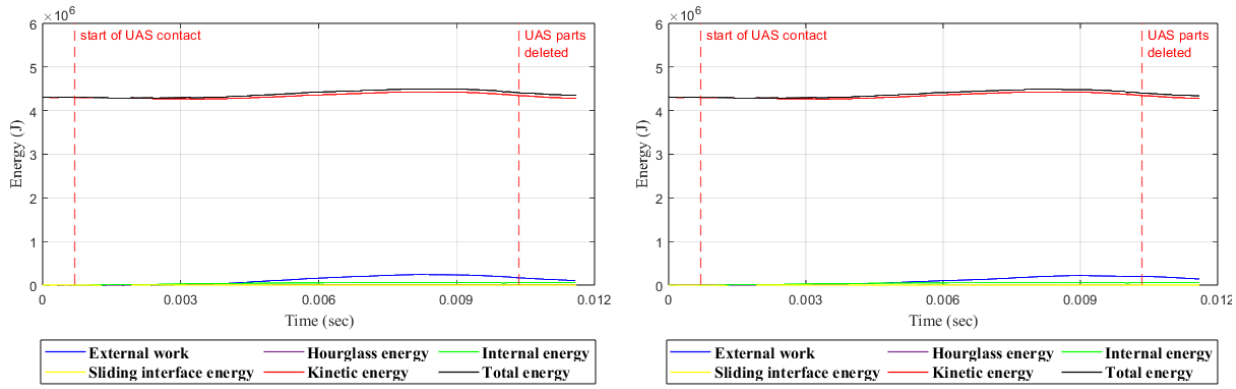

(a) CFM56-7B (b) Representative

Figure 56. Comparison of total energy during the simulation.

The internal and kinetic energies of the UAS projectile for both simulations can be seen in Figure 57 until they are deleted from the simulation. As the UAS contacts the fan blades, both the internal and kinetic energies of the UAS increase. This is because when the UAS contacts the fan blades, plastic deformation, and element failure occur, increasing the internal energy of the UAS. Also, while the UAS is impacting the rotating fan blades, the UAS parts are swept outwards by the angular velocity of the fan blades, which imparts more kinetic energy to the UAS. The kinetic energy of the UAS then decreases when the UAS parts impact the casing, reducing the speed of the UAS parts and transferring energy into the casing.

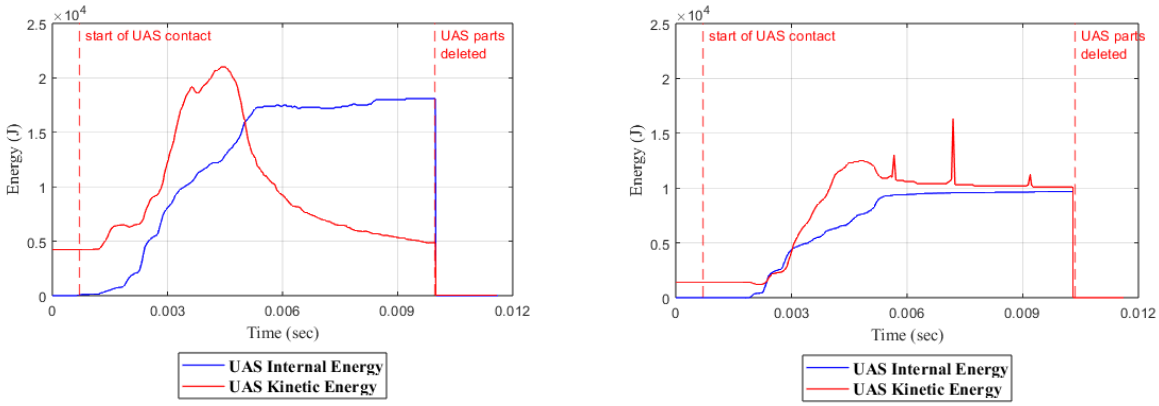

(a) CFM56-7B (b) Representative

Figure 57. Comparison of energy in UAS during ingestion simulation.

Figure 58 shows the velocities of the key components of the UAS, showing similar trends to those of the internal and kinetic energy plots of the UAS. The velocities of the parts increase when the individual parts come in contact with the fan blades. Note the similarity in the time the velocity starts to increase for each of the individual parts. The actual amount the velocity increases and how it accelerates and interacts with the casing is different between the models, as is expected since they have different geometries, but overall, they are in good agreement.

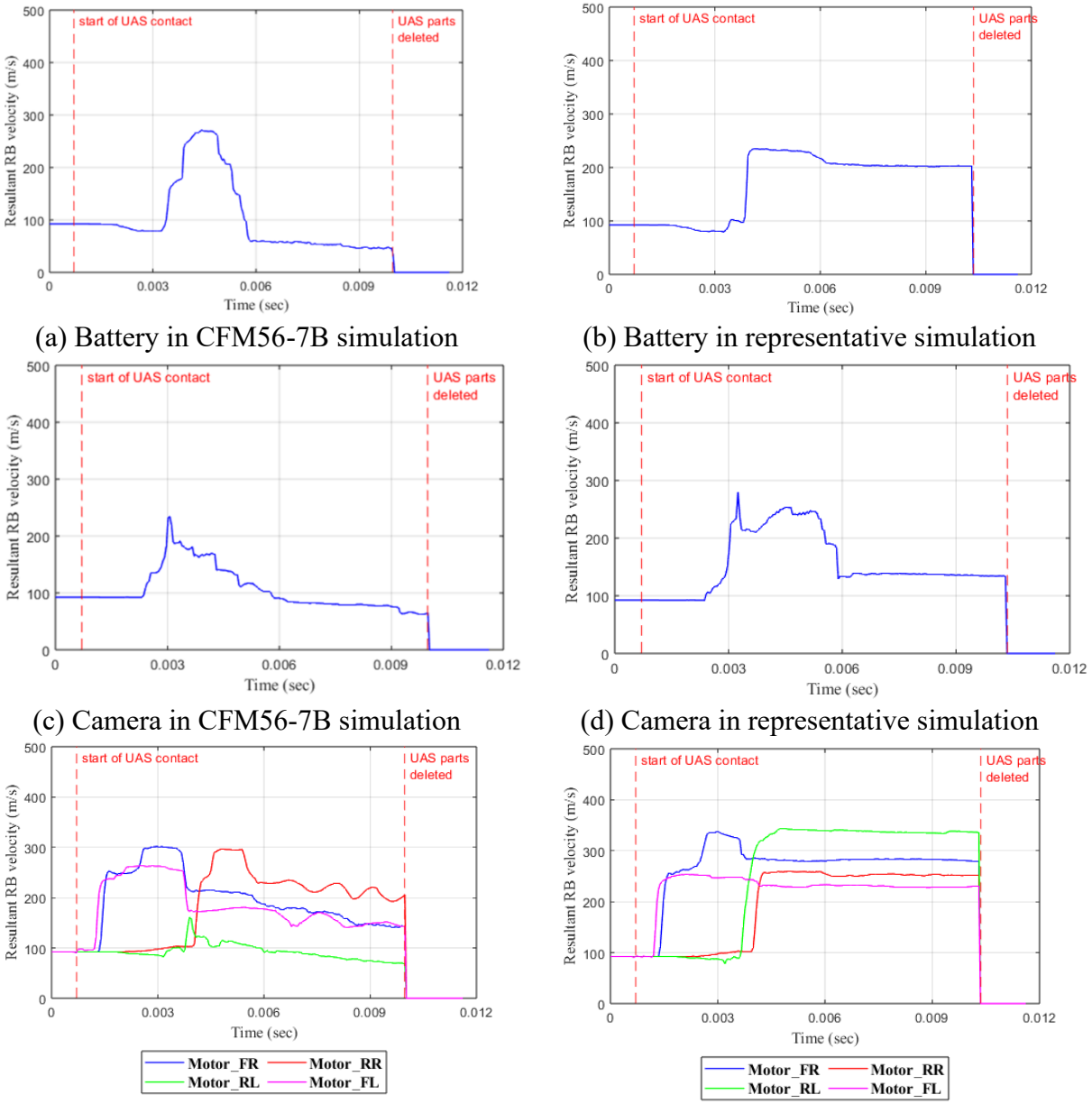

(a) Battery in CFM56-7B simulation

(b) Battery in representative simulation

(c) Camera in CFM56-7B simulation

(d) Camera in representative simulation

(e) Motors in CFM56-7B simulation

(f) Motors in representative simulation

Figure 58. Comparison of velocities of key UAS components during ingestion simulation.

Lastly, a breakdown of the internal and kinetic energies of the individual fan blades for both simulations can be seen in Figure 59. For both computational models, the fan blades were numbered to match the experimental fan blade numbering, with the top vertical blade at 0 seconds being labeled blade number 18 with the following blades in the clockwise direction counting down to 1 and the blades in the counterclockwise direction from blade number 18 counting up to 24 for a total of 24 blades in each computational model. The increase of kinetic and internal energies in the fan blades can be attributed to the UAS impact, causing the fan blades to deflect, increasing the kinetic energy, and causing plastic deformation and damage to the fan blades, creating internal energy. For both computational model setups, the bulk of the UAS contact with the fan blades was

between fan blades 10 through 18, with fan blade 13 having the highest internal and kinetic energies, followed by blades 14, 15, 12, and 11. It is also important to note the increase in internal energy in all fan blades that were not in contact with the UAS, as seen with the blue lines for the CFM56-7B model. This is due to several assumptions made during the model development process described in Section 5.3.2, which can be seen in the plastic strain in the model, specifically the leading edge of all the CFM56-7B blades in Figure 53.

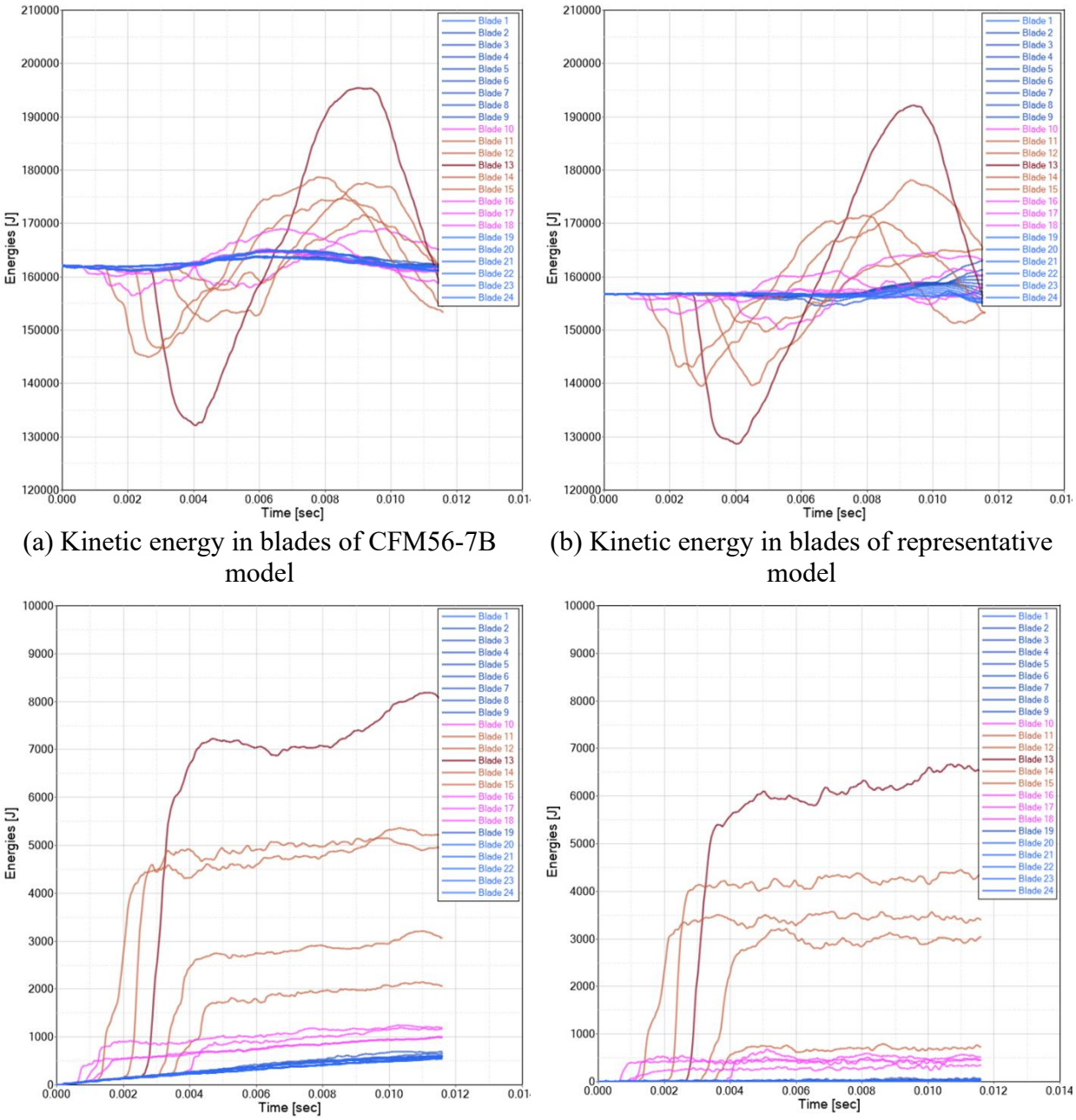

(a) Kinetic energy in blades of CFM56-7B model

(b) Kinetic energy in blades of representative model

(c) Internal energy in blades of CFM56-7B model

(d) Internal energy in blades of representative model

Figure 59. Energy in individual blades during ingestion simulations.

8.2 ADDITIONAL INGESTION SIMULATION COMPARISONS

Four additional computational studies were defined for this work using different UAS orientations, relative velocities, and impact locations matching those conducted in previous UAS engine ingestion research into the generic representative fan assembly model[4]. The additional computational studies matching the previous engine ingestion research are defined in Table 8.

Table 8. Description of additional ingestion simulations.

Simulation identification	Fan Speed	Relative translational velocity	Impact location	Orientation of UAS	Fan damage severity level
HFS_LRV_HRS_Nom	High	Low	High	0°	Level 3
HFS_HRV_HRS_180R	High	High	High	180° roll	Level 3
HFS_HRV_LRS_90P	High	High	Low	90° pitch	Level 1
HFS_HRV_LRS_Nom	High	High	Low	0°	Level 2

The nomenclature for the simulation identification in Table 8 is given in Table 9. The high and low parameters defined for the simulations correspond to two different values for ease of referencing. The high fan speed corresponds to the maximum speed for the fan, which is 5,175 RPM (541.9 rad/s). The low relative translational velocity corresponds to the minimum takeoff speed for this engine of 66.88 m/s (130 knots). The high translational relative velocity corresponds to the maximum speed for an aircraft below 3,048 m (10,000 ft) of 128.6 m/s (250 knots). The low radial impact location corresponds to around a 10% radial span impact, and a high impact location to around an 80% radial span impact location. It should be noted that the impact locations were chosen to be the highest and lowest impact locations for the center of mass of the UAS where no portion of the UAS directly impacts the casing or the nose cone.

Table 9. Nomenclature of additional simulations.

Definitions	Parameters
Rotational fan speed	High fan speed (HFS)
Relative translational velocity	High relative translational velocity (HRV) and low relative translational velocity (LRV)
Span impact location	High radial span (HRS) and low radial span (LRS)
UAS impact orientation	0° (Nom), 90° pitch (90P), and 180° roll (180R)

The orientation and radial location of the UAS before it hits the fan for each of the cases defined in Table 8 is shown in Figure 60.

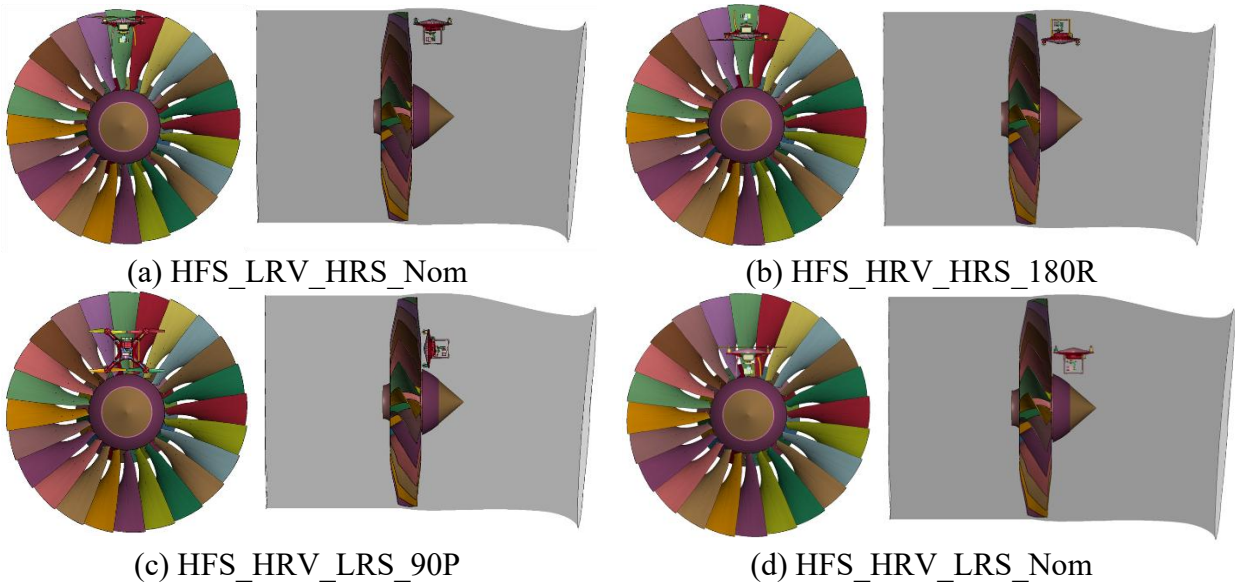

(a) HFS_LRV_HRS_Nom (b) HFS_HRV_HRS_180R

(c) HFS_HRV_LRS_90P (d) HFS_HRV_LRS_Nom

Figure 60. Orientation of UAS for additional simulations.

These simulations were specifically chosen to verify if the fan blade model developed from the CFM56-7B engine behaves similarly to the representative fan assembly model used in previous UAS ingestion research for a wide spectrum of conditions. HFS_LRV_ HRS_Nom was chosen due to the high levels of blade damage seen, while HFS_HRV_HRS_180R was chosen for the high levels of disk force seen. Both HFS_HRV_LRS_90P and HFS_HRV_LRS_Nom were chosen for their decreased damage severity levels to see if the CFM56-7B fan assembly model would have the same damage severity level (defined in Table 7) for the different ingestion simulations.

It is important to note that all the simulations using the CFM56-7B fan assembly model and the simulation of the representative fan assembly model matching the experimental test were run on LS-DYNA R11.0.0. In contrast, simulations of the representative fan assembly model used to study additional UAS ingestion conditions were run on LS-DYNA R10.1.0, which may account for some differences in the results in this section. The additional simulations were a comparison with the previous work carried out in the A17 project, and the older version of LS-DYNA was no longer available to the researchers when carrying out the current study.

The following subsections compare the ingestion of the UAS into the CFM56-7B and representative fan assembly models for the four cases given in Table 8. The simulations were carried out in a very similar manner to the live ingestion case, and the previous study focused on the representative fan assembly model[4]. Each of the cases will compare the kinematics, effective plastic strain, D_{fan}, damage severity level, and center of mass of the blades. The overall force in the disk and energy in the casing will also be discussed in Section 8.3. Note that the resultant force and moments in a sectional plane of the blade, energies in the overall system and component parts, and velocities of the UAS were also studied and found to be similar and consistent with the discussion for the live engine ingestion test case. For each of the simulations, the fan blade model was rotated for one full revolution, which is about 11.6 ms.

8.2.1 HFS_LRV_HRS_Nom

This additional computational study corresponded to a high fan speed, low UAS relative velocity, high UAS radial span impact, and nominal UAS position. The kinematics of the ingestion event for the CFM56-7B fan assembly model can be seen in Figure 61. The fan was simulated to make one full revolution, which was around 11.6 ms. It should be noted that the UAS parts were deleted once they cleared the contact region with the fan blades, which was around 7.3 ms for the CFM56-7B fan assembly model and around 6.4 ms for the representative fan assembly model to increase the computational efficiency of the simulation.

For the CFM56-7B fan assembly model, it is important to note that at around 3.4 ms, elements 90,119,534 and 90,119,551 from the front right motor anchor were deleted due to excessive element deformation. This represents 0.00071% of the total UAS mass, and these elements were deleted after passing through the contact region of the fan blades, so manually removing these elements has little effect on the overall simulation. Additionally, at around 5.4 ms, several UAS parts had to be deleted from the simulation due to high hourglass energy, which are given in Table 10.

Table 10. UAS parts deleted for high hourglass energy in HFS_LRV_HRS_Nom.

Part ID	Part	% of total UAS mass	Past fan blade contact region
90000019	Bottom PC Board Connector	0.03	Yes
90000023	Battery Cells 1 1	3.04	No
90000024	Battery Cells 1 2	3.04	No
90000028	Battery Cells 2 1	3.04	No
90000029	Battery Cells 2 2	3.04	Yes
90000033	Battery Cells 3 1	3.04	No
90000034	Battery Cells 3 2	3.04	Yes
90000038	Battery Cells 4 1	3.04	Yes
90000039	Battery Cells 4 2	3.04	No
90000082	Motor Stator Front Right	2.22	No
90000086	Motor Stator Rear Right	2.22	No
90000094	Motor Stator Front Left	2.22	Yes
90000101	Circuit Board Solids	3.55	Yes
90000104	Camera Carcass	1.96	Yes
90000120	Back Casing 0.813mm	0.12	No

A total of 36.6% of the total UAS mass was deleted at around 5.4 ms, with the most common part with high hourglass energy being battery parts. However, when only looking at the deleted UAS parts that were not past the fan blade contact region, the total mass deleted is reduced to 26.1% of the total UAS mass. While this is a significant amount of the total UAS mass, this should not significantly affect the overall results of the simulation as the parts were deleted after the primary impact between the UAS and fan blades, so most of the energy would have already been transferred with smaller secondary impacts occurring afterward.

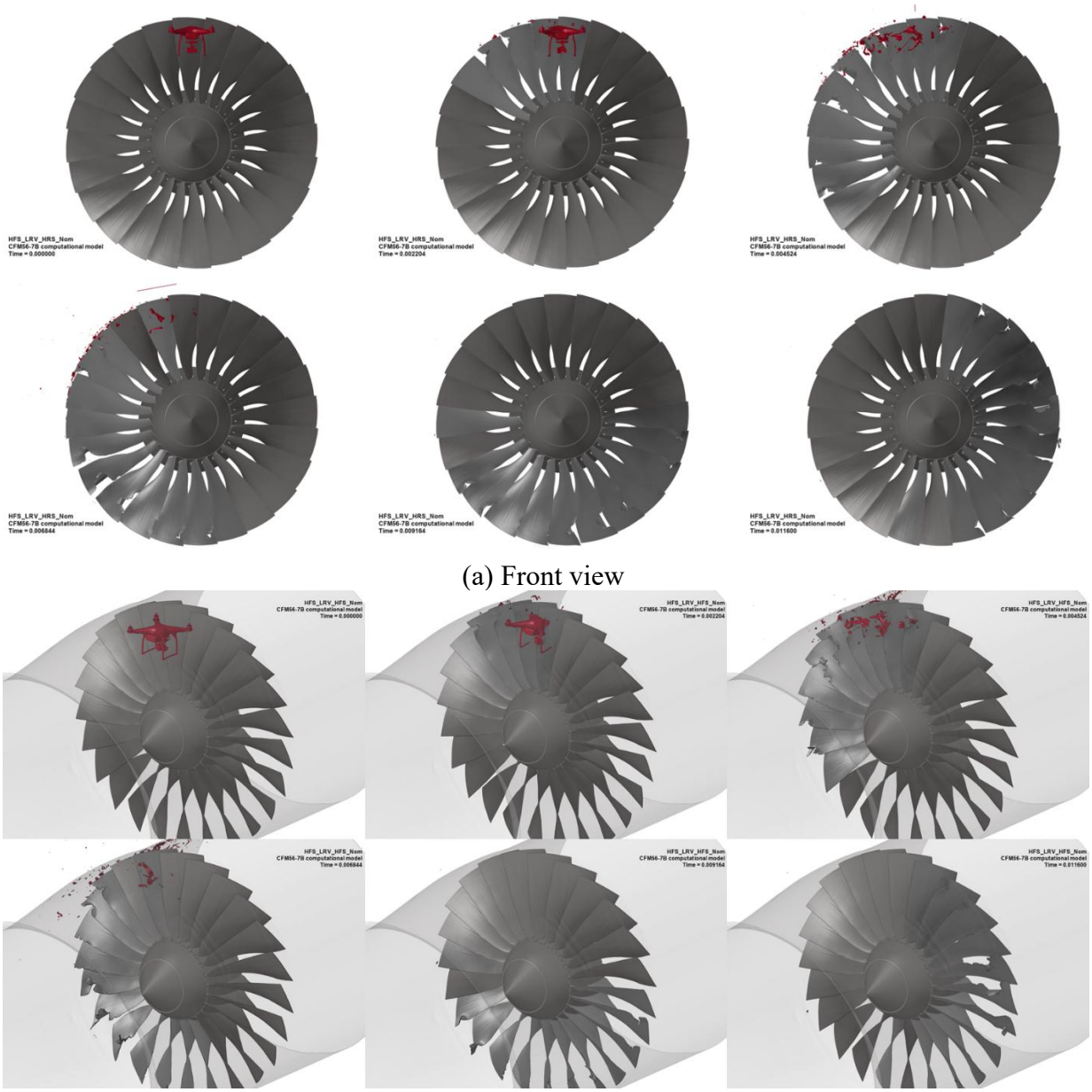

(a) Front view

(b) Isometric view

Figure 61. HFS_LRV_HRS_Nom CFM56-7B fan assembly model ingestion kinematics.

The kinematics of the ingestion event for the representative fan assembly model can be seen in Figure 62.

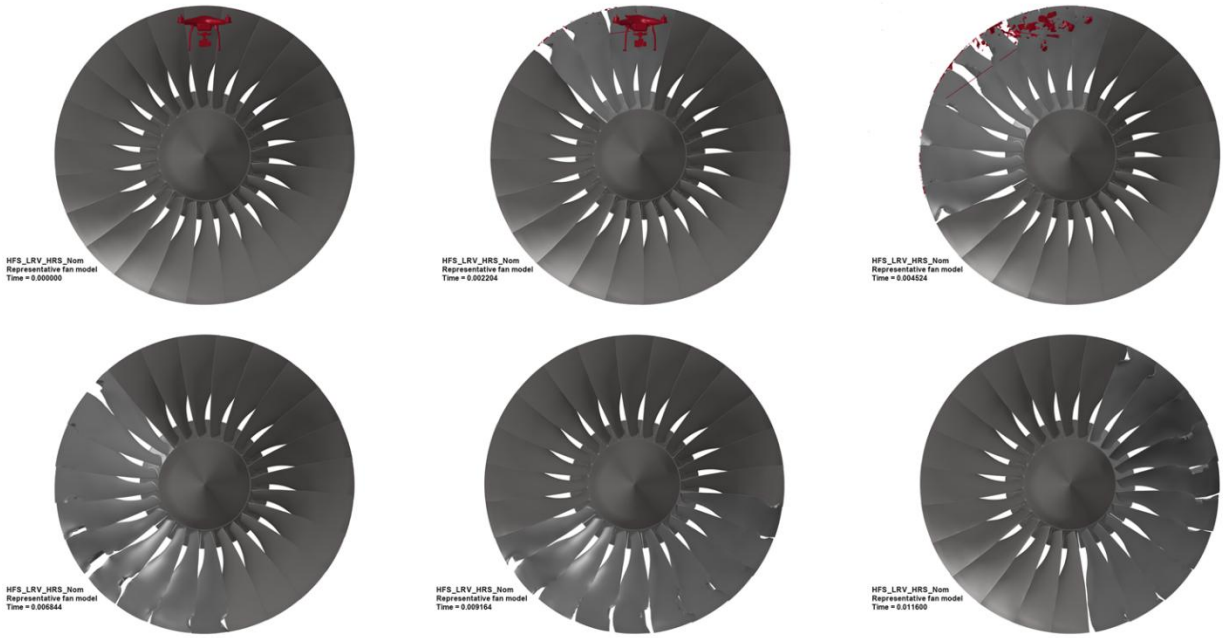

(a) Front view

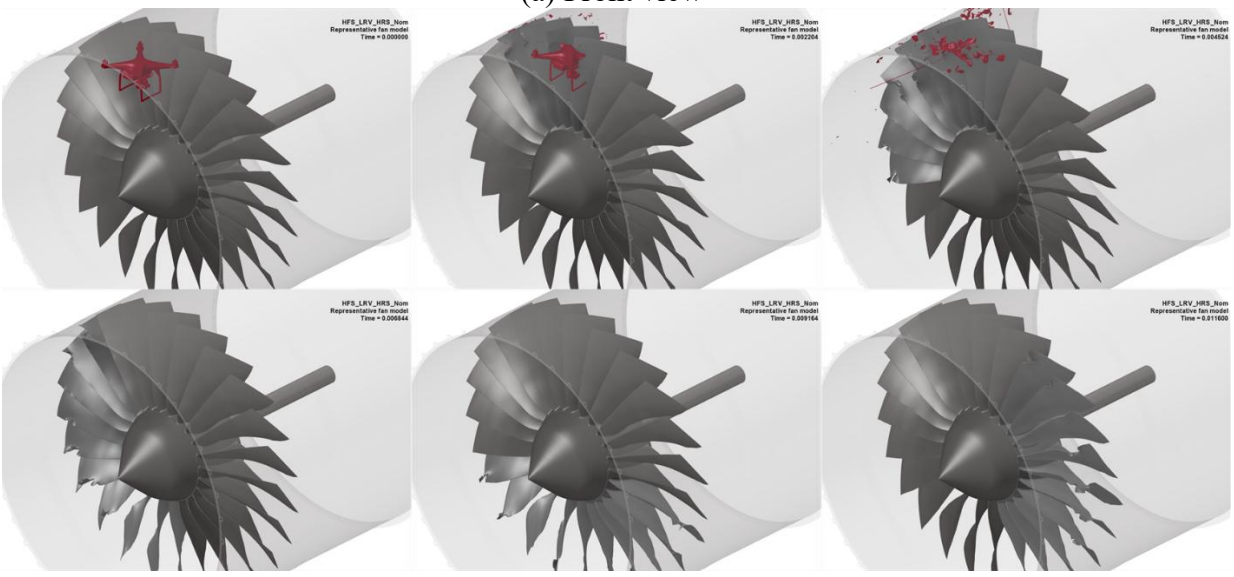

(b) Isometric view

Figure 62. HFS_LRV_HRS_Nom representative fan assembly model ingestion kinematics.

The similarity in the ingestion kinematics is evident for the two models. The UAS is completely obliterated during the ingestion, and very similar blades in the fan are impacted and damaged.

Contour plots of the front and rear views of the CFM56-7B and representative fan assembly models' effective plastic strain can be seen in Figure 63. These contour plots highlight the areas that sustained the most damage in the ingestion event. It should be noted that while similar plastic strain distribution is seen in the damaged blades, there is some small plastic strain in the leading edge area for all blades of the CFM56-7B model that is not seen in the representative model.

Additionally, there is more plastic strain in the disk of the CFM56-7B model when compared to the representative model, which can be attributed to the manner in which the model was created, as discussed in Section 5.3.2. Figure 63 shows that the damage is focused on the leading edge of several fan blades, causing plastic deformation with several blades exhibiting material loss along the leading edge and a couple of blades potentially leading to a liberation of their blade tip above the mid-span line. This would create an imbalance in the fan that would be less than the loss of a full fan blade, corresponding to a damage severity level 3 for both computational models. The damage level D_{fan} is 0.00172 for the CFM56-7B model and 0.00176 for the representative model, so there is slightly more overall damage in the representative fan assembly model.

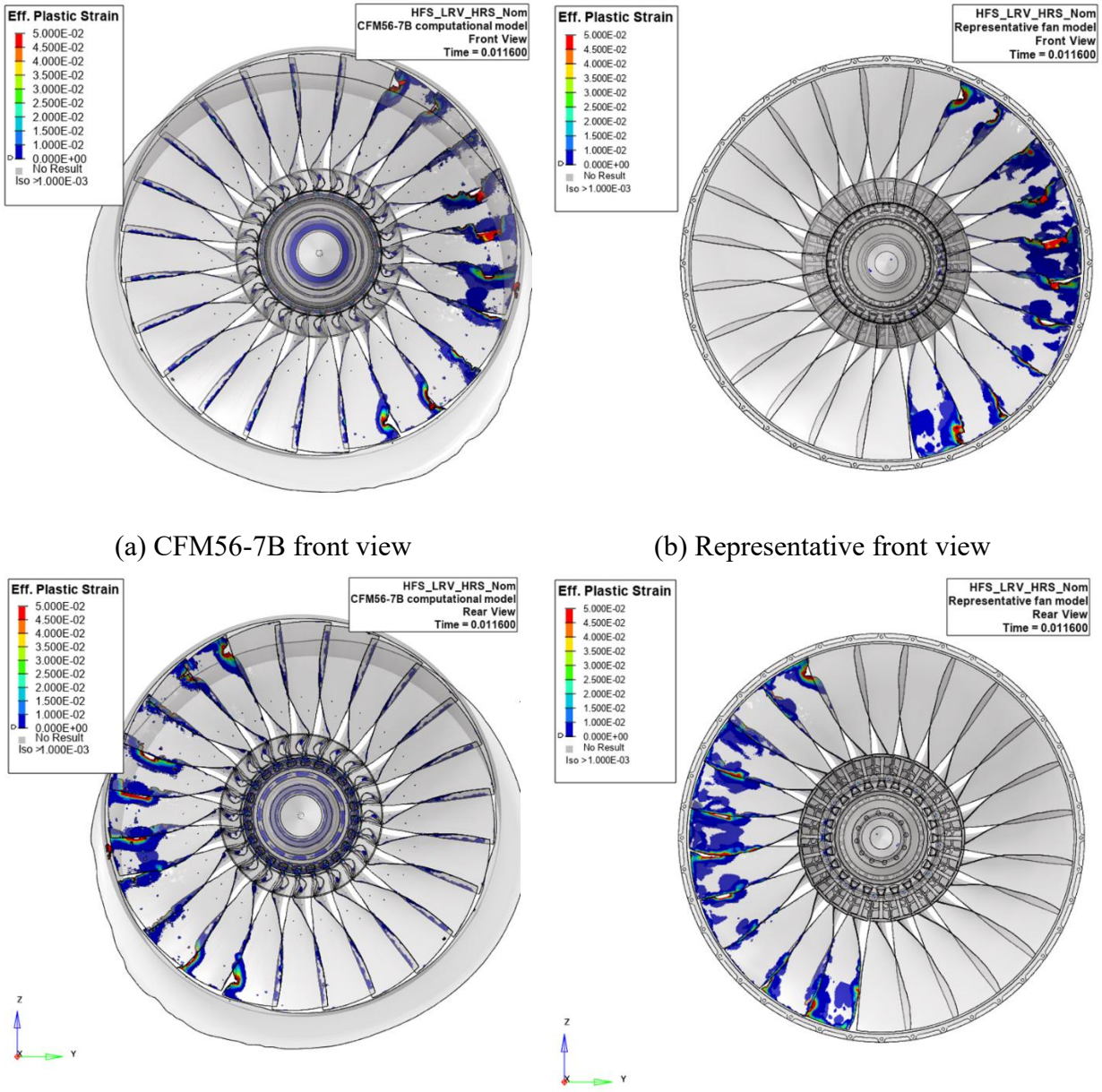

(a) CFM56-7B front view

(b) Representative front view

(c) CFM56-7B rear view

(d) Representative rear view

Figure 63. HFS_LRV_HRS_Nom effective plastic strain in the fan assembly models.

The steady-state imbalances in the fan assembly models can be related to the change in position of the center of mass of each fan blade from the ingestion event. The plots of this change for the CFM56-7B and representative fan assembly models are shown in Figure 64. It is clear that the change is very similar for both models, with a decrease in the center of mass of the blades that sustained the most damage. It should be noted that even though both computational models have similar fan diameters, the representative fan assembly model does not account for the dovetail in the center of mass calculation. In contrast, the CFM56-7B fan assembly model does. This accounts for the large difference in the average center of mass of the fan blades, given the fan diameters are similar in size. The resultant force in the disk is also looked at to gain an understanding of transient loads in the fan assembly during and just after the impact, with those results discussed in Section 8.3.

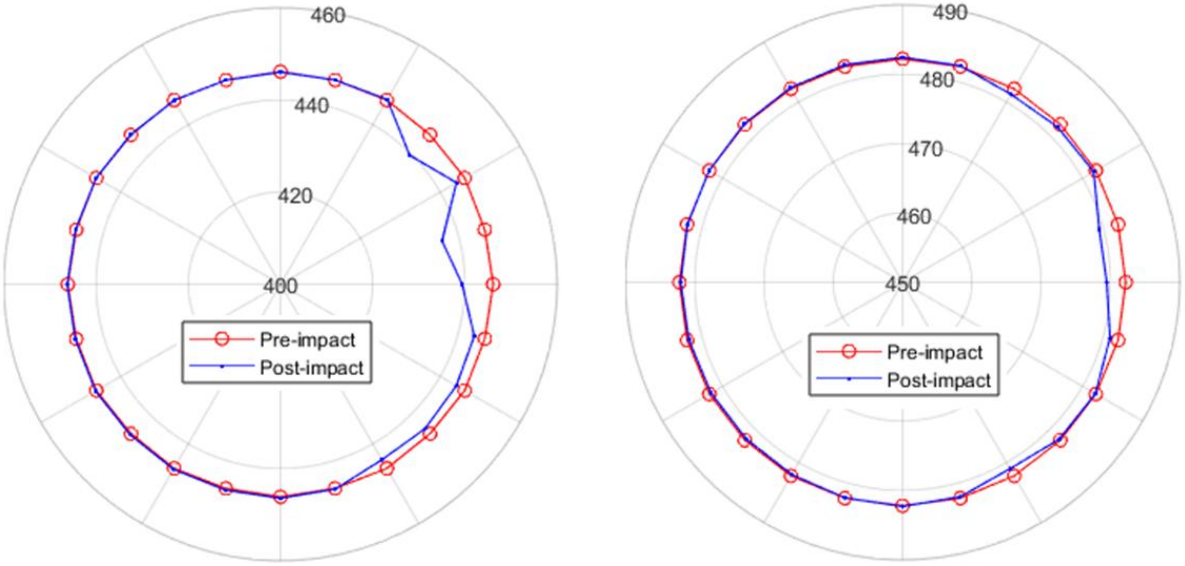

(a) CFM56-7B (b) Representative

Figure 64. HFS_LRV_HRS_Nom center of mass of blades pre- and post-impact.

8.2.2 HFS_HRV_HRS_180R

This additional computational study corresponded to a high fan speed, high UAS relative velocity, high UAS radial span impact, and 180° roll orientation for the UAS. The kinematics of the ingestion event for the CFM56-7B fan assembly model can be seen in Figure 65. The fan was simulated to make one full revolution, which was around 11.6 ms. It should be noted that the UAS parts were deleted once they cleared the contact region with the fan blades, which was around 5.7 ms for the CFM56-7B fan assembly model and 7.3 ms for the representative fan assembly model to increase the computational efficiency of the simulation.

For the CFM56-7B fan assembly model, it is important to note that at around 5.1 ms, elements 90,137,616 and 90,137,621 from the rear right motor anchor were deleted due to excessive element deformation. This represents 0.00026% of the total UAS mass, and these elements were deleted after passing through the contact region of the fan blades, so manually removing these elements has little effect on the overall simulation.

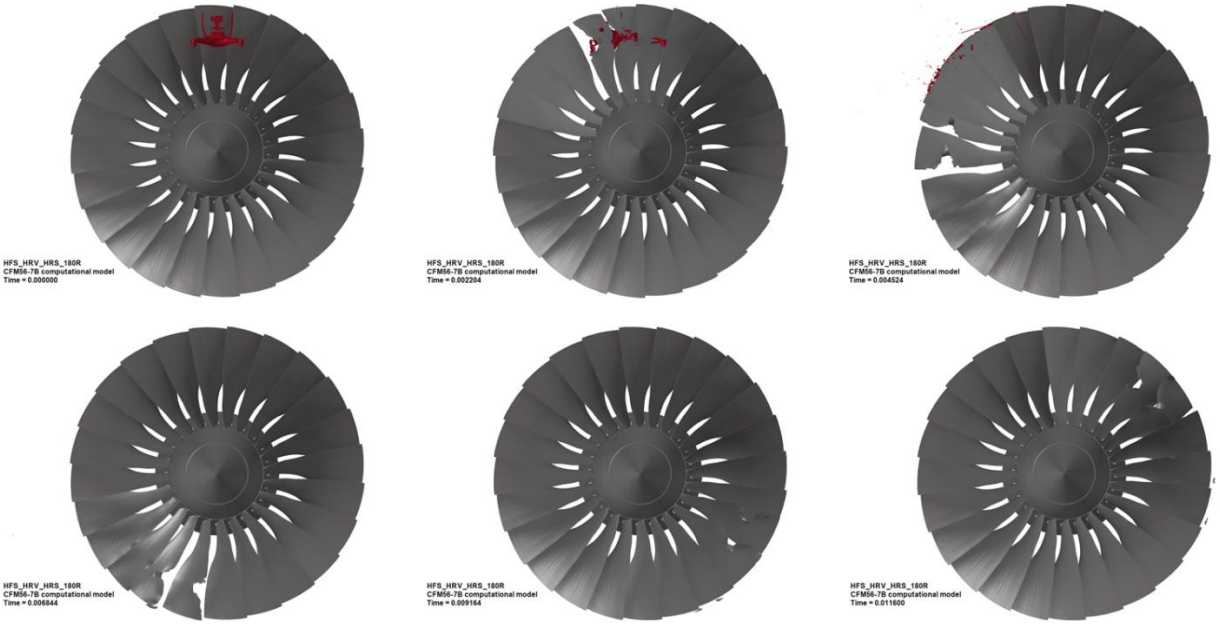

(a) Front view

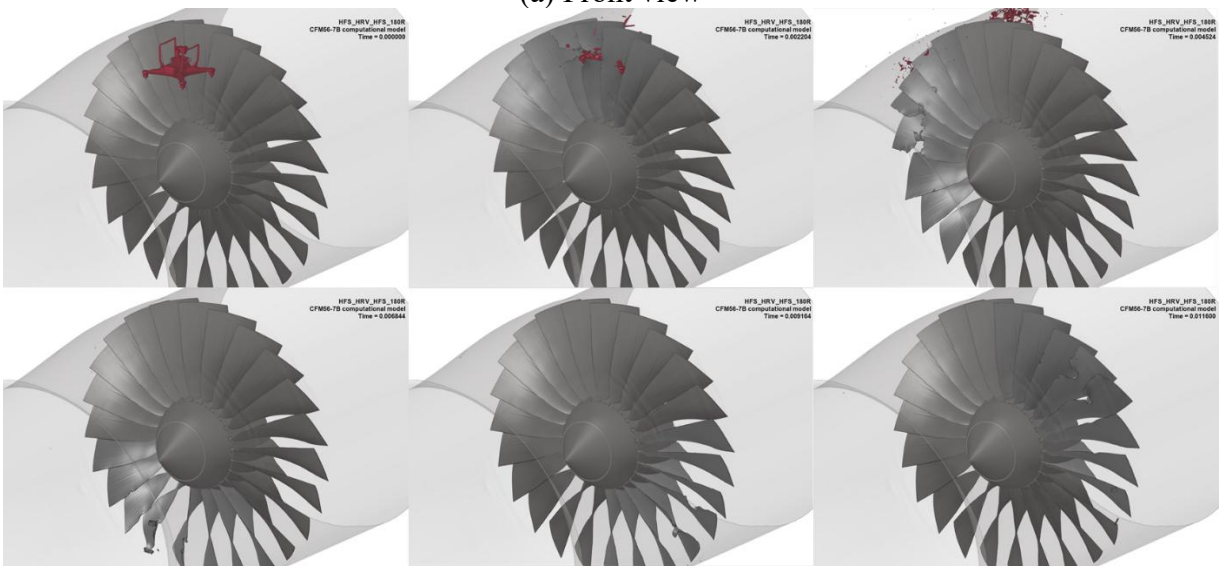

(b) Isometric view

Figure 65. HFS_HRV_HRS_180R CFM56-7B fan assembly model ingestion kinematics.

The kinematics of the ingestion event for the representative fan assembly model can be seen in Figure 66.

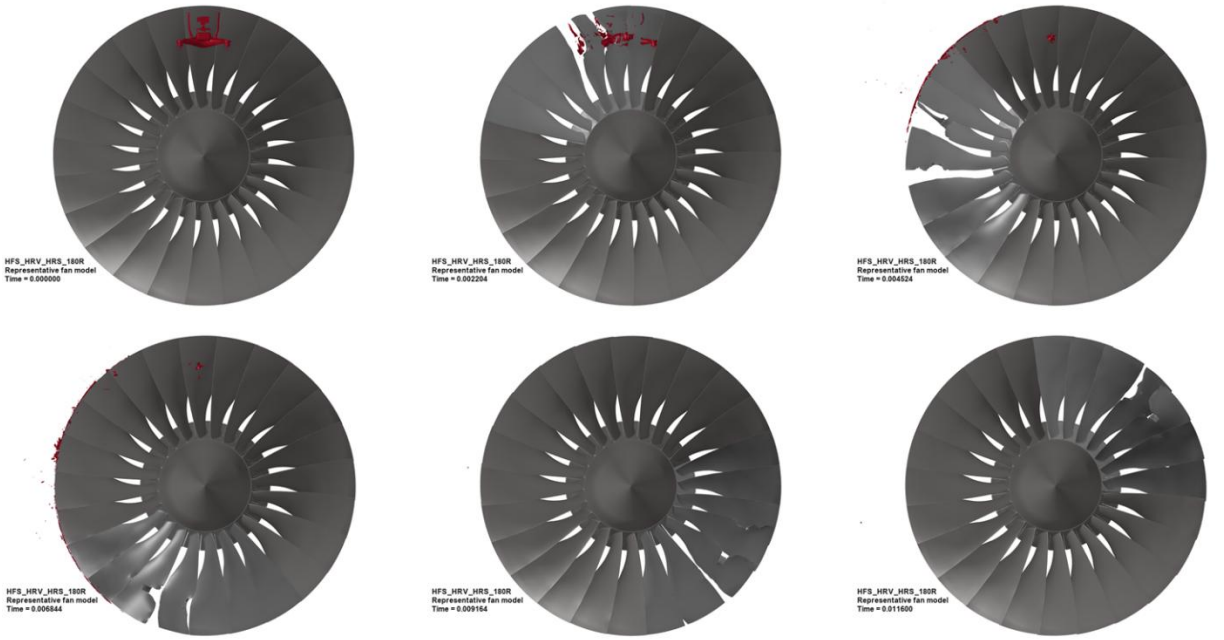

(a) Front view

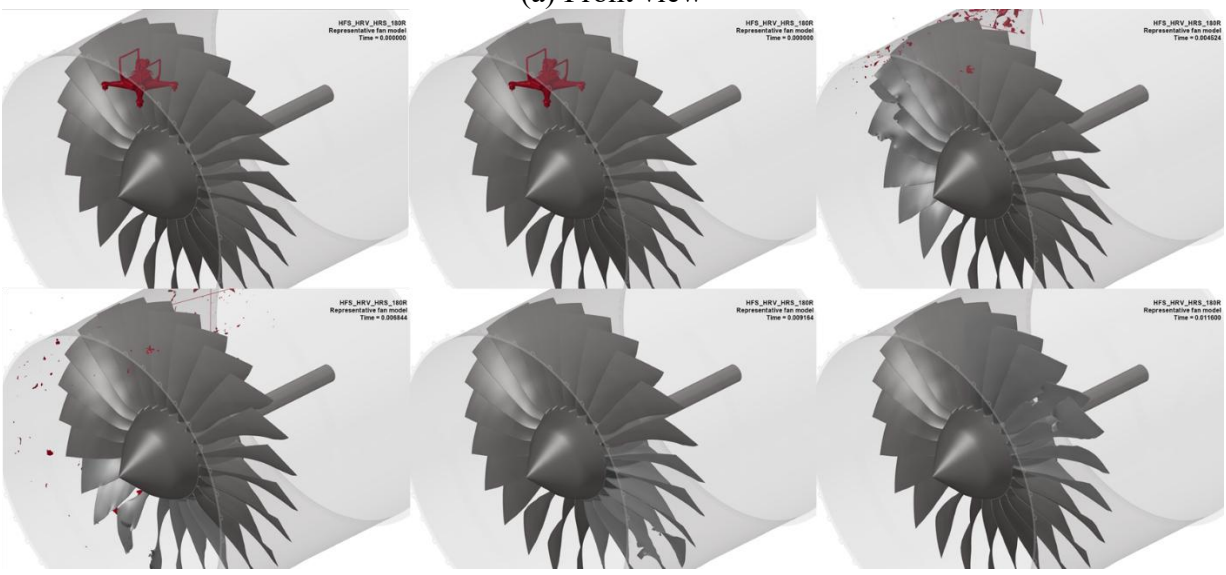

(b) Isometric view

Figure 66. HFS_HRV_HRS_180R representative fan assembly model ingestion kinematics.

The similarity in the ingestion kinematics is evident for the two models. The UAS is completely obliterated during the ingestion, and very similar blades in the fan are impacted and damaged.

Contour plots of the front and rear views of the CFM56-7B and representative fan assembly models' effective plastic strain can be seen in Figure 67. These contour plots highlight the areas that sustained the most damage in the ingestion event. It should be noted that while similar plastic strain distribution is seen in the damaged blades, there is some small plastic strain in the leading edge area for all blades of the CFM56-7B model that is not seen in the representative model.

Additionally, there is more plastic strain in the disk of the CFM56-7B model when compared to the representative model, which can be attributed to the manner in which the model was created, as discussed in Section 5.3.2. Figure 67 shows that the damage is focused on the leading edge of two fan blades, causing plastic deformation and the formation of a significant crack along the leading edge of these two blades, which could potentially lead to the liberation of their blade tip above the mid-span line. This would create an imbalance in the fan that would be less than the loss of a full fan blade, corresponding to a damage severity level 3 for both computational models. The damage level D_{fan} is 0.00121 for the CFM56-7B model and 0.00112 for the representative model, so there is slightly more overall damage in the CFM56-7B fan assembly model.

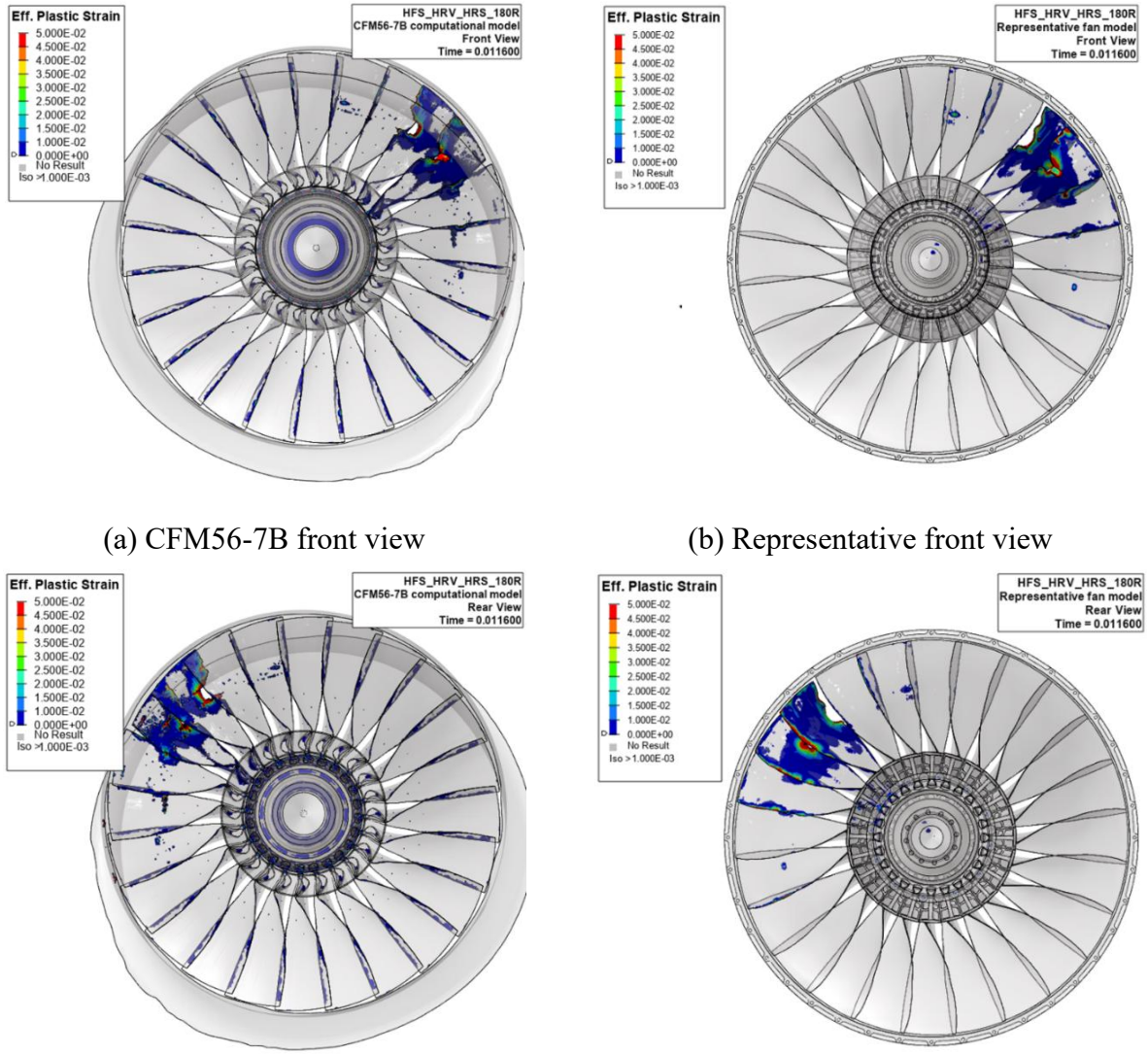

(a) CFM56-7B front view

(b) Representative front view

(c) CFM56-7B rear view

(d) Representative rear view

Figure 67. HFS_HRV_HRS_180R effective plastic strain in the fan assembly models.

The steady-state imbalances in the fan assembly models can be related to the change in position of the center of mass of each fan blade from the ingestion event. The plots of this change for the

CFM56-7B and representative fan assembly models are shown in Figure 68. It is clear that the change is similar for both models, with a decrease in the center of mass of the blades that sustained the most damage. It should be noted that even though both computational models have similar fan diameters, the representative fan assembly model does not account for the dovetail in the center of mass calculation, while the CFM56-7B fan assembly model does. This accounts for the large difference in the average center of mass of the fan blades, given the fan diameters are similar in size. The resultant force in the disk is also looked at to gain an understanding of transient loads in the fan assembly during and just after the impact, and those results are included in Section 8.3.

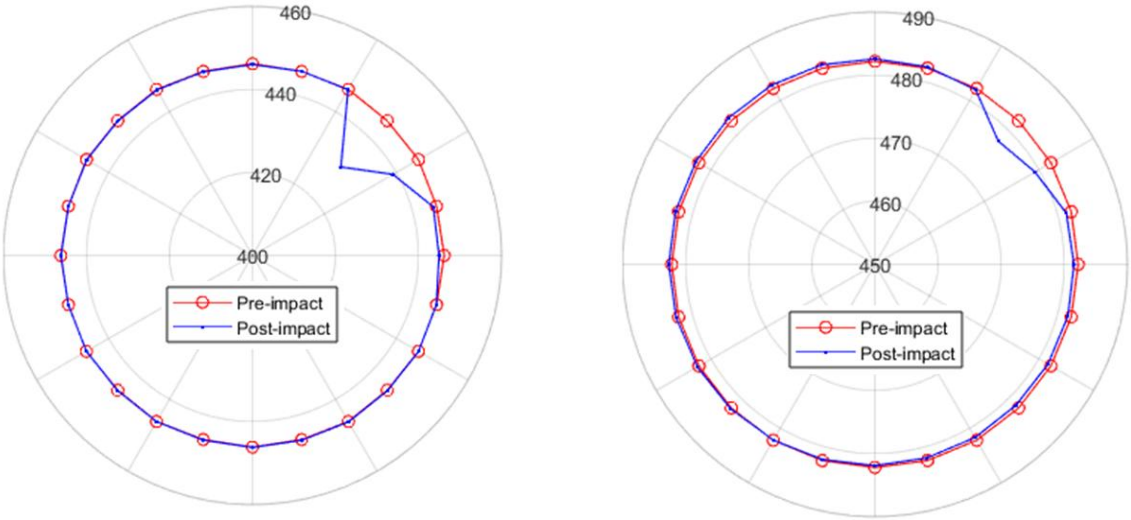

(a) CFM56-7B (b) Representative

Figure 68. HFS_HRV_HRS_180R center of mass of blades pre- and post-impact.

8.2.3 HFS_HRV_LRS_90P

This additional computational study corresponded to a high fan speed, high UAS relative velocity, low UAS radial span impact, and 90° pitch orientation for the UAS. The kinematics of the ingestion event for the CFM56-7B fan assembly model can be seen in Figure 69. The fan was simulated to make one full revolution, which is around 11.6 ms. It should be noted that the UAS parts were deleted once they cleared the contact region with the fan blades, which was around 5.9 ms for the CFM56-7B fan assembly model and 5.3 ms for the representative fan assembly model to increase the computational efficiency of the simulation. For the CFM56-7B fan assembly model, it is important to note that the UAS was translated back 15 mm (axial direction of fan blades) to prevent a fictitious contact with a gimbal part and the fan blade where the fan blade fictitiously passed through the gimbal part causing the parts to become stuck to one another. This small translation should have little to no effect on the overall results of the simulation.

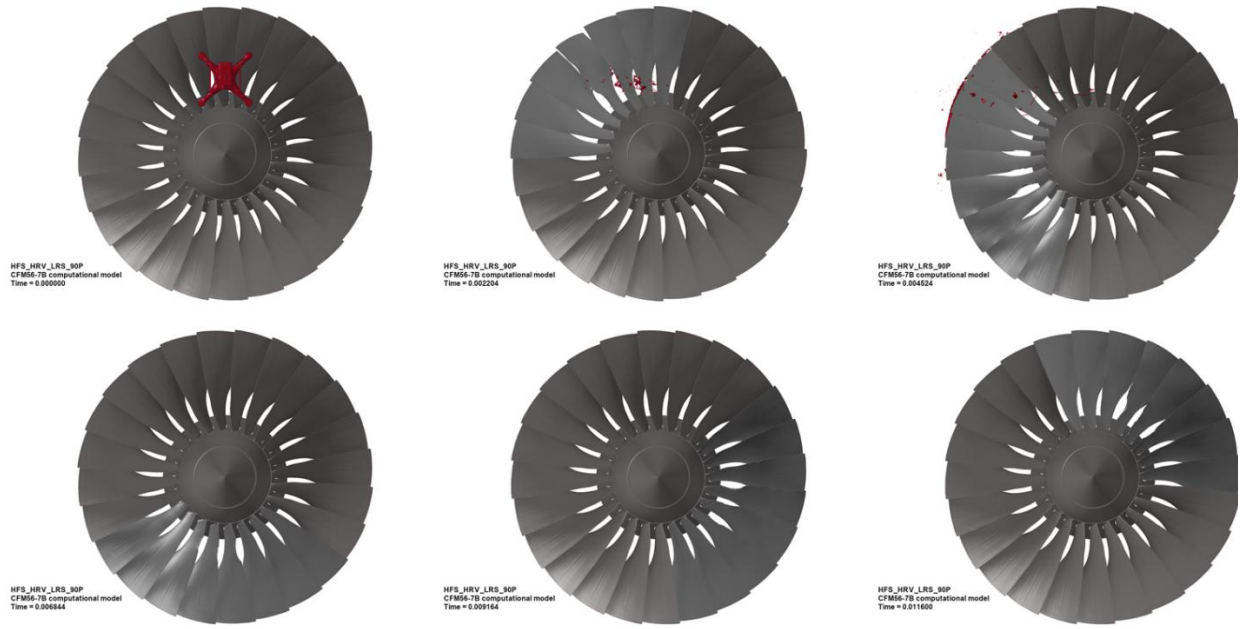

(a) Front view

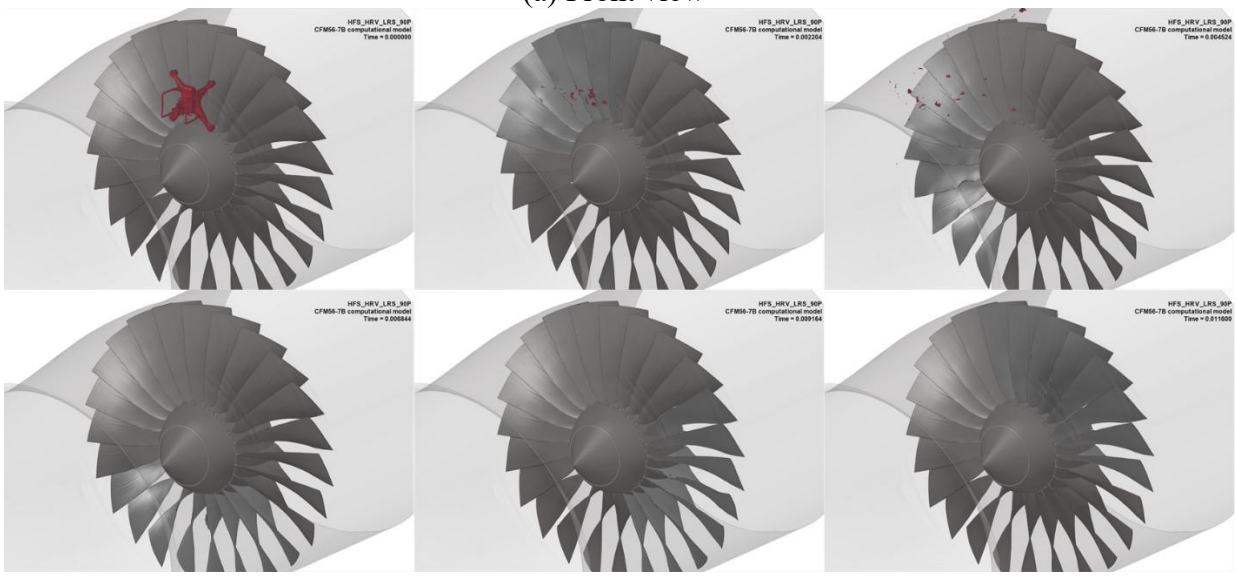

(b) Isometric view

Figure 69. HFS_HRV_LRS_90P CFM56-7B fan assembly model ingestion kinematics.

The kinematics of the ingestion event for the representative fan assembly model can be seen in Figure 70.

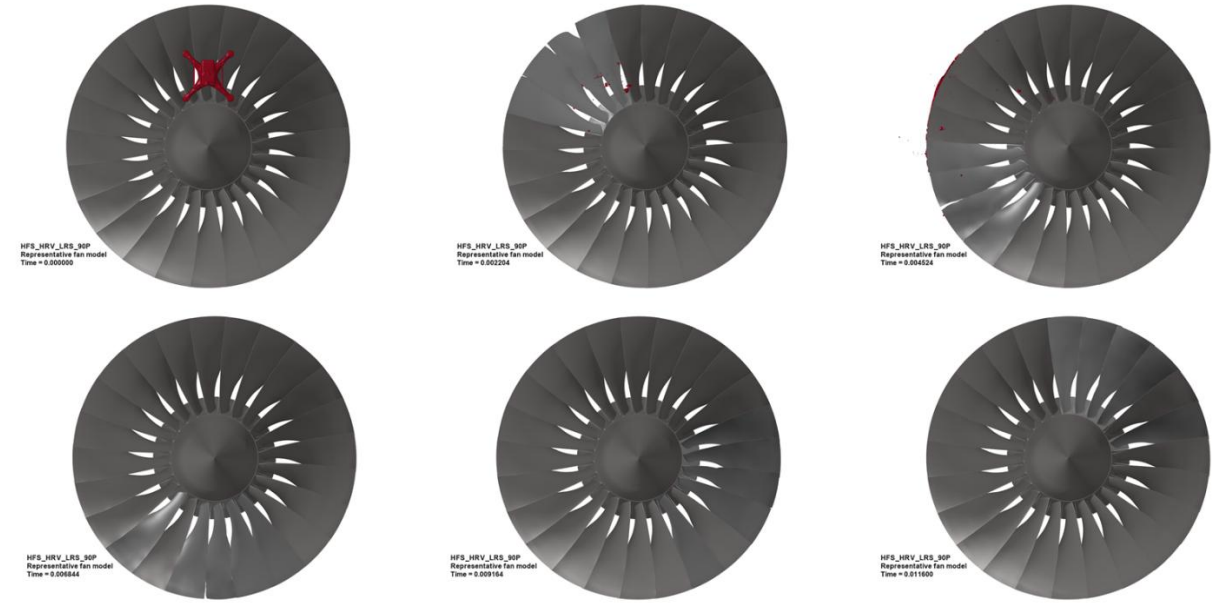

(a) Front view

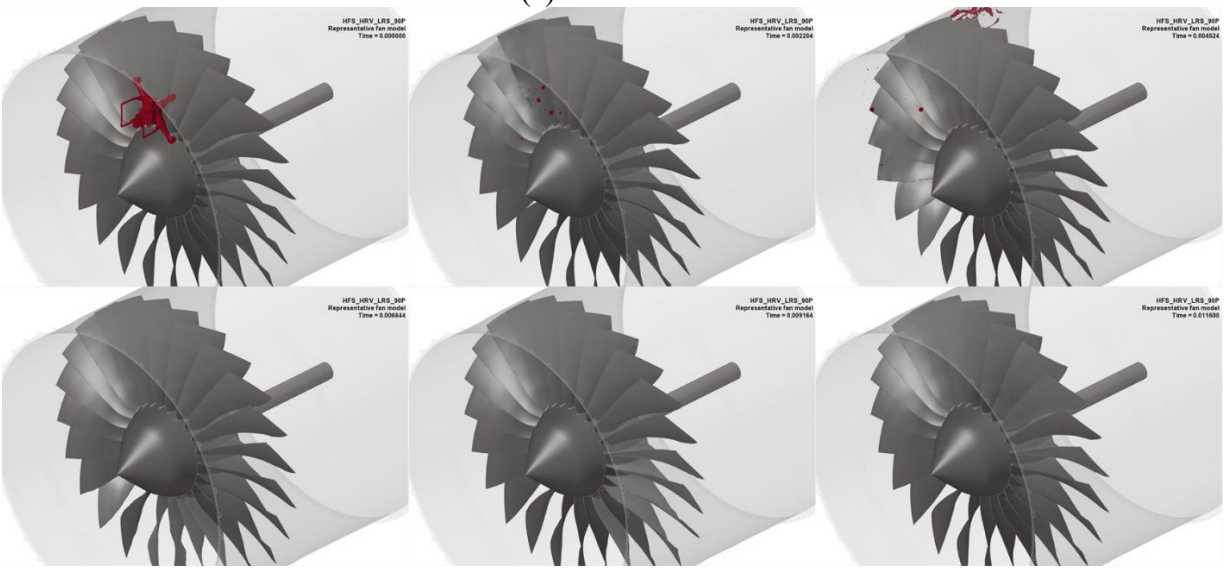

(b) Isometric view

Figure 70. HFS_HRV_LRS_90P representative fan assembly model ingestion kinematics.

The similarity in the ingestion kinematics is evident for the two models. The UAS is completely obliterated during the ingestion, and very similar blades in the fan are impacted and damaged.

Contour plots of the front and rear views of the CFM56-7B and representative fan assembly models' effective plastic strain can be seen in Figure 71. These contour plots highlight the areas that sustained the most damage in the ingestion event. It should be noted that while similar plastic strain distribution is seen in the damaged blades, there is some small plastic strain in the leading edge area for all blades of the CFM56-7B model that is not seen in the representative model. Additionally, there is more plastic strain in the disk of the CFM56-7B model when compared to

the representative model, which can be attributed to the manner in which the model was created, as discussed in Section 5.3.2. Figure 71 shows that the damage is focused on one blade that had mainly plastic deformation and some minor material loss. The damage from this ingestion event caused minor deformation and material loss in the fan blade leading edge, corresponding to a damage severity level 1 for both computational models. The damage level D_{fan} is 0.00037 for the CFM56-7B model and 0.00023 for the representative model, so there is slightly more overall damage in the CFM56-7B fan assembly model.

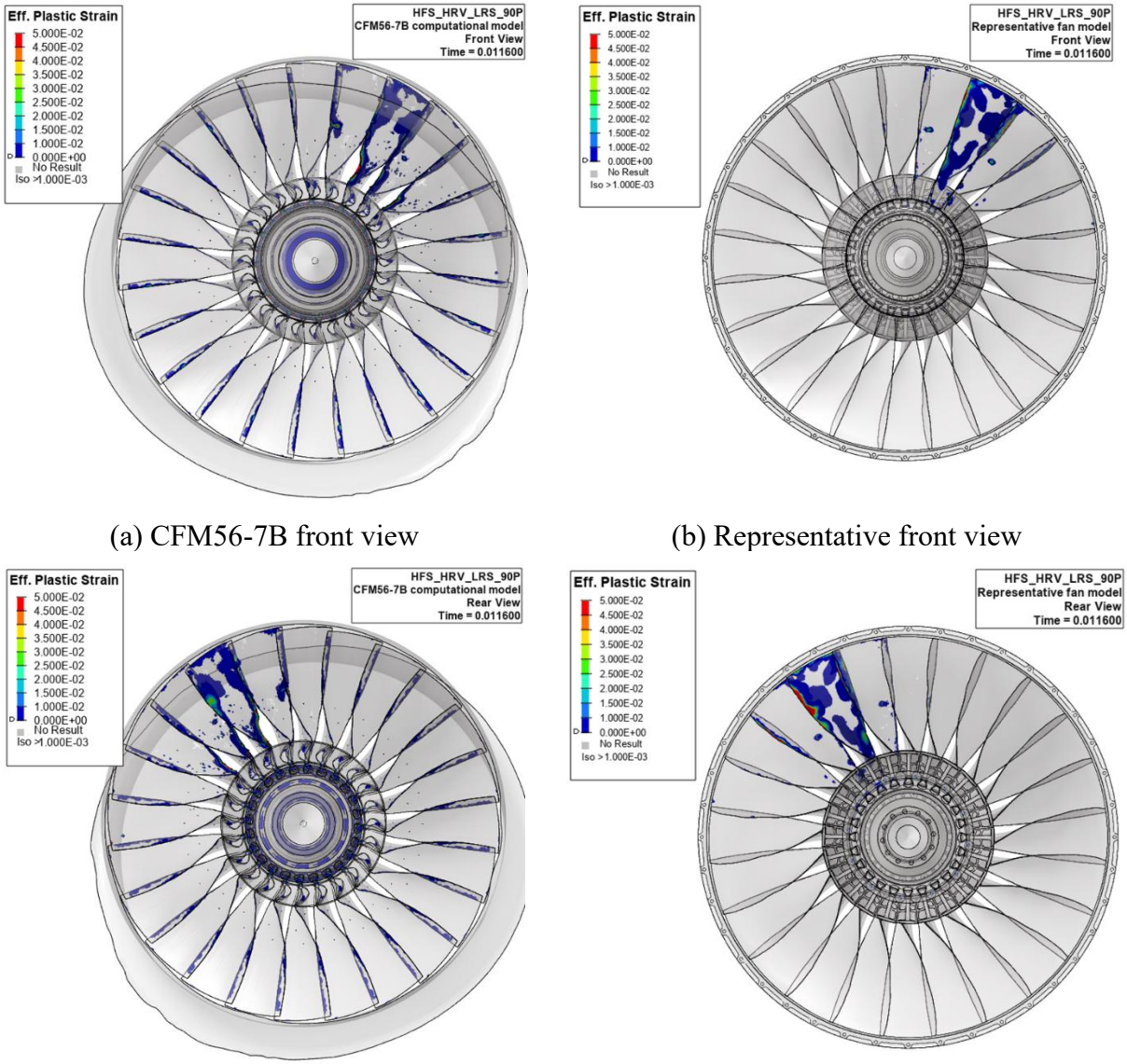

(a) CFM56-7B front view

(b) Representative front view

(c) CFM56-7B rear view

(d) Representative rear view

Figure 71. HFS_HRV_LRS_90P effective plastic strain in the fan assembly models.

The steady-state imbalances in the fan assembly models can be related to the change in position of the center of mass of each fan blade from the ingestion event. The plots of this change for the

CFM56-7B and representative fan assembly models are shown in Figure 72. As expected for a damage severity level of 1, the blade center of masses for each case does not change much from the ingestion event. It should be noted that even though both computational models have similar fan diameters, the representative fan assembly model does not account for the dovetail in the center of mass calculation, while the CFM56-7B fan assembly model does. This accounts for the large difference in the average center of mass of the fan blades, given the fan diameters are similar in size. The resultant force in the disk is also looked at to gain an understanding of transient loads in the fan assembly during and just after the impact, and those results are included in Section 8.3.

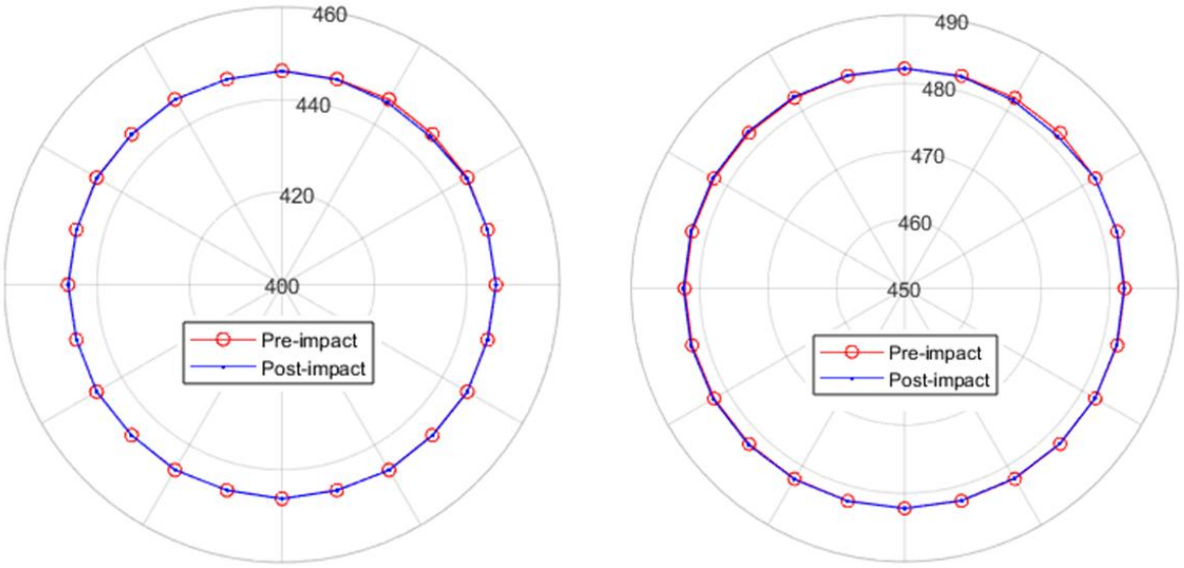

(a) CFM56-7B (b) Representative

Figure 72. HFS_HRV_LRS_90P center of mass of blades pre- and post-impact.

8.2.4 HFS_HRV_LRS_Nom

This additional computational study corresponded to a high fan speed, high UAS relative velocity, low UAS radial span impact, and nominal UAS position. The kinematics of the ingestion event for the CFM56-7B fan assembly model can be seen in Figure 73. The fan was simulated to make one full revolution, which is around 11.6 ms. It should be noted that the UAS parts were deleted once they cleared the contact region with the fan blades, which was around 9.1 ms for the CFM56-7B fan assembly model and 8.0 ms for the representative fan assembly model to increase the computational efficiency of the simulation.

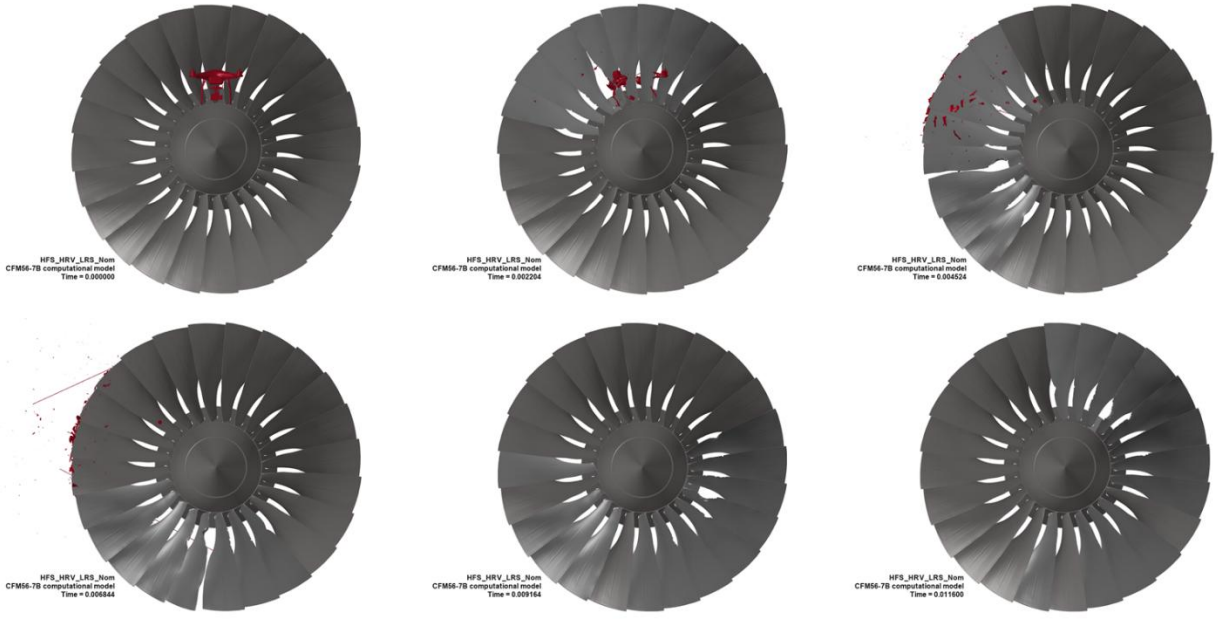

(a) Front view

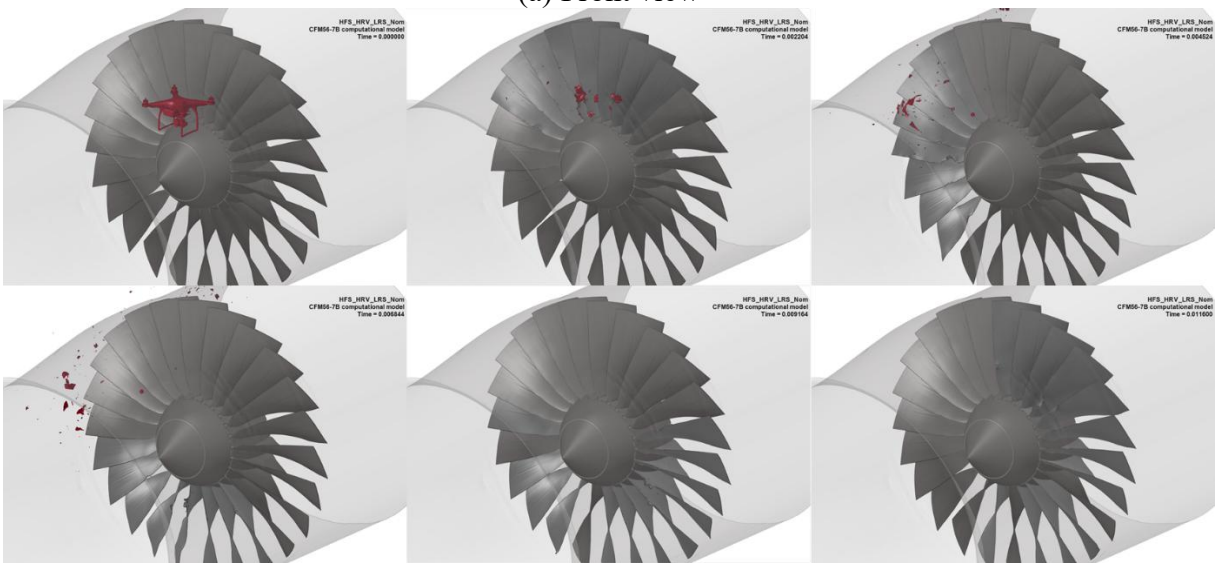

(b) Isometric view

Figure 73. HFS_HRV_LRS_Nom CFM56-7B fan assembly model ingestion kinematics.

The kinematics of the ingestion event for the representative fan assembly model can be seen in Figure 74.

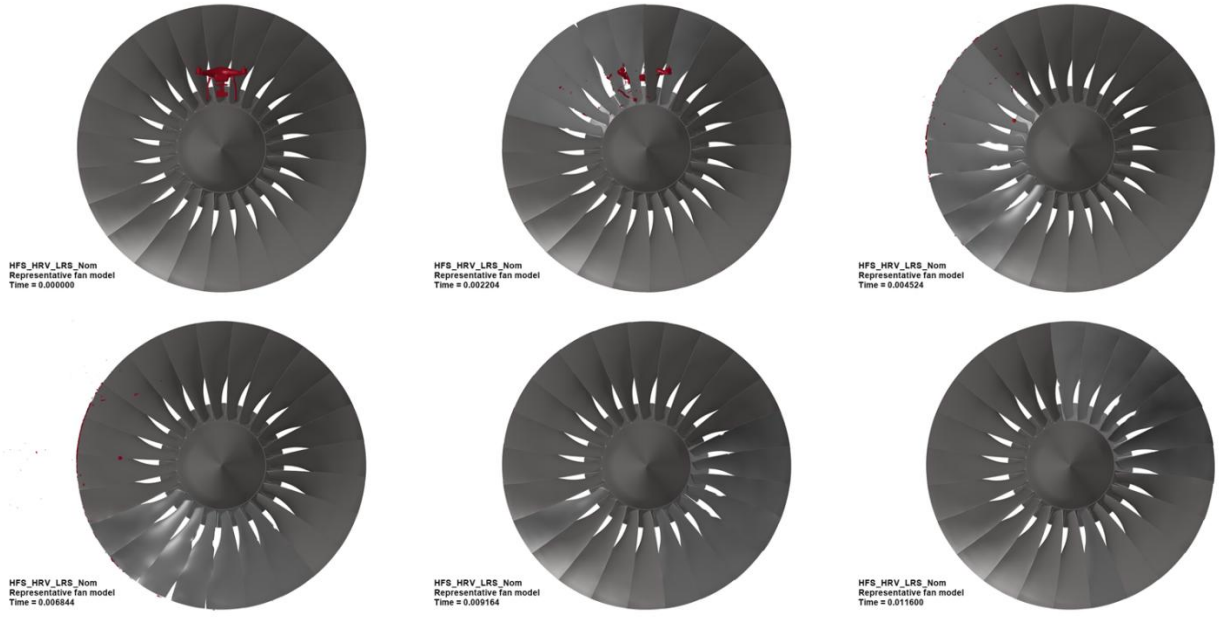

(a) Front view

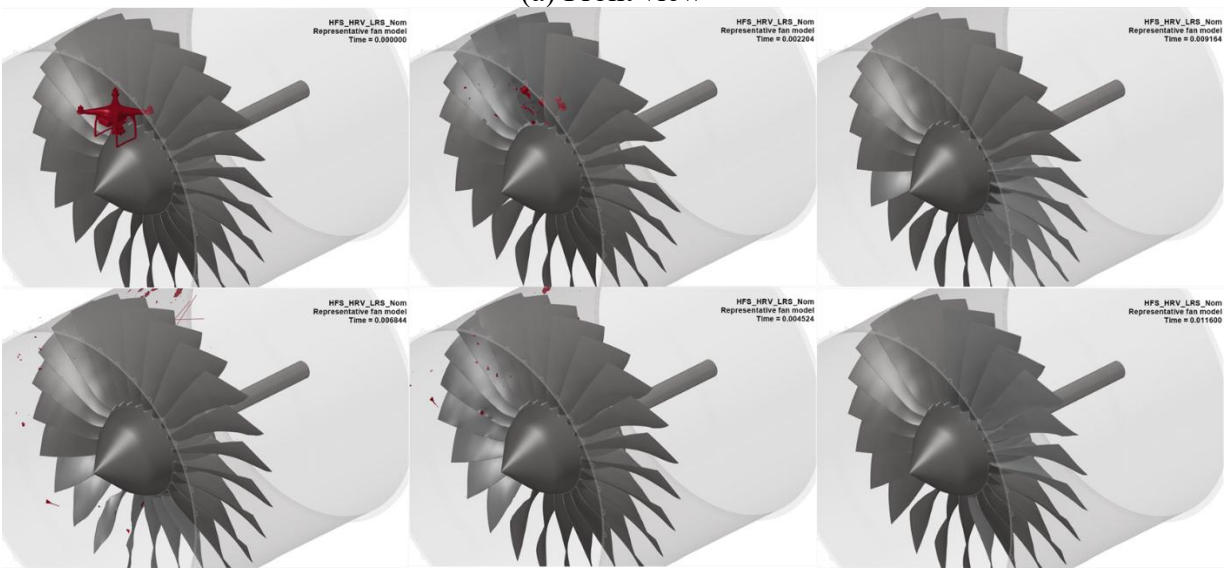

(b) Isometric view

Figure 74. HFS_HRV_LRS_Nom representative fan assembly model ingestion kinematics.

The similarity in the ingestion kinematics is evident for the two models. The UAS is completely obliterated during the ingestion, and very similar blades in the fan are impacted and damaged.

Contour plots of the front and rear views of the CFM56-7B and representative fan assembly models' effective plastic strain can be seen in Figure 75. These contour plots highlight the areas that sustained the most damage in the ingestion event. It should be noted that while similar plastic strain distribution is seen in the damaged blades, there is some small plastic strain in the leading edge area for all blades of the CFM56-7B model that is not seen in the representative model. Additionally, there is more plastic strain in the disk of the CFM56-7B model when compared to

the representative model, which can be attributed to the manner in which the model was created, as discussed in Section 5.3.2. Figure 75 shows that the damage is focused on the leading edge of a few fan blades, causing plastic deformation and the formation of a few small notches along the leading edge of several blades. The damage from this ingestion event caused deformation and material loss in the leading edge of multiple fan blades, corresponding to a damage severity level of 2 for both computational models. The damage level D_{fan} is 0.00062 for the CFM56-7B model and 0.00035 for the representative model, so there is a bit more overall damage in the CFM56-7B fan assembly model.

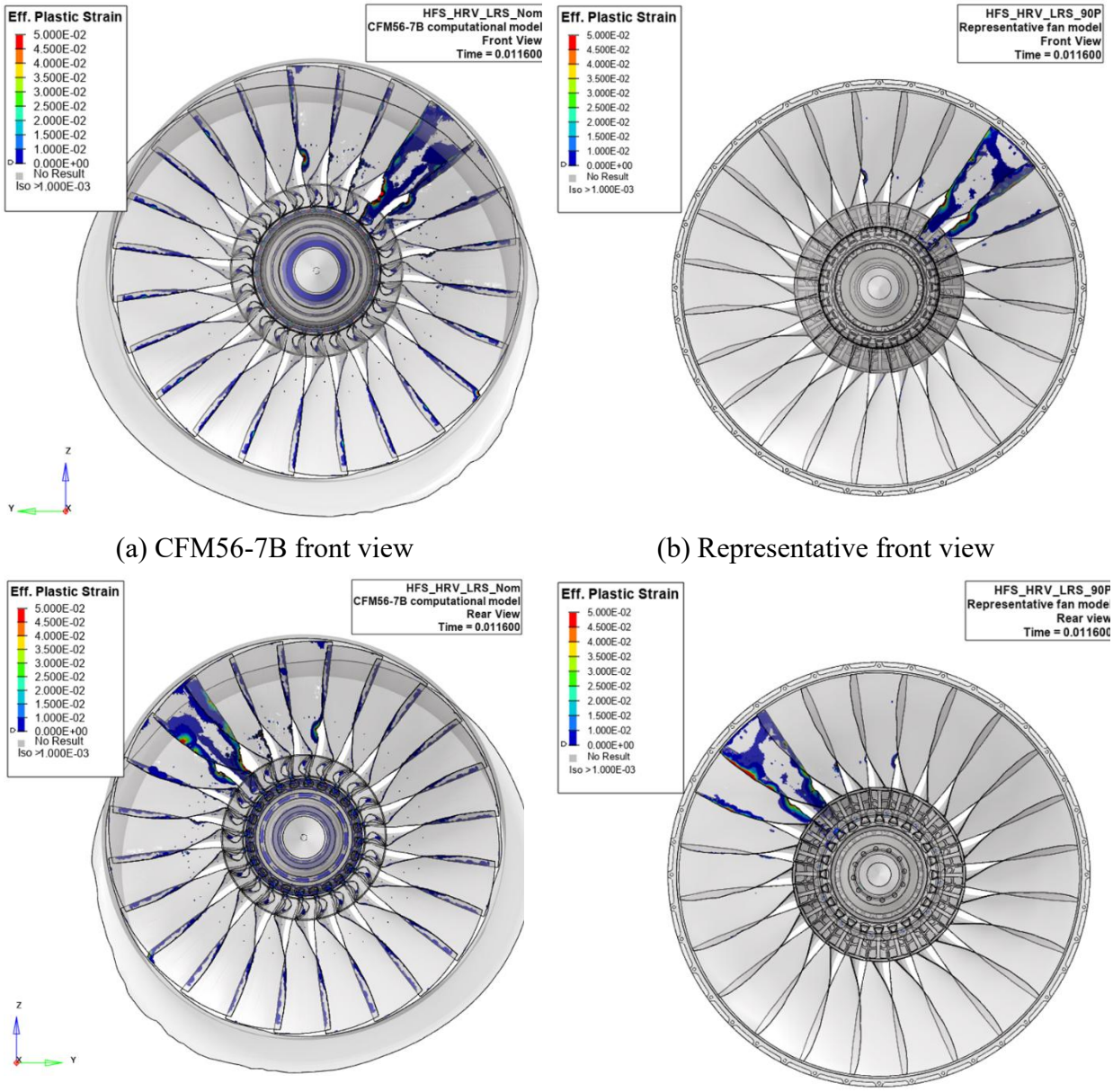

(a) CFM56-7B front view

(b) Representative front view

(c) CFM56-7B rear view

(d) Representative rear view

Figure 75. HFS_HRV_LRS_Nom effective plastic strain in the fan assembly models.

The steady-state imbalances in the fan assembly models can be related to the change in position of the center of mass of each fan blade from the ingestion event. The plots of this change for the CFM56-7B and representative fan assembly models are shown in Figure 76. It is clear that the change is similar for both models, with a slight decrease in the center of mass of the blade, which sustained the most damage. It should be noted that even though both computational models have similar fan diameters, the representative fan assembly model does not account for the dovetail in the center of mass calculation, while the CFM56-7B fan assembly model does. This accounts for the large difference in the average center of mass of the fan blades, given the fan diameters are similar in size. The resultant force in the disk is also looked at to gain an understanding of transient loads in the fan assembly during and just after the impact, and those results are included in Section 8.3.

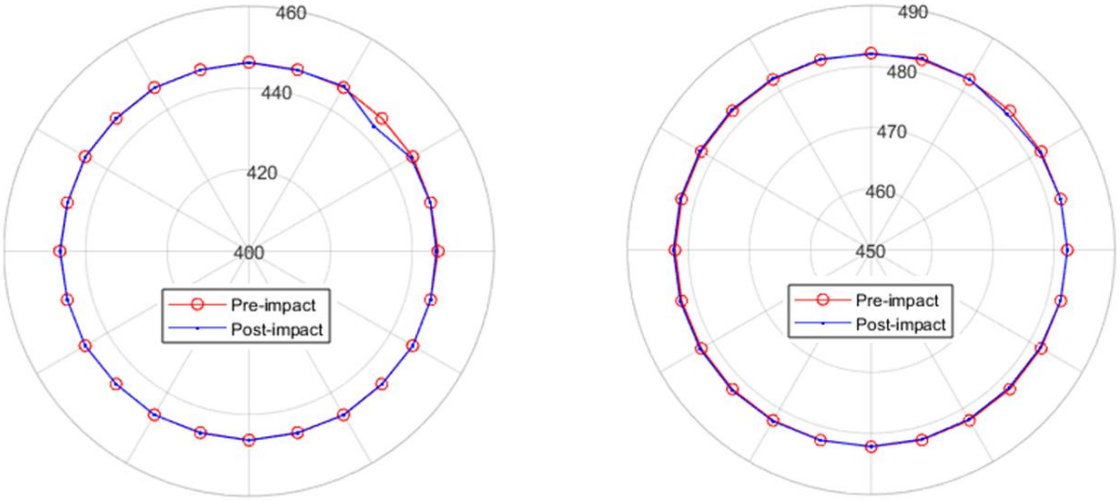

(a) CFM56-7B (b) Representative

Figure 76. HFS_HRV_LRS_Nom center of mass of blades pre- and post-impact.

8.3 SUMMARY OF COMPUTATIONAL INGESTION SIMULATIONS

The previous subsections showed that there are many similarities between the ingestion of a UAS in the CFM56-7B and representative fan assembly models for a wide variety of cases, from significant material loss and crack initiation along the leading edges of multiple blades to just a small deformation along the leading edge of a couple of blades. In general, the energy distribution in the fan and UAS components is very similar for the two cases, and importantly, the key UAS parts impact the same blades in a similar manner to result in similar effective plastic strain and failure patterns in the fan assemblies. This section highlights and compares all the cases together to better understand how the models compare and the effectiveness of the representative fan assembly in capturing appropriate trends in overall damage, transient disk force loads, and casing energies for different ingestion scenarios.

A comparison of the cumulative fan blade damage seen in the CFM56-7B and the representative fan assembly model is shown in Figure 77. The predicted level of damage is very close for higher levels of damage. Note that the CFM56-7B model shows larger damage when compared to the representative model for the lower energy (less severe ingestion) cases due to the fictitious plastic

strain predicted along the leading edge of the blades, as previously discussed. These results show that the representative fan assembly can capture the expected overall fan damage for different UAS ingestion events.

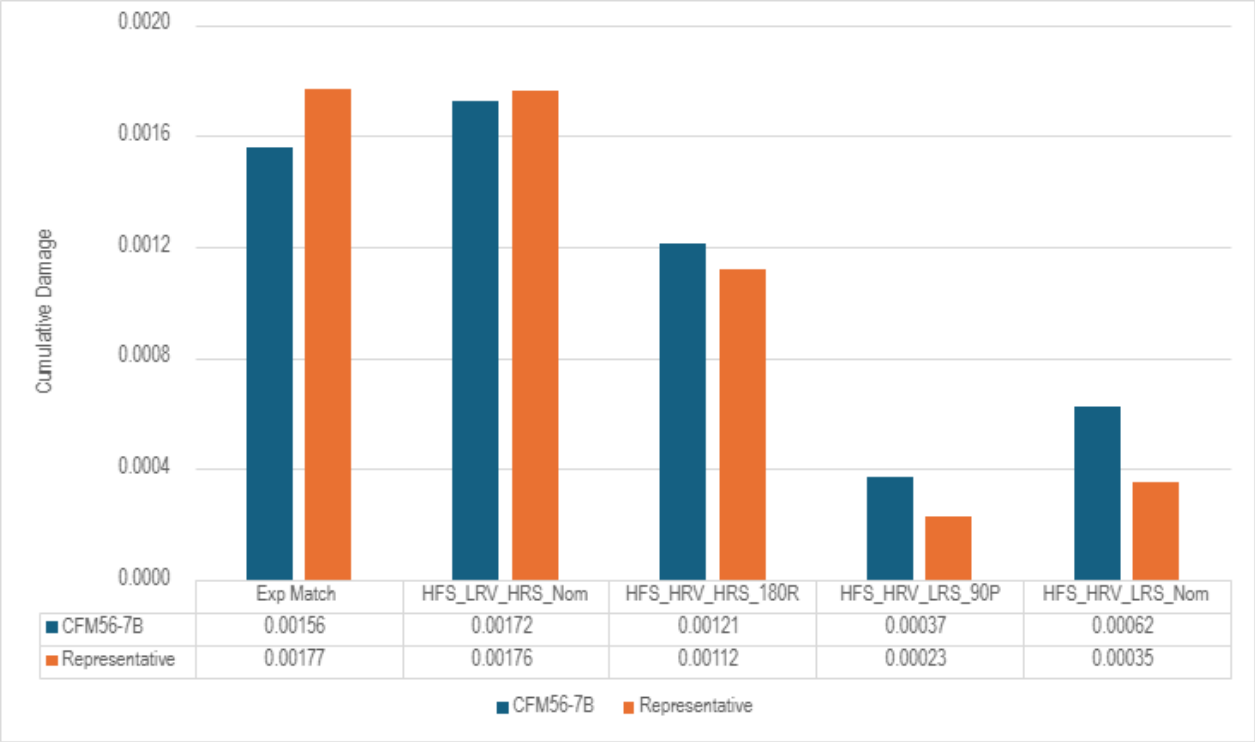

Figure 77. Cumulative fan damage (D_{fan}) comparison for different ingestion conditions.

Steady-state loads on the shaft from the fan due to imbalance can be calculated from the changes in the center of mass of the blades that were highlighted in the previous subsections and were found to be in pretty good agreement for the UAS ingestions into the CFM56-7B and representative fan assembly models. The overall transient loads at the base of the disk during the ingestion are given in Figure 78. The figure plots the disk force for the simulations with the solid lines corresponding to the CFM56-7B model and the dashed lines corresponding to the representative computational model. The average and maximum disk loads for each case are given in Figure 79. It should be noted that the average and maximum disk forces are consistently higher for the representative model compared to the CFM56-7B model. This can be attributed to the differences in boundary conditions between the two models, with the representative model having a retaining ring part on the back of the disk and a retainer on the front part of the disk to prevent axial motion in the fan blade while the CFM56-7B model had the nodes on the back of the fan blade fixed in the axial direction with the shim part in the front to prevent axial motion in the fan blade. This difference in boundary conditions causes the CFM56-7B model to transmit less force to the disk when compared to the representative model due to the fan blades being fixed axially by nodes rather than being axially fixed by a component that allows for more motion in the fan blade and the transmission of higher loads to the disk.

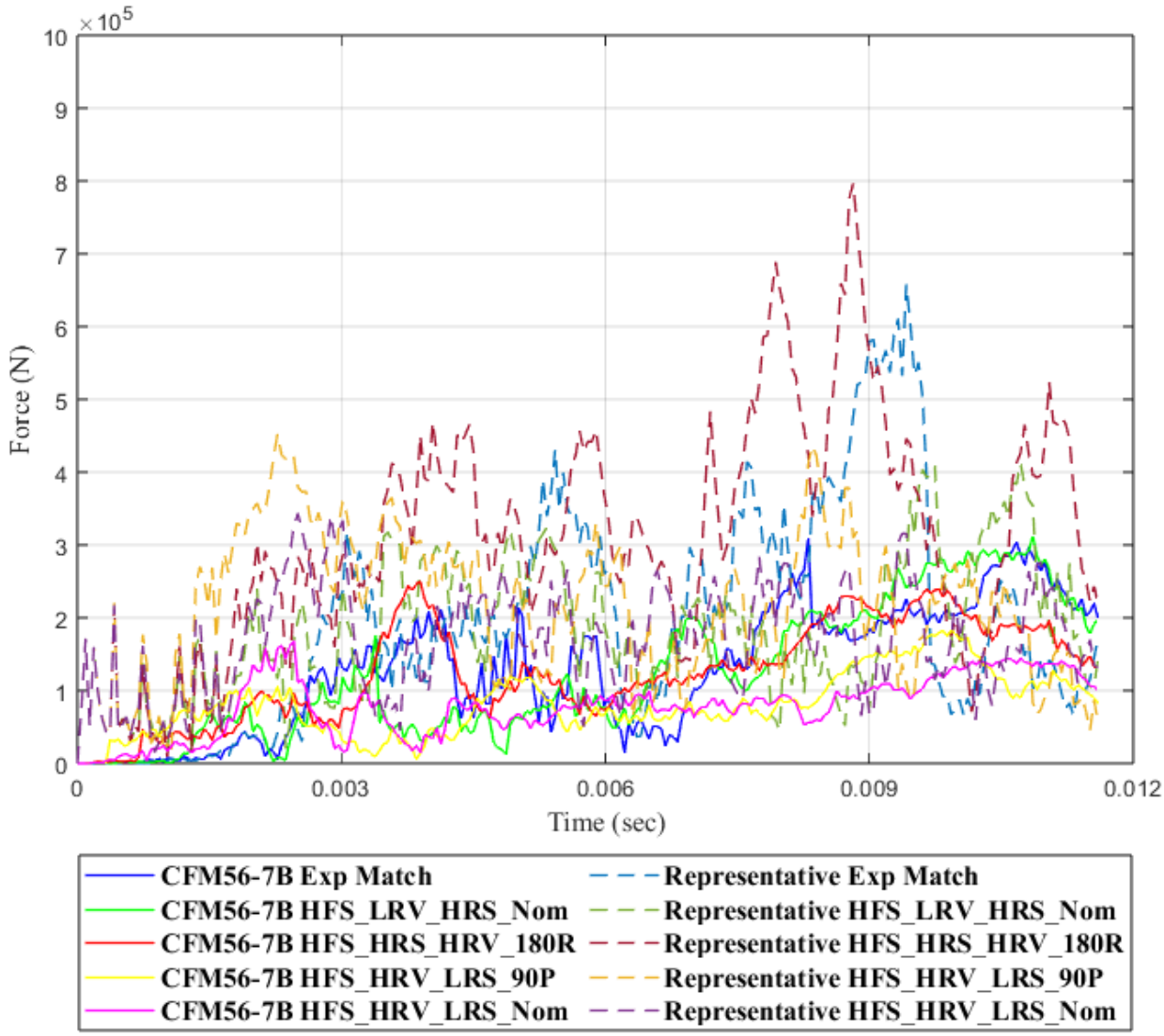

Figure 78. Transient forces at base of disk for different UAS ingestion cases.

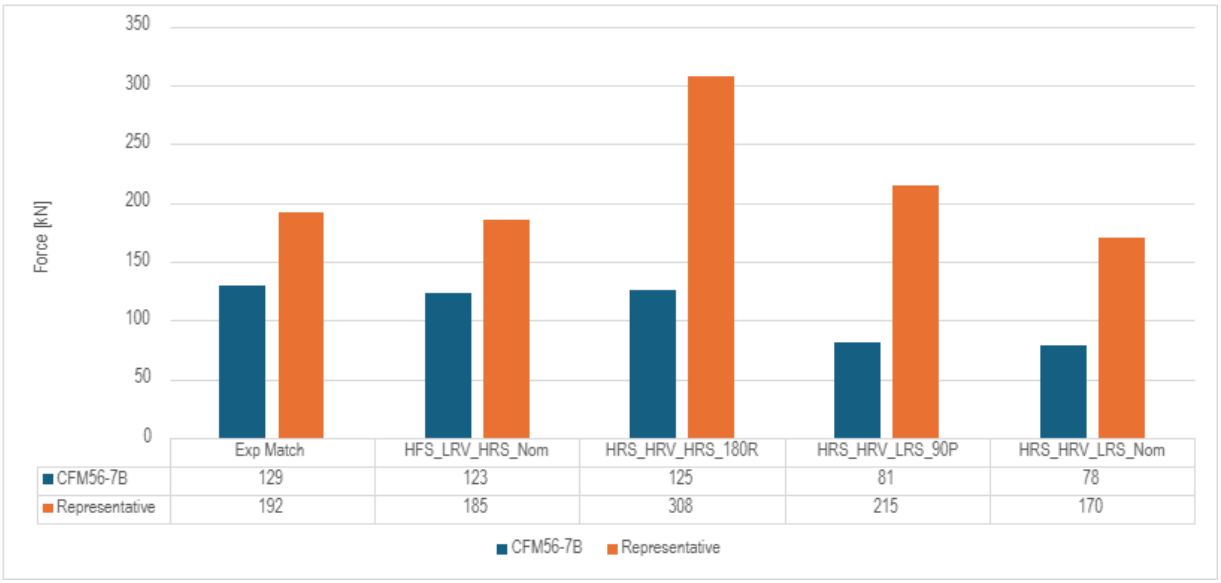

(a) Average force

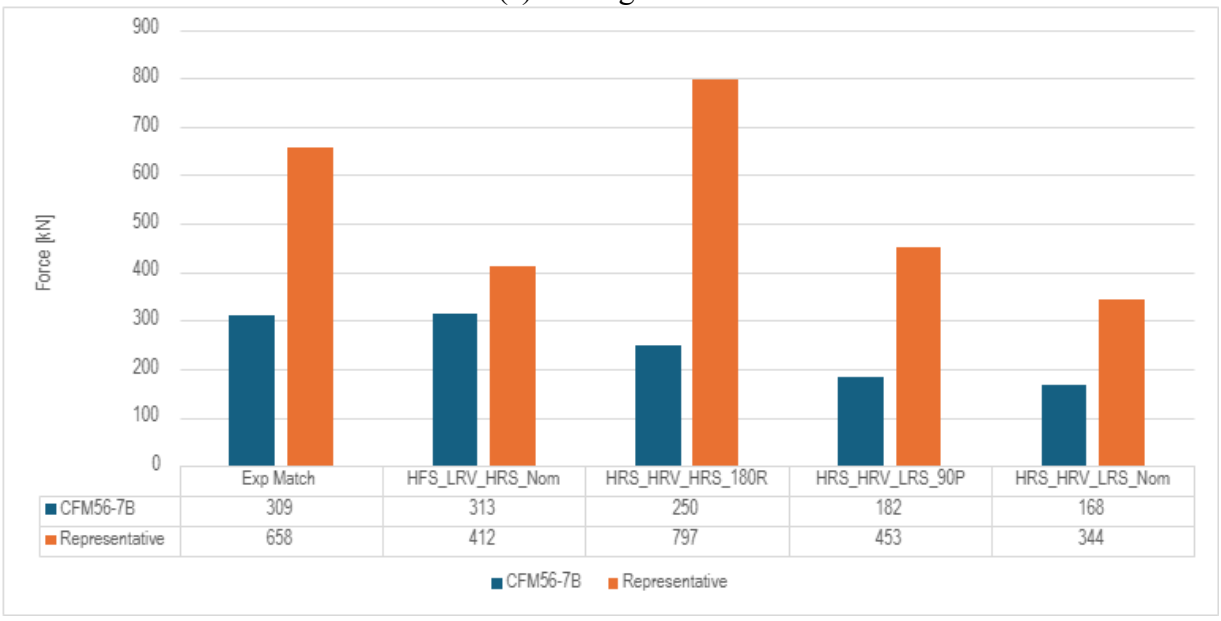

(b) Maximum force

Figure 79. Average and maximum transient forces at the base of the disk during UAS ingestion cases.

Figure 80 shows the maximum internal and kinetic energies in the casings from when the UAS first makes contact with the casing to when the UAS parts are deleted, while Figure 81 shows the average internal and kinetic energy over the same time period. It should be noted that the representative fan assembly model consistently has higher internal and kinetic energy when compared to the CFM56-7B fan assembly model. This makes sense as the casing for the CFM56-7B model is longer and has a larger mass than the representative model, as well as a different shell thickness. So, when the UAS impacts the casing for both models, the velocity of the casing from the CFM56-7B model is lower than the representative model casing. This lower velocity in the

CFM56-7B model casing reduces its kinetic energy due to the velocity term being squared in the calculation of kinetic energy.

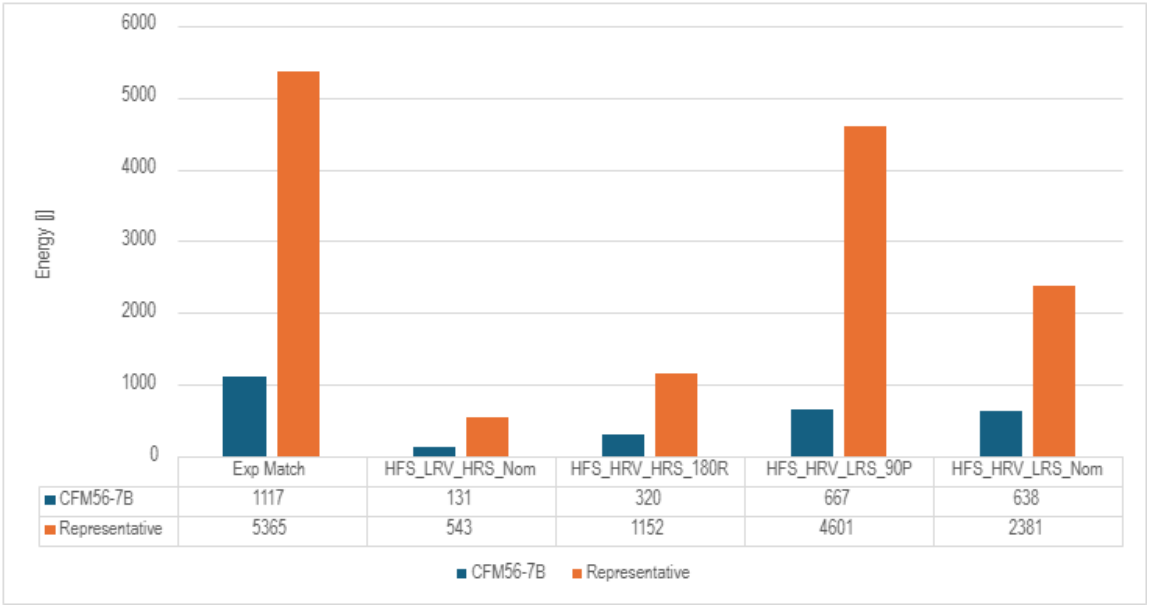

(a) Internal energy

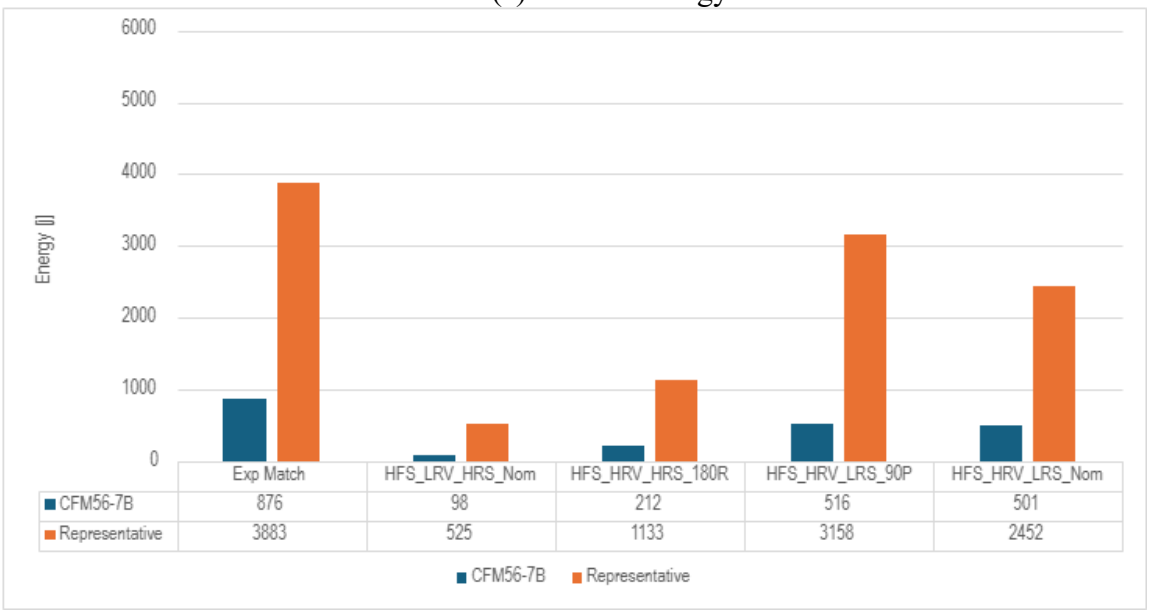

(b) Kinetic energy

Figure 80. Maximum energy in casing during ingestion simulations.

Additionally, since the UAS parts were deleted at different times for the simulations, the average energy values are skewed to be smaller for the simulations where the UAS parts were deleted later due to having a longer time period to calculate the average energies from. However, both computational models show similar trends for their respective simulations, with the UAS impacting a lower radial span having higher energy than those where it impacts a higher radial span location. This makes sense since, when the UAS impacts the fan blade model lower, this

allows for more time for the UAS to gain kinetic energy from the rotation of the fan blades so it can impart more energy into the casing. The one exception is the experimental match case where the UAS impacted at a pretty high radial span location but resulted in the highest maximum and average energy in the casing. This can be explained by the fact that in this case, the UAS's original trajectory was angled upwards towards the casing at the start of the simulation as opposed to all the other cases where the UAS was ingested with an initial velocity purely in the axial direction. The average and peak forces tend to scale pretty consistently with the same trends, in addition to the internal and kinetic energy, which has previously been observed[4].

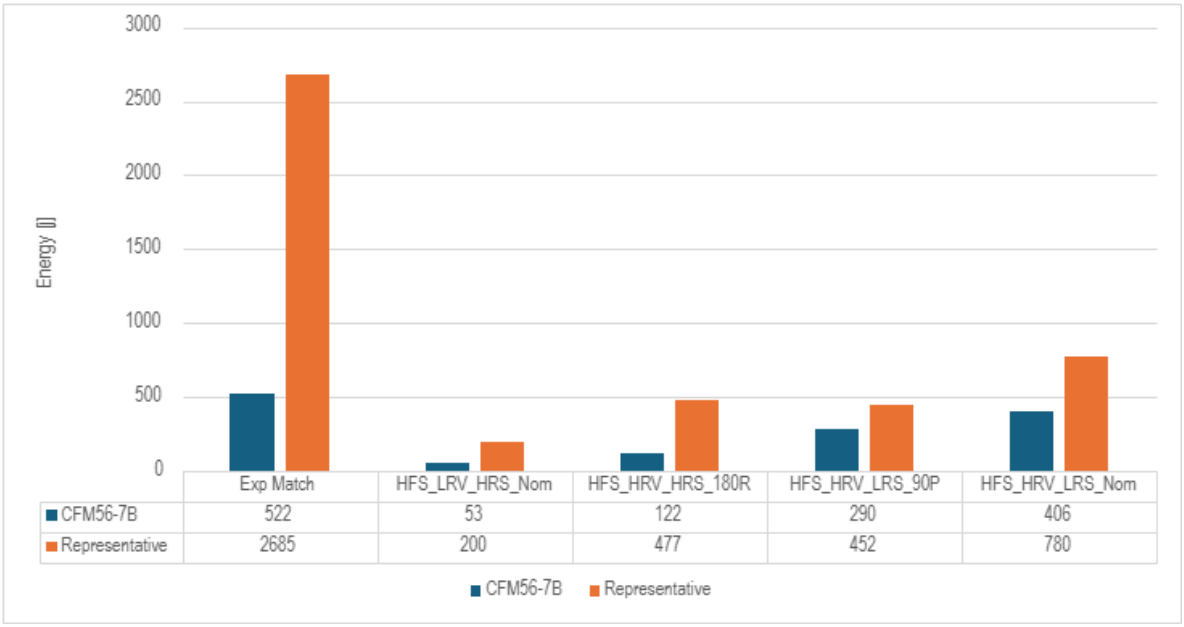

(a) Internal energy

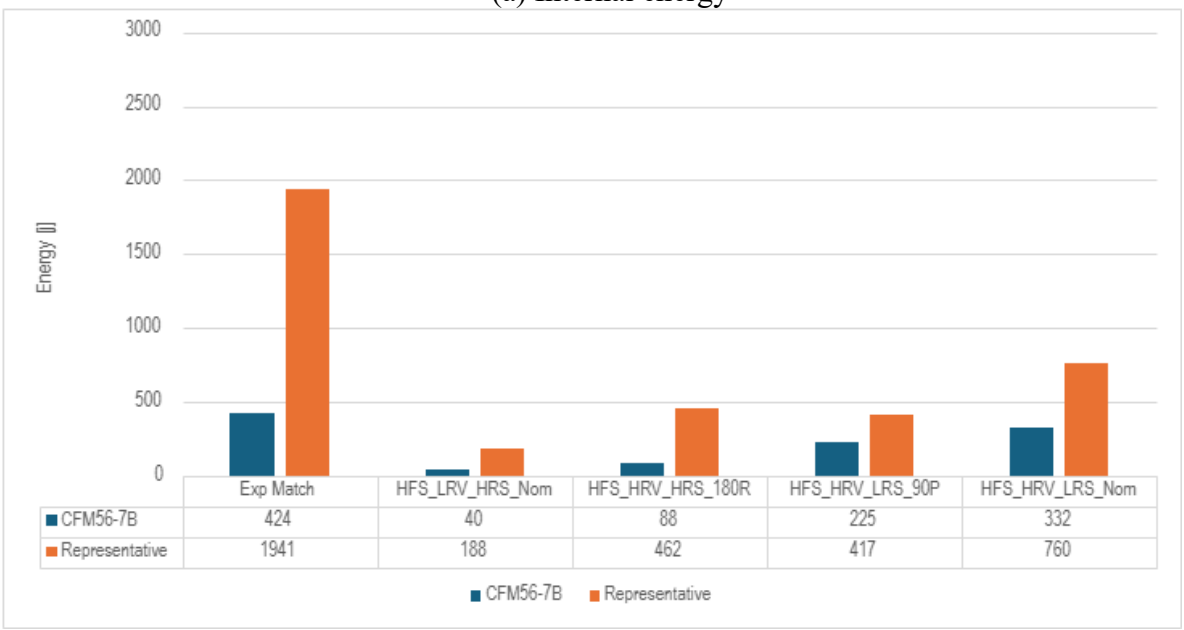

(b) Kinetic energy

Figure 81. Average energy in casing during ingestion simulations.

A summary of the key results comparing each of the ingestion simulations for the two fan assembly models is given in Table 11.

Table 11. Summary of ingestion results for each model.

Simulation ID	Average force in Disk (kN)	Average internal energy in casing (J)	Average kinetic energy in casing (J)	D_{fan}	Severity level	Associated damage
Experimental match CFM56-7B	129	522	424	0.00156	Level 3	Significant material loss on leading edge of multiple blades
Experimental match Representative	192	2,685	1,941	0.00177	Level 3	Significant material loss on leading edge of multiple blades
HFS_LRV_HRS_Nom CFM56-7B	123	53	40	0.00172	Level 3	Significant material loss on leading edge of multiple blades
HFS_LRV_HRS_Nom Representative	185	200	188	0.00176	Level 3	Significant material loss on leading edge of multiple blades
HFS_HRV_HRS_180R CFM56-7B	125	122	88	0.00121	Level 3	Significant material loss on leading edge of multiple blades
HFS_HRV_HRS_180R Representative	308	477	462	0.00112	Level 3	Significant material loss on leading edge of multiple blades
HFS_HRV_LRS_90P CFM56-7B	81	290	225	0.00037	Level 1	Small deformation of blades and no crack initiation
HFS_HRV_LRS_90P Representative	215	452	417	0.00023	Level 1	Small deformation of blades and no crack initiation
HFS_HRV_LRS_Nom CFM56-7B	78	406	332	0.00062	Level 2	Small material loss along leading edge of multiple blades and plastic deformation of blades
HFS_HRV_LRS_Nom Representative	170	780	760	0.00035	Level 2	Small material loss along leading edge of multiple blades and plastic deformation of blades

9. KEY CONCLUSIONS AND RECOMMENDATIONS

The completion of this research program resulted in overseeing a live ingestion of a UAS into a CFM56-7B engine to gather as much data as possible for validating the computational modeling approach, as well as generating a large data set that can be used in future studies. The test conditions were chosen to result in one of the more severe ingestion scenarios for the given UAS while also leveraging past research.

A representative engine was chosen for the test, a flightworthy CFM56-7B engine. The DJI Phantom 3 standard UAS was chosen as the projectile to capitalize on the considerable effort that was expended in developing a high-fidelity FE model that was validated at the conditions of an ingestion event[6, 8, 9, 14]. The ingestion conditions were selected to be at takeoff conditions for the engine, with the UAS impacting the outer radial span. Key data collected from the experiment to validate the modeling approach include several high-definition and high-speed cameras capturing the ingestion, DIC, strain gauges, and post-test documentation.

A fan assembly model was developed to capture many of the key geometric features of the CFM56-7B fan. Some key fan components were scanned and then stitched together to provide the baseline geometry of key components of the fan assembly. The parts were assembled and meshed following the best practices of the Aerospace Working Group[13]. The key material model used for the fan material was a publicly available Ti-6Al-4V model that was developed from previous FAA research[17]. The material model is the closest publicly available model since the actual material properties are proprietary. The general development of the fan assembly model was in line with the previous development of the representative fan assembly model created in prior research[4].

The developed computational CFM56-7B fan assembly model was simulated in LS-DYNA under the same conditions as the live engine ingestion test in a manner similar to the previous computational work[4]. The conditions of the ingestion (UAS speed, orientation, and location just before impact) were computed by analyzing the DIC data. Comparisons were made between the data gathered from the test and the numerical simulation. The overall damage to the fan blades was in very good agreement. There was a small amount of extra damage at the tips of all blades in the live ingestion due to the severe blade rub that occurred during the testing that was not present in the simulation. The main notable difference in damage between the two cases was that the upper portion of one blade in the experiment broke free, whereas there was a significant crack along the leading edge in the simulation for the corresponding blade. It is important to note that LS-DYNA is not a crack propagation tool but rather a tool that can accurately predict the onset of damage and was not developed to predict subsequent fracture mechanic growth. This was noted in the previous UAS ingestion research, and anywhere there is severe cracking and damage to the leading edge of a blade, there is the potential for a crack to propagate through the entire chord of the blade[4]. The overall fan damage severity level as defined in the previous engine ingestion research[4], was matched between the experiment and numerical simulation. The strain gauge data and out-of-plane displacement on the impacted blades were compared with the simulation results and were in reasonably good agreement, considering all the assumptions and limitations in the model. Also, the kinematics of the ingestion were very similar except for the fireball that was created in the experiment, which was not replicated in the numerical simulation.

The open representative fan assembly model that was developed in the previous research effort for studying UAS ingestions was also compared with the live ingestion experiment and CFM56-7B fan assembly simulation. The blade damage was the only data from the experiment that the representative fan assembly model was compared with, and it was again found to be in good agreement with all the impacted blades having similar levels of damage. Again, the simulation did not predict the liberation of the blade tip but did predict severe damage at the same location, which could lead to the same portion of the blade breaking off as in the experiment. A more detailed comparison of many factors, such as the overall blade damage in the fans (D_{fan}), effective plastic

strain in the blades, energy in the fan blades and UAS during the ingestion, force and moments in a sectional plane of damaged and undamaged blades, transient forces in the disk, center of mass of the blades after the ingestion, and energy in the casing were able to be compared for the simulations. Due to differences, particularly in the boundary conditions of the fan blades and the size of the casing, a direct comparison of some of these parameters is not useful, and only trends from multiple simulations can be observed. To this end, multiple additional simulations with the CFM56-7B fan assembly model were completed to match a wide assortment of damage levels from the previous engine ingestion research[4]. It was found that, in general, the overall damage in the fan blades (D_{fan}), the effective plastic strain, force and moments in a sectional plane of a damaged and undamaged blade, change in center of mass of the blades, and general energy distributions in parts compared pretty well between the two fan assembly models. The transient forces in the disk during the ingestion and casing energies tended to be very different due to the differences in the boundary conditions. However, even in these cases, the trends in the results for the different fan assembly models were quite evident. Most importantly, the overall fan damage severity levels were predicted to be the same in all five cases studied.

The completion of this research program has validated the overall computational modeling approach for the ingestion of a UAS into a fan assembly model. Moreover, the open representative fan assembly model that was previously developed was compared with a fan assembly rig model of an actual engine in service (CFM56-7B) and found to be in good agreement. This gives high confidence in using this open representative fan assembly model in future foreign object ingestion studies in industry and academia to improve models and compare results with prior work.

10. REFERENCES

[1] http://osc.edu/ark:/19495/f5s1ph73. Ohio Supercomputer Center. Columbus, OH: Ohio Supercomputer Center; 1987.
[2] D'Souza K, Lyons T, Lacy T, Kota K. Volume IV: UAS Airborne Collision Severity Evaluation: Engine Ingestion. FAA; 2017.
[3] Lyons T, D'Souza K. Parametric Study of an UAV Ingestion into a Business Jet Size Fan Assembly Model. ASME Journal of Engineering for Gas Turbines and Power 2019;141(7).
[4] D'Souza K, Sirivolu D, Wong M, Kurstak E. Annex A to Task A17: OSU Representative Fan Model and sUAS Ingestion Studies. 2023.
[5] Lyons T, Sirivolu D, D'Souza K. Stress State Characterization for a Generic Titanium Fan During Bird Ingestion. AIAA Journal 2022:1-12.
[6] Olivares G, Gomez L, Ly H. Annex B to Task A17: NIAR/WSU sUAS Numerical Model Validation (Component and Full-Scale Level) for Engine Ingestion Analysis. 2023.
[7] Duling C, Zweiner M, Arteburn D. Annex C to Task A17: UAH High Speed Impacts of Full sUAS and Components with Angled Plates 2023.
[8] D'Souza K, Wong M, Sirivolu D, Perrin Z, Zwiener M, Duling C, Gomez L, Olivares G. Experimental Validation of a UAS at Engine Ingestion Conditions: Part I Experiments. Aerospace Science and Technology 2024.
[9] D'Souza K, Wong M, Sirivolu D, Gomez L, Olivares G, Perrin Z, Zwiener M, Duling C. Experimental Validation of a UAS at Engine Ingestion Conditions: Part 2 Model Validation. Aerospace Science and Technology 2024.
[10] Mattar R, Sirivolu D, D'Souza K. Comparison of Ingestion of Different Size Hard and Soft Bodies into a Representative Fan Assembly Model. Journal of Engineering for Gas Turbines and Power 2024;147(2).
[11] D'Souza K, Sirivolu D, Gomez L, Olivares G. Damage to a High Bypass Ratio Fan During UAS Ingestions. Journal of Engineering for Gas Turbines and Power 2024;146(12).
[12] D'Souza K, Olivares G, Arteburn D. Task A17: Airborne Collision Severity Evaluation – Engine Ingestion. 2023.
[13] http://awg.lstc.com/tiki/tiki-index.php?page=MGD. LS-DYNA Aerospace Working Group Modeling Guidelines Document. 2016.
[14] Olivares G, Gomez L, Monteros JE, Baldridge R, Zinzuwadia C, Aldag T. Volume II – UAS Airborne Collision Severity Evaluation – Quadcopter. FAA; 2017.
[15] Olivares G, Monteros J, Baldridge R, Zinzuwadia C, Gomez L. Volume II – UAS Airborne Collision Severity Evaluation – Quadcopter. FAA Report; 2016.
[16] CFM. Training Manual CFM56-5B, Basic Engine. 2000.
[17] Haight S, Wang, L., Du Bois, P., Carney K., Kan C. D. Development of a Titanium Alloy Ti-6Al-4V Material Model Used in LS-DYNA. FAA.
[18] Hammer JT. Plastic Deformation and Ductile Fracture of Ti-6Al-4V under Various Loading Conditions. FAA Report DOT/FAA/TC-TT14/2; 2014.
[19] LS-DYNA Keyword User's Manual Vol. 1. Livermore, California; 2016.
[20] http://awg.lstc.com/tiki/tiki-index.php?page=Resources. LS-DYNA Aerospace Working Group *Mat_224 User Guide. 2016.
[21] Seidt JD. Part 3: Plastic Deformation and Ductile Fracture of 2024 Aluminum under Various Loading Conditions. Development of a New Metal Material Model in LS-DYNA: FAA Report DOT/FAA/TC-13/25, P3; 2014.
[22] https://awg.ansys.com/Welcome. LS-DYNA Aerospace Working Group 2016.

[23] Sengoz K, Kan S, Eskandarian A. Development of a Generic Gas Turbine Engine Fan Blade-out Full Fan Rig Model. FAA Report DOT/FAA/TC-14/43; 2015.
[24] https://www.cfmaeroengines.com/engines/cfm56/. The Cfm56 Engine Family. CFM; 2024.
[25] https://www.safran-group.com/products-services/cfm56-best-selling-engine-commercial-aviation-history. Cfm56 - the Best-Selling Engine in Commercial Aviation History. 2024.